

EUROPEAN ORGANISATION FOR NUCLEAR RESEARCH (CERN)



Submitted to: Phys. Rev. D.



CERN-PH-EP-2015-237
26th September 2018

Measurement of the differential cross-section of highly boosted top quarks as a function of their transverse momentum in $\sqrt{s} = 8$ TeV proton–proton collisions using the ATLAS detector

The ATLAS Collaboration

Abstract

The differential cross-section for pair production of top quarks with high transverse momentum is measured in 20.3 fb^{-1} of proton–proton collisions at a center-of-mass energy of 8 TeV. The measurement is performed for $t\bar{t}$ events in the lepton+jets channel. The cross-section is reported as a function of the hadronically decaying top quark transverse momentum for values above 300 GeV. The hadronically decaying top quark is reconstructed as an anti- k_t jet with radius parameter $R = 1.0$ and identified with jet substructure techniques. The observed yield is corrected for detector effects to obtain a cross-section at particle level in a fiducial region close to the event selection. A parton-level cross-section extrapolated to the full phase space is also reported for top quarks with transverse momentum above 300 GeV. The predictions of a majority of next-to-leading-order and leading-order matrix-element Monte Carlo generators are found to agree with the measured cross-sections.

Contents

1	Introduction	2
2	The ATLAS detector	3
3	Data and Monte Carlo samples	3
4	Object definition and event selection	5
5	Background estimation	7
6	Systematic uncertainties	9
6.1	Detector modeling	9
6.2	Signal and background modeling	10
7	Data and MC comparison at detector level	11
8	Differential cross-section determination	11
8.1	Combination of decay channels	13
8.2	Particle- and parton-levels fiducial region definitions	13
8.3	Unfolding to particle and parton levels	14
8.4	Propagation of statistical and systematic uncertainties	17
9	Results and interpretation	19
10	Conclusions	22
A	Detailed tables of systematic uncertainties	26

1. Introduction

The large number of top–antitop quark ($t\bar{t}$) pairs produced at the LHC provide a unique opportunity to improve our understanding of $t\bar{t}$ production and test the Standard Model (SM) at the TeV scale. New phenomena beyond the Standard Model may distort the top quark transverse momentum (p_T) spectrum, in particular at high p_T (see, e.g., Refs. [1, 2]), and could thus be revealed by a precise measurement. Moreover, due to their high cross-section at the LHC and rich experimental signature, $t\bar{t}$ events constitute a dominant background to a wide range of searches for new massive particles. A better understanding of the production of high-momentum top quarks, including a more precise determination of the parton distribution functions (PDF) of the proton, would be of great benefit to the broader LHC program.

The initial measurements of $t\bar{t}$ production at the LHC have focused on a determination of the inclusive production cross-section. Now that the experimental uncertainties on these measurements (see, e.g., Refs. [3–5]) are comparable to or lower than the uncertainties on the next-to-next-to-leading-order plus next-to-next-to-leading-logarithmic order (NNLO+NLL) theory prediction [6–11], the interest in differential top quark cross-section measurements has gained traction. Measurements of the differential cross-section as a function of the kinematics of the top quark, or the top–antitop quark pair, have

been performed by the ATLAS [12–14] and CMS collaborations [15, 16], where the highest measured top quark p_T range is 350–800 GeV [13].

In this paper a measurement using techniques specifically designed to deal with the collimated decay topology of highly boosted top quarks is presented. In particular, the hadronic top quark decay is reconstructed as a single large-radius (large- R) jet. The selection and reconstruction are based on an algorithm developed [17] and used in $t\bar{t}$ resonance searches [18–21] that increases the $t\bar{t}$ selection efficiency at high top quark p_T and extends the kinematic reach into the TeV range. This analysis utilizes the lepton+jets channel where one W boson decays hadronically and the other leptonically to an electron or a muon, assuming each top quark decays to a W boson and a b -quark. The cross-section is measured as a function of the hadronically decaying top quark p_T . A particle-level cross-section is measured in a kinematic region close to the detector-level selection, referred to in the following as fiducial region. A parton-level differential cross-section is also reported as a function of the hadronically decaying top quark p_T , by further extrapolating to the full kinematic phase space except for a lower limit on top quark p_T of 300 GeV. The measured cross-sections are compared to the predictions of several MC generators and PDF sets.

The object definition, event selection, and background determination used in this analysis follow closely the ones used in the search for $t\bar{t}$ resonances [20]. More details of these aspects of the measurement can be found in the corresponding reference.

2. The ATLAS detector

ATLAS is a multipurpose detector [22] that provides nearly full solid angle¹ coverage around the interaction point. Charged-particle trajectories are reconstructed by the inner detector, which covers pseudorapidity $|\eta| < 2.5$ and is composed of a silicon pixel detector, a silicon microstrip detector, and a transition radiation tracker (TRT). The inner detector is surrounded by a solenoid that provides a 2 T magnetic field. Sampling calorimeters with several different designs span the pseudorapidity range up to $|\eta| = 4.9$. High-granularity liquid-argon (LAr) electromagnetic (EM) calorimeters are used up to $|\eta| = 3.2$. Hadronic calorimetry based on scintillator-tile active material covers $|\eta| < 1.7$ while LAr technology is utilized for hadronic calorimetry from $|\eta| = 1.5$ to $|\eta| = 4.9$. The calorimeters are surrounded by a muon spectrometer. A magnetic field in the spectrometer is provided by air-core toroid magnets. Three layers of precision gas chambers track muons up to $|\eta| = 2.7$ and muon trigger chambers cover $|\eta| < 2.4$.

3. Data and Monte Carlo samples

The cross-section is measured using data from the 2012 LHC pp run at $\sqrt{s} = 8$ TeV, which corresponds to an integrated luminosity of $20.3 \pm 0.6 \text{ fb}^{-1}$. The luminosity was measured using techniques similar to those described in Ref. [23] with a calibration of the luminosity scale derived from beam-overlap scans performed in November 2012. The average number of pp interactions per bunch

¹ ATLAS uses a right-handed coordinate system with its origin at the nominal interaction point (IP) in the center of the detector and the z -axis along the beam pipe. The x -axis points from the IP to the center of the LHC ring, and the y -axis points upward. Cylindrical coordinates (r,ϕ) are used in the transverse plane, ϕ being the azimuthal angle around the beam pipe. The pseudorapidity is defined in terms of the polar angle θ as $\eta = -\ln \tan(\theta/2)$.

crossing (pileup) in 2012 was around 21. The sample was collected using the logical OR of two single-electron triggers with transverse momentum thresholds of 60 GeV, lowered to 24 GeV in the case of isolated electrons, and two single-muon triggers with transverse momentum thresholds of 36 GeV, lowered to 24 GeV in the case of isolated muons.

Samples of Monte Carlo (MC) simulated events are used to characterize the detector response and efficiency to reconstruct $t\bar{t}$ events, estimate systematic uncertainties, predict the background contributions from various physics processes, and to compare the theoretical predictions with the measurement. The simulated events are weighted such that the distribution of the average number of pp interactions per bunch crossing agrees with data. The samples were processed through the GEANT4[24] simulation of the ATLAS detector [25]. For the evaluation of some systematic uncertainties, generated samples are passed to a fast simulation using a parameterization of the performance of the ATLAS electromagnetic and hadronic calorimeters [26]. Simulated events are reconstructed using the same algorithms that are applied to the data.

The nominal signal $t\bar{t}$ sample is generated using the PowHEG (PowHEG-hvq patch4) [27] method, as implemented in the PowHEG-Box generator [28], which is based on next-to-leading-order (NLO) QCD matrix elements. The h_{damp} parameter, which effectively regulates the high- p_T radiation in PowHEG, is set to the top quark mass. The CT10 [29] PDF are employed and the top quark mass is set to $m_{\text{top}} = 172.5$ GeV. Parton showering and hadronization are simulated with PYTHIA v6.425 [30] using the Perugia 2011 C set of tuned parameters (tune) [31] and the corresponding leading-order (LO) CTEQ6L1 [32] PDF set. Unless otherwise noted, electroweak corrections extracted with HATHOR 2.1-ALPHA [33], implementing the theoretical calculations of Refs. [34–36], are applied as weights to the events of this sample. The prediction of PowHEG is compared to that obtained with other generators such as MC@NLO v4.01 [37] with CT10 for the PDF set, interfaced to HERWIG v6.520 [38] for parton showering and hadronization, JIMMY v4.31 [39] for the modeling of multiple parton scattering. In Herwig and Jimmy the CT10 PDF is used and the ATLAS AUET2 tune [40] is employed for the parton shower and hadronization settings. In addition, the LO multileg generator ALPGEN v2.13 [41] interfaced to HERWIG is used where up to four additional partons in the matrix element are produced; the MLM [42] matching scheme is employed to avoid double counting of configurations generated by both the parton shower and the matrix-element calculation; the CTEQ6L1 [32] PDF set is employed; heavy-flavor quarks are included in the matrix-element calculations to produce the $t\bar{t} + b\bar{b}$ and $t\bar{t} + c\bar{c}$ processes; the overlap between the heavy-flavor quarks produced from the matrix-element calculations and from the parton shower is removed. For the evaluation of systematic uncertainties due to the parton showering and hadronization models, a PowHEG+HERWIG sample is compared to a PowHEG+PYTHIA sample. The uncertainties due to QCD initial- and final-state radiation (ISR and FSR) modeling are estimated with samples generated with AcerMC v3.8 [43], interfaced to PYTHIA for which the parton shower parameters are varied according to a measurement of the additional jet activity in $t\bar{t}$ events [44]. The tunes for samples used to describe $t\bar{t}$ production show a reasonable agreement over a broad range of observables and kinematic regions in $t\bar{t}$ events [45–47]. The electroweak corrections that are applied to the nominal PowHEG+PYTHIA sample are not applied to the other samples. The $t\bar{t}$ samples are normalized to the NNLO+NNLL cross-section² [6–11]: $\sigma_{t\bar{t}} = 253^{+13}_{-15}$ pb.

Leptonic decays of vector bosons produced in association with several high- p_T jets, referred to as $W+\text{jets}$ and $Z+\text{jets}$, constitute the largest background in this analysis. Samples of simulated $W/Z+\text{jets}$ events with up to five additional partons in the LO matrix elements are produced with the ALPGEN

² The top++2.0 [48] calculation includes the next-to-next-to-leading-order QCD corrections and resums next-to-leading logarithmic soft gluon terms. The quoted cross-section corresponds to a top quark mass of 172.5 GeV.

generator interfaced to PYTHIA for parton showering using the MLM matching scheme. Heavy-flavor quarks are included in the matrix-element calculations to produce the $Wb\bar{b}$, $Wc\bar{c}$, W_c , $Zb\bar{b}$, and $Zc\bar{c}$ processes. The overlap between the heavy-flavor quarks produced by the matrix element and by parton showering is removed. W +jets samples are normalized to the inclusive W boson NNLO cross-section [49, 50] and corrected by applying additional scale factors derived from data, as described in Sec. 5.

Single top quark production in the t -channel is simulated using the AcerMC generator, while production in the s -channel and the production of a top quark in association with a W boson are modeled with PowHEG [51–54]. Both generators are interfaced with PYTHIA using the CTEQ6L1 PDF set and the Perugia 2011 tune for parton shower modeling. The cross-sections multiplied by the branching ratios for the leptonic W decay employed for these processes are 28.4 pb (t -channel) [55], 22.4 pb (Wt production) [56], and 1.8 pb (s -channel) [57], as obtained from NLO+NNLL calculations.

Diboson production is modeled using SHERPA [58] with the CT10 PDF set and the yields are normalized to the NLO cross-sections [59].

4. Object definition and event selection

Jets are reconstructed using the anti- k_t algorithm [60] implemented in the FASTJET package [61] with radius parameter $R = 0.4$ or $R = 1.0$, respectively called small- R and large- R jets in the following, using as input calibrated topological clusters [62–64]. These clusters are assumed to be massless when computing the jet four-vectors and substructure variables. Large- R jets containing hadronically decaying top quarks are selected by applying jet substructure requirements, which exploit the fact that they contain several high- p_T objects and have a high mass, unlike most jets originating from the fragmentation of other quarks or gluons. The trimming algorithm [65] with parameters $R_{\text{sub}} = 0.3$ and $f_{\text{cut}} = 0.05$ is applied to large- R jets to mitigate the impact of initial-state radiation, underlying-event activity, and pileup. A correction for the number of additional pp interactions per bunch crossing is applied to small- R jets [66–69]. The p_T of small- R jets and large- R trimmed jets and the large- R jet mass, obtained from the four-momentum sum of all jet constituents, are calibrated using energy- and η -dependent correction factors. After this calibration, the p_T and mass of the jets in simulated events correspond on average to the ones of the corresponding particle-level jets, which are built from the stable particles produced by the MC event generator [70, 71]. Differences between the small- R jet response in data and MC simulation are evaluated from control samples and corresponding corrections are applied to data. Small- R jets are required to be in the fiducial region $|\eta| < 2.5$ and must have $p_T > 25$ GeV. The jet vertex fraction (JVF) is a measure of the fraction of the jet’s track momenta that originate from the primary vertex. It is computed as the summed p_T of all tracks matched to the jet and the primary vertex, divided by the summed p_T of all tracks matched to the jet. Small- R jets with $p_T < 50$ GeV and $|\eta| < 2.4$ are rejected when $\text{JVF} < 0.5$, to reduce the contribution of jets generated by pileup interactions.³ Trimmed large- R jets are considered for the analysis if $|\eta| < 2.0$ and $p_T > 300$ GeV. More details on the reconstruction and performance of highly boosted top quarks in ATLAS can be found in Ref. [71, 72].

Small- R jets containing a b -hadron are tagged using a neural-network-based algorithm (MV1) [73] that combines information from the track impact parameters, secondary vertex location, and decay

³ The jet is retained if no tracks are assigned to the jet.

topology inside the jets. The operating point corresponds to an overall 70% b -tagging efficiency in $t\bar{t}$ events, and to a probability to mistag light-flavor jets of approximately 1%.

Electron candidates are reconstructed as charged-particle tracks in the inner detector associated with energy deposits in the EM calorimeter. They must satisfy identification criteria based on the shower shape in the EM calorimeter, on track quality, and on the transition radiation observed in the TRT detector [74]. Electrons are required to be in the pseudorapidity region $|\eta| < 2.47$, excluding the transition region between the barrel and the endcap calorimeters ($1.37 < |\eta| < 1.52$). The EM clusters must have a transverse energy $E_T > 25$ GeV. The associated track must have a longitudinal impact parameter $|z_0| < 2$ mm with respect to the primary vertex, which is the vertex with the highest $\sum p_T^2$ of the associated tracks in the event.

Muon candidates are defined by matching track segments in the muon spectrometer with tracks in the inner detector. The track p_T is determined through a global fit of the track that takes into account the energy loss in the calorimeters [75]. The track is required to have a longitudinal impact parameter $|z_0| < 2$ mm, and a transverse impact parameter significance $|d_0/\sigma(d_0)| < 3$, indicating the track is consistent with originating from the hard-scattering vertex. Muons are required to have $p_T > 25$ GeV and be in the fiducial region $|\eta| < 2.5$.

Lepton candidates are required to be isolated to suppress background leptons originating from jets. The variable “mini-isolation” [76] is used. It is defined as $I_{\text{mini}} = \sum_{\text{tracks}} p_T^{\text{track}} / p_T^\ell$, where p_T^ℓ is the lepton transverse momentum and the sum is over all good-quality tracks (excluding the lepton track) that have $p_T > 0.4$ GeV and a distance from the lepton $\Delta R = \sqrt{(\Delta\eta)^2 + (\Delta\phi)^2} < K_T / p_T^\ell$. The parameter K_T is set to 10 GeV and the isolation requirement $I_{\text{mini}} < 0.05$ is applied for both the electrons and muons. An isolation cone that decreases in size with increasing p_T^ℓ improves the selection efficiency of the decay of high- p_T top quarks.

Since leptons deposit energy in the calorimeters, an overlap removal procedure is applied in order to avoid double counting of leptons and small- R jets. In order to improve the reconstruction efficiency in the highly boosted topology, the same overlap removal procedure as used in Ref. [20] has been adopted. First, jets close to electrons, with $\Delta R(e, \text{jet}_{R=0.4}) < 0.4$ are corrected by subtracting the electron four-vector from the jet four-vector and the JVF is recalculated after removing the electron track. The new e -subtracted jet is retained if it satisfies the jet selection criteria listed above, otherwise it is rejected. After this procedure, electrons that lie within $\Delta R(e, \text{jet}_{R=0.4}) = 0.2$ from a small- R jet are removed and their four-momentum added back to that of the jet. The muon–jet overlap removal procedure removes muons that fall inside a cone of size $\Delta R(\mu, \text{jet}_{R=0.4}) < 0.04 + 10 \text{ GeV}/p_{T,\mu}$ around a small- R jet axis.

The missing transverse momentum E_T^{miss} is the magnitude of the vector sum of the transverse energy of all calorimeter cells [77]. Their energy is corrected on the basis of the associated physics object. The contribution of muons is added using their transverse momentum obtained from the tracking system and the muon spectrometer.

The event selection proceeds as follows. Each event must have a reconstructed primary vertex with five or more associated tracks with $p_T > 0.4$ GeV. The events are required to contain exactly one reconstructed lepton candidate with $p_T > 25$ GeV. The transverse mass of the lepton and E_T^{miss} is defined as $m_T^W = \sqrt{2p_T^\ell E_T^{\text{miss}}(1 - \cos\Delta\phi)}$, where $\Delta\phi$ is the azimuthal angle between the lepton and E_T^{miss} . Events are retained if $E_T^{\text{miss}} > 20$ GeV and $E_T^{\text{miss}} + m_T^W > 60$ GeV to suppress QCD multijet events.

The selection exploits the fact that the highly boosted top quark decay products tend to be collimated. Therefore events are selected by requiring the presence of at least one small- R jet close to the lepton ($\Delta R(\ell, \text{jet}_{R=0.4}) < 1.5$) and the existence of a reconstructed large- R trimmed jet with mass $m_{\text{jet}} > 100$ GeV. To improve the rejection of background jets, originating from light quarks or gluons, a cut on the k_t splitting scale [68, 69] of the large- R jets is made. The k_t splitting scale is calculated by reclustering the large- R jet with the k_t -clustering algorithm, and taking the k_t distance between the two subjets of the final clustering step to be $\sqrt{d_{12}} = \min(p_{T1}, p_{T2})\Delta R_{12}$, where p_{T1} and p_{T2} are the transverse momenta of the two subjets and ΔR_{12} is the distance between them. It is expected to have large values for jets containing two hard subjets, as expected in the decay of massive objects. Events are selected if the large- R jet has $\sqrt{d_{12}} > 40$ GeV. The large- R jet must be well separated from the lepton ($\Delta\phi(\ell, \text{jet}_{R=1.0}) > 2.3$) and from the small- R jet associated with the lepton ($\Delta R(\text{jet}_{R=1.0}, \text{jet}_{R=0.4}) > 1.5$). The leading- p_T trimmed large- R jet satisfying these requirements is referred to as the *top-jet* candidate. Finally, at least one of the two top quark candidates must be b -tagged. This implies that either the highest- p_T small- R jet close to the lepton ($\Delta R(\ell, \text{jet}_{R=0.4}) < 1.5$) or at least one small- R jet close to the large- R jet ($\Delta R(\text{jet}_{R=1.0}, \text{jet}_{R=0.4}) < 1.0$) is b -tagged⁴.

The event selection is summarized in Table 1. After these requirements the data sample contains 4145 and 3603 events in the electron channel and muon channel, respectively, of which $\approx 85\%$ are expected to be semileptonic $t\bar{t}$ events.

5. Background estimation

After the event selection the background is composed primarily, in order of importance, of W +jets, $t\bar{t}$ dilepton, single top, and QCD multijet events. The W +jets background is obtained from MC simulation with normalization and heavy-flavor content adjusted in data control regions. The $t\bar{t}$ dilepton background is determined as a fraction of the full $t\bar{t}$ sample predicted by MC simulation. QCD multijet events are estimated with a fully data-driven method. Single top production as well as minor backgrounds (Z +jets and diboson) are determined from MC simulation normalized to the best available theoretical calculation of their cross-sections.

The W +jets background estimate uses as a starting point the ALPGEN+PYTHIA samples normalized to the inclusive W boson NNLO cross-section. The normalization and heavy-flavor fraction of the W +jets background have large theoretical uncertainties, and are then determined from data. The overall W +jets normalization is obtained by exploiting the expected charge asymmetry in the production of W^+ and W^- bosons at a pp collider [12, 78]. This asymmetry is predicted precisely by theory, and other processes in the $t\bar{t}$ sample are symmetric in charge except for a small contamination from single top and WZ events, which is corrected by MC simulation. The total number of W +jets events in the sample can thus be estimated with the following equation:

$$N_{W^+} + N_{W^-} = \left(\frac{r_{\text{MC}} + 1}{r_{\text{MC}} - 1} \right) (D_+ - D_-), \quad (1)$$

where r_{MC} is the ratio of the number of events with positive leptons to the number with negative leptons in the MC simulation, and D_+ and D_- are the number of events with positive and negative leptons in the data, respectively. The signal sample has too few events to apply Eq. (1) directly. Instead

⁴ The reconstruction of a large- R jet does not prevent the reconstruction of small- R jets overlapping with it.

Cut	Detector level		Particle level
	$e + \text{jets}$	$\mu + \text{jets}$	
Leptons	$ z_0 < 2 \text{ mm}$ $I_{\text{mini}} < 0.05$ $ \eta < 1.37 \text{ or } 1.52 < \eta < 2.47$ $p_T > 25 \text{ GeV}$	$ z_0 < 2 \text{ mm} \text{ and } d_0/\sigma(d_0) < 3$ $I_{\text{mini}} < 0.05$ $ \eta < 2.5$ $p_T > 25 \text{ GeV}$	$ \eta < 2.5$ $p_T > 25 \text{ GeV}$
Anti- $k_t R = 0.4$ jets	$p_T > 25 \text{ GeV}$ $ \eta < 2.5$ JVF > 0.5 (if $p_T < 50 \text{ GeV}$ and $ \eta < 2.4$)		$ \eta < 2.5$ $p_T > 25 \text{ GeV}$
Overlap removal	if $\Delta R(e, \text{jet}_{R=0.4}) < 0.4$: $\text{jet}'_{R=0.4} = \text{jet}_{R=0.4} - e$ if $\Delta R(e, \text{jet}'_{R=0.4}) < 0.2$: e removed and $\text{jet}''_{R=0.4} = \text{jet}'_{R=0.4} + e$	if $\Delta R(\mu, \text{jet}'_{R=0.4}) < 0.04 + 10 \text{ GeV}/p_T(\mu)$: μ removed	None
E_T^{miss}, m_T^W	$E_T^{\text{miss}} > 20 \text{ GeV}, E_T^{\text{miss}} + m_T^W > 60 \text{ GeV}$		
Leptonic top	At least one anti- $k_t R = 0.4$ jet with $\Delta R(\ell, \text{jet}_{R=0.4}) < 1.5$		
Hadronic top	The leading- p_T trimmed anti- $k_t R = 1.0$ jet has: $p_T > 300 \text{ GeV}, m > 100 \text{ GeV}, \sqrt{d_{12}} > 40 \text{ GeV}$ $\Delta R(\text{jet}_{R=1.0}, \text{jet}_{R=0.4}) > 1.5, \Delta\phi(\ell, \text{jet}_{R=1.0}) > 2.3$		
b -tagging	At least one of: 1) the leading- p_T anti- $k_t R = 0.4$ jet with $\Delta R(\ell, \text{jet}_{R=0.4}) < 1.5$ is b -tagged 2) at least one anti- $k_t R = 0.4$ jet with $\Delta R(\text{jet}_{R=1.0}, \text{jet}_{R=0.4}) < 1.0$ is b -tagged		

Table 1: Summary of event selections for detector-level and MC-generated particle-level events described in Secs. 4 and 8.2, respectively.

a sample enhanced in $W+\text{jets}$ events is obtained by removing the b -tagging, $\Delta\phi(\text{jet}_{R=1.0}, \ell)$, jet mass, and $\sqrt{d_{12}}$ requirements. The heavy-flavor fraction scale factors correct for potential mismodeling in the generator of the fractions of W production associated with different flavor components ($W + b\bar{b}$, $W + c\bar{c}$, $W + c$). They are estimated in a sample with the same lepton and E_T^{miss} selections as the signal selection, but with only two small- R jets and no b -tagging requirements. The b -jet multiplicity, in conjunction with knowledge of the b -tagging and mistag efficiency, is used to extract the heavy-flavor fraction in this sample. A common scale factor is used for the $W + b\bar{b}$ and $W + c\bar{c}$ components. This information is extrapolated to the signal region using the MC simulation, assuming constant relative rates for the signal and control regions. The overall normalization and heavy-flavor scale factors are extracted iteratively because the various flavor components have different charge asymmetries. After correction the $W+\text{jets}$ events are expected to make up approximately 5% of the total events in the signal region.

QCD multijet events can mimic the lepton+jets signature. This background is estimated directly from data by using the matrix-method technique [79]. A sample enhanced in fake leptons, i.e., nonprompt leptons or jets misidentified as prompt leptons, is obtained by loosening the lepton identification

requirements. The number of events with fake leptons in the signal region can be predicted as:

$$N_{\text{multijet}} = \frac{(\epsilon - 1) f}{\epsilon - f} N_T + \frac{\epsilon f}{\epsilon - f} N_L,$$

where ϵ and f are the efficiencies for leptons that passed the loose selections to also pass the tight (signal) selections, for real and fake leptons respectively, N_T is the number of events with a tight lepton, and N_L is the number of events with a loose lepton that failed the tight cuts. The efficiency f is measured using data in fake-lepton-enhanced control regions and ϵ is extracted from MC simulation and validated in data. QCD multijet events contribute to the total event yield at approximately the percent level.

Top quark pair events with both the top and antitop quarks decaying leptonically (including decays to τ) can sometimes pass the event selection, contributing approximately 5% of the total event yield, and are treated as background in the analysis. The fraction of dileptonic $t\bar{t}$ events in each p_T bin is estimated using the same MC sample used to model the signal.

6. Systematic uncertainties

Systematic uncertainties, which arise from object reconstruction and calibration, MC generator modeling, and background estimation, are described below. The propagation of systematic uncertainties through the unfolding procedure is described in Sec. 8.4.

6.1. Detector modeling

The uncertainty on the large- R jet energy scale (JES), jet mass scale (JMS), and k_t splitting scale is obtained using two different data-driven methods. For $p_T > 800$ GeV for JES, and for all p_T for the JMS and k_t splitting scale, the ratio of the large- R jets kinematic variables reconstructed from the calorimeter clusters to those from inner-detector tracks is compared between data and MC simulation. For $p_T < 800$ GeV for JES, the p_T of large- R jets are compared to the well-calibrated p_T of photons in a large sample of photon+jets events. An additional MC-based uncertainty, referred to as large- R JES topology uncertainty, is included to reflect the fact that the jets in these calibration samples have a different response (gluon or light-quark jets) than those in $t\bar{t}$ events (top-jets). The full difference between the response to these two types of jets is conservatively assigned as the corresponding systematic uncertainty. The uncertainty on the large- R jet energy resolution (JER) is determined by smearing the jet energy such that the resolution is degraded by 20% [80, 81] and evaluating the effect on the final result. The same smearing procedure is applied to determine the uncertainty due to the large- R jet mass resolution (JMR). The uncertainties on the large- R jets JES are the dominant contribution to the total uncertainty of this measurement, in particular the topology and photon+jet calibration uncertainties.

The small- R jet energy scale uncertainty is derived using a combination of simulations, test beam data, and *in situ* measurements [63, 70, 82]. Additional contributions from the jet flavor composition, calorimeter response to different jet flavors, and pileup are taken into account. Uncertainties in the jet energy resolution are obtained with an *in situ* measurement of the jet p_T balance in dijet events [83].

The efficiency to tag b -jets and mistag light jets is corrected in Monte Carlo events by applying b -tagging scale factors, extracted in $t\bar{t}$ and dijet samples, that compensate for the residual difference between data and simulation. The associated systematic uncertainty is computed by varying the scale factors within their uncertainty [84–86]. The b -jet calibration is performed for jets with p_T up to 300 GeV; for larger transverse momenta an additional MC-based extrapolation uncertainty is applied, which ranges from approximately 10% to 30%, increasing with b -jet p_T from 300 GeV to 1200 GeV.

The lepton reconstruction efficiency in simulation is corrected by scale factors derived from measurements of these efficiencies in data using $Z \rightarrow \ell^+ \ell^-$ enriched control regions. The lepton trigger and reconstruction efficiency scale factors, energy scale, and energy resolution are varied within their uncertainties [75, 87].

The uncertainty associated with E_T^{miss} is calculated by propagating the energy scale and resolution systematic uncertainties on all physics objects to the E_T^{miss} calculation. Additional E_T^{miss} uncertainties arising from energy deposits not associated with any reconstructed objects are also included [77].

The uncertainty on the integrated luminosity is $\pm 2.8\%$ and is derived following a methodology similar to that defined in Ref. [23].

6.2. Signal and background modeling

The $t\bar{t}$ parton shower and hadronization uncertainty is computed by comparing the results obtained with PowHEG+PYTHIA (without electroweak corrections applied) and PowHEG+HERWIG. The $t\bar{t}$ generator uncertainty is evaluated by taking the difference between the results obtained with PowHEG+HERWIG and MC@NLO+HERWIG. Both uncertainties are symmetrized. The procedure to compute the PDF uncertainty on the signal is based on the PDF4LHC recommendations [88] using the MC@NLO+HERWIG sample with three different PDF sets (CT10 [29], MSTW [89] and NNPDF [90]). An intra-PDF uncertainty is obtained for each PDF set by following its respective prescription while an inter-PDF uncertainty is computed as the envelope of the three intra-PDF uncertainties. The modeling of ISR and FSR is evaluated separately using dedicated ACERMC + PYTHIA samples with variation of the PYTHIA parameters for QCD radiation.

The W +jets shape uncertainty is extracted by varying the renormalization and matching scales in ALPGEN. The W +jets MC statistical uncertainty is also computed and its contribution to the cross-section uncertainty increases with the top-jet candidate p_T from approximately 1% to 6%. A new set of W +jets normalization and heavy-flavor scale factors is extracted for each variation of the most important detector modeling uncertainties, allowing their correlated effect on the W +jets background, $t\bar{t}$ signal and background, and other MC-based background processes to be assessed.

The uncertainty on the fake-lepton background is determined by varying the definition of loose leptons, changing the selection used to form the fake-enhanced control region, and propagating the statistical uncertainty of parameterizations of the efficiency and the fake rate.

The single-top background is assigned an uncertainty associated with the theory calculations used for its normalization [55–57]. A generator uncertainty is included for the Wt channel, which provides the largest single-top contribution, by taking the difference between the yields predicted by PowHEG and MC@NLO. An uncertainty on the interference between the $t\bar{t}$ and Wt processes is also included. A conservative uncertainty of 50% is applied to the normalization of the subdominant Z +jets and diboson backgrounds.

7. Data and MC comparison at detector level

Table 2 gives the number of observed and expected events for each process, where the systematic uncertainties on the background estimates, objects' energy scales and reconstruction efficiencies, and MC statistics are taken into account. The prediction is generally found to overestimate the data by approximately one standard deviation.

	$e+\text{jets}$	$\mu+\text{jets}$
$t\bar{t} \ell+\text{jets}$	3880 ± 430	3420 ± 380
$t\bar{t}$ dilepton	199 ± 27	169 ± 24
$W+\text{jets}$	235 ± 54	226 ± 50
Single top	133 ± 22	134 ± 29
Multijet	91 ± 17	3 ± 1
$Z+\text{jets}$	34 ± 18	14 ± 8
Dibosons	22 ± 12	18 ± 10
Prediction	4600 ± 470	3980 ± 410
Data	4145	3603

Table 2: Observed and expected number of events in the signal $e+\text{jets}$ and $\mu+\text{jets}$ samples. The systematic uncertainties include the background estimation techniques, objects' energy scales and reconstruction efficiencies, and MC statistics.

Agreement of the data with the prediction is further tested by studying the distributions of several variables of interest in Fig. 1. The systematic uncertainties on the objects' energy scales and reconstruction efficiencies, on the background estimates, luminosity and MC statistics are shown. While the prediction generally overestimates the data, as already seen in Table 2, the simulation reproduces the observed shapes in most cases. Exceptions include the tails of some kinematic variables such as the top-jet candidate p_{T} . The distribution of the top-jet candidate p_{T} constitutes the input to the unfolding procedure and is studied in more detail in the following sections.

8. Differential cross-section determination

Differential cross-sections are measured as a function of the p_{T} of the top-jet candidate at particle level and the p_{T} of the top quark at parton level. The electron and muon channels are first combined into a $\ell+\text{jets}$ sample at the detector level. The detector-level p_{T} spectrum is corrected for detector inefficiencies and finite resolution to obtain particle- and parton-level differential cross-sections. The particle-level measurement is performed in a specific fiducial region of phase space close to the event selection. The systematic and statistical uncertainties are propagated through the unfolding procedure. Finally a covariance matrix is computed to perform a quantitative comparison of the measured cross-sections with MC predictions.

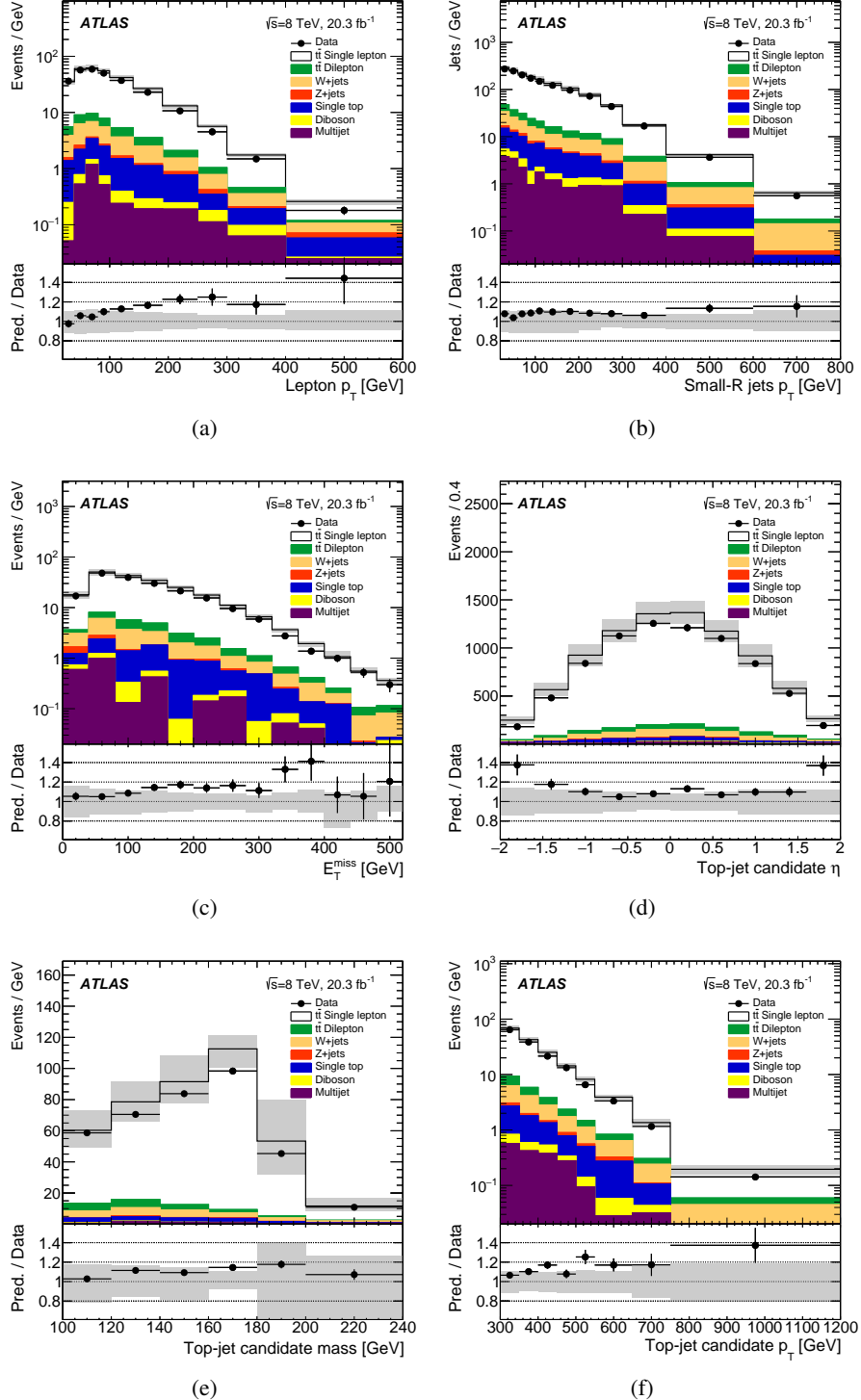


Figure 1: Distributions of (a) transverse momentum p_T of the lepton candidates, (b) p_T of selected small- R jets, (c) missing transverse momentum E_T^{miss} , (d) and pseudorapidity η , (e) mass and (f) p_T of the leading selected anti- k_t $R=1.0$ jets for the $\ell+\text{jets}$ channel. The $t\bar{t}$ prediction is obtained using the nominal POWHEG+PYTHIA sample. The ratio of the MC prediction to the data is shown in the insets below the histograms. The hashed area includes all the object-related uncertainties (on the jet, lepton, and E_T^{miss}), and the uncertainties from the background estimation, luminosity and MC statistics. The vertical lines indicate the data statistical uncertainty.

8.1. Combination of decay channels

The e -jets and μ -jets selections are combined into a ℓ -jets sample at the detector level. The combined ℓ -jets signal and background samples take into account the efficiencies of the two selections. This procedure is well motivated given that the relative yields of the two channels agree well between data and MC simulation, as shown in Table 2. The combination method is cross-checked by performing the unfolding in each channel individually to the ℓ -jets phase space described in Sec. 8.2 and comparing these alternative cross-section estimates with the one based on the combined data. The final results are found to be consistent.

8.2. Particle- and parton-levels fiducial region definitions

Particle-level corrections to the data are derived from leptons and jets in simulated $t\bar{t}$ events that are constructed using stable particles, with a mean lifetime greater than 0.3×10^{-10} seconds, which result directly from the hard-scattering pp interaction or from subsequent decays of particles with a shorter lifetime.

All leptons ($e, \mu, \nu_e, \nu_\mu, \nu_\tau$) not from hadron decays are considered as prompt isolated leptons. The leptons from τ decays are accepted only if the parent τ is not a hadron decay product itself. The four-momenta of photons within a cone of $\Delta R = 0.1$ around the electron or muon direction are added to those of the leptons (dressed leptons). Both the small- R and large- R jets are reconstructed using all stable particles except for the selected dressed leptons. The trimming procedure applied to detector-level jets is also applied to particle-level jets. A small- R jet with $p_T > 25$ GeV and $|\eta| < 2.5$ is considered to be “ b -tagged” if there exists at least one b -hadron with $p_T > 5$ GeV clustered in the jet.⁵

The missing transverse momentum E_T^{miss} is the magnitude of the vector sum of the momenta of neutrinos not resulting from hadron decays.

To minimize the theoretical input to the measurement, the fiducial region is chosen to follow the detector-level event selections closely, including the kinematic requirements on the objects and the requirements on the event topology. In contrast to the detector-level selection, no overlap removal procedure is applied to the leptons and jets, and no isolation requirement is imposed on the leptons. Using the particle-level objects defined above, the fiducial region is defined by requiring:

- Exactly one lepton (electron or muon) with $p_T > 25$ GeV, $|\eta| < 2.5$.
- $E_T^{\text{miss}} > 20$ GeV and $E_T^{\text{miss}} + m_T^W > 60$ GeV.
- At least one small- R jet with $p_T > 25$ GeV, $|\eta| < 2.5$, and a distance $\Delta R < 1.5$ from the lepton. If there is more than one such jet, the one with the largest p_T is considered to be the leptonic b -jet candidate (the b -jet associated to the leptonic top quark decay).
- At least one trimmed large- R jet with $p_T > 300$ GeV, mass > 100 GeV, $\sqrt{d_{12}} > 40$ GeV, and $|\eta| < 2$, well separated from both the lepton ($\Delta\phi > 2.3$) and the leptonic b -jet candidate ($\Delta R > 1.5$). The jet mass is reconstructed from the four-vector sum of the particles constituting the jet.

⁵ The b -hadrons are not stable and do not contribute to the total four-vector of the jet, only their decay products do. However, they are clustered with their energy set to a negligible value to check that they match the jet geometrically [66].

If more than one large- R jet satisfies these criteria, the one with largest p_T is chosen. The jet passing this selection is referred to as the particle-level top-jet candidate.

- At least one b -tagged small- R jet such that $\Delta R(\text{jet}_{R=1.0}, \text{jet}_{R=0.4}) < 1$ and/or the leptonic b -jet candidate is b -tagged.

The particle-level event selection is summarized in Table 1. Fiducial particle-level corrections are determined by using only simulated $t\bar{t}$ events in which exactly one of the W bosons, resulting from the decay of the $t\bar{t}$ pair, decays to an electron or a muon either directly or through a τ lepton decay. All other $t\bar{t}$ events are not used. The cross-section is then determined as a function of the particle-level top-jet candidate transverse momentum, $p_{T,\text{ptcl}}$.

For the parton level, the top quark that decays to a hadronically decaying W boson is considered just before the decay and after QCD radiation, selecting events in which the momentum of such a top quark, $p_{T,\text{parton}}$, is larger than 300 GeV. Parton-level corrections are determined by using only simulated $t\bar{t}$ events in which exactly one of the W boson decays to an electron or a muon or a τ lepton (including hadronic τ decays). The correction to the full parton-level phase space defined above is obtained by accounting for the branching ratio of $t\bar{t}$ pairs to the $\ell+\text{jets}$ channel.

8.3. Unfolding to particle and parton levels

The procedure to unfold the distribution of $p_{T,\text{reco}}$, the p_T of the detector-level leading- p_T trimmed large- R jet, to obtain the differential cross-section as a function of $p_{T,\text{ptcl}}$ is composed of several steps, outlined in:

$$\begin{aligned} \frac{d\sigma_{t\bar{t}}}{dp_{T,\text{ptcl}}} (p_{T,\text{ptcl}}^i) &= \frac{N_{\text{ptcl}}^i}{\Delta p_{T,\text{ptcl}}^i \mathcal{L}} \\ &= \frac{1}{\Delta p_{T,\text{ptcl}}^i \mathcal{L} f_{\text{ptcl!reco}}^i} \cdot \sum_j M_{ij}^{-1} f_{\text{reco!ptcl}}^j f_{t\bar{t},\ell+\text{jets}} (N_{\text{reco}}^j - N_{\text{reco,bgnd}}^j), \end{aligned} \quad (2)$$

where N_{reco}^j is the number of observed events in bin j of $p_{T,\text{reco}}$ with the detector-level selection applied, N_{ptcl}^i is the total number of events in bin i of $p_{T,\text{ptcl}}$ that meet the fiducial region selection, $\Delta p_{T,\text{ptcl}}^i$ is the size of bin i of $p_{T,\text{ptcl}}$, and \mathcal{L} is the integrated luminosity of the data sample. The corrections that are applied to $p_{T,\text{reco}}$ are all extracted from the nominal PowHEG+PYTHIA $t\bar{t}$ sample.

First, the non- $t\bar{t}$ background contamination, $N_{\text{reco,bgnd}}^j$, is subtracted from the observed number of events in each $p_{T,\text{reco}}$ bin. The contribution from non- $\ell + \text{jets}$ $t\bar{t}$ events is taken into account by the multiplicative correction $f_{t\bar{t},\ell+\text{jets}}$, which represents the fraction of $\ell+\text{jets}$ $t\bar{t}$ events extracted from the nominal PowHEG+PYTHIA $t\bar{t}$ sample.

In a second step the correction factor $f_{\text{reco!ptcl}}^j$, also referred to as acceptance correction, corrects the $p_{T,\text{reco}}$ spectrum for the $t\bar{t}$ events that pass the detector-level selection but fail the particle-level selection. For each $p_{T,\text{reco}}$ bin j , $f_{\text{reco!ptcl}}^j$ is defined as the ratio of the number of events that meet both the detector-level and particle-level selections to the number of events that satisfy the detector-level selection. The distribution of the acceptance correction $f_{\text{reco!ptcl}}^j$ is shown in Fig. 2(a) for various MC generators.

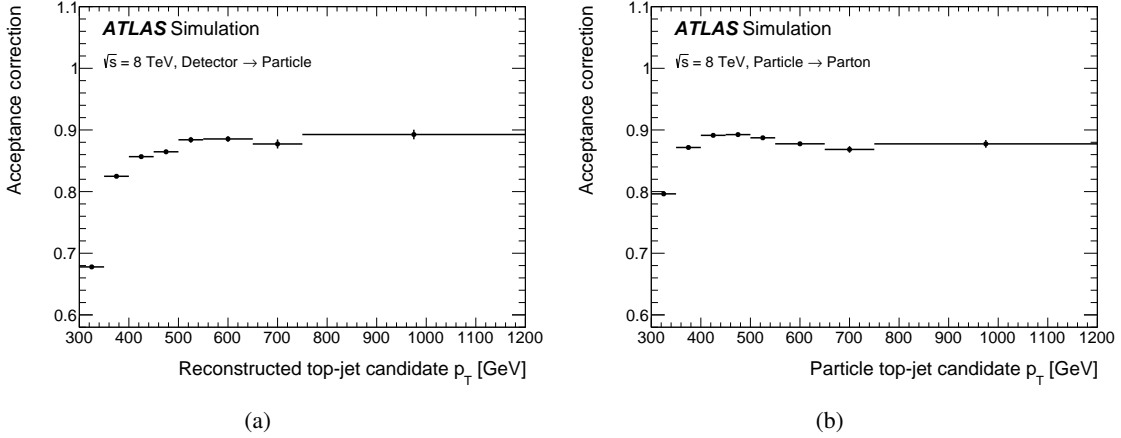


Figure 2: (a) Distribution of the correction factor $f_{\text{reco!ptcl}}$ as a function of $p_{T,\text{reco}}$. It represents the ratio of the number of events that meet both the detector-level and particle-level to the number of events that satisfy the detector-level selection requirements. (b) Distribution of the correction factor $f_{\text{ptcl!parton}}$ as a function of $p_{T,\text{ptcl}}$. It represents the ratio of the number of events that meet both the parton-level and particle-level to the number of events that satisfy only the particle-level selection requirements.

The third step corrects for detector resolution effects. A migration matrix is constructed to correlate the $p_{T,\text{reco}}$ -binned distribution to the $p_{T,\text{ptcl}}$ distribution. The matrix M_{ij} represents the probability for an event with $p_{T,\text{ptcl}}$ in bin i to have a $p_{T,\text{reco}}$ in bin j . This matrix is shown in Fig. 3(a). It shows that approximately 50% to 85% of events have values of $p_{T,\text{ptcl}}$ and of $p_{T,\text{reco}}$ that fall in the same bin.

The inversion of the migration matrix to correct $p_{T,\text{reco}}$ to the particle level is carried out by an unfolding scheme based on Tikhonov regularization which is implemented through the singular value decomposition (SVD) of the matrix [91]. This scheme is chosen to reduce sizable statistical fluctuations that are introduced by instabilities in the inversion procedure. The unfolding regularization parameter, which characterizes the size of the expansion of the solution to the inversion problem, is optimized according to the procedure described in Ref. [91]. In parallel the bin size for the $p_{T,\text{ptcl}}$ (and $p_{T,\text{reco}}$) distribution is optimized such that systematic uncertainties are larger than statistical uncertainties in each bin, and such that the width of each bin corresponds to at least one and a half times the expected resolution in that bin. The former requirement is introduced to minimize statistical fluctuations when estimating systematic uncertainties. The typical expected fractional resolution for $p_{T,\text{reco}}$ in $t\bar{t}$ simulated events ranges from 7% to 3% for $p_{T,\text{reco}}$ values between 250 GeV and 1.2 TeV. Finally, the optimization requires the unfolding to be unbiased, i.e., that a given input $p_{T,\text{ptcl}}$ spectrum is recovered on average by the unfolding procedure. After rounding to the nearest 50 GeV, this procedure results in bin widths of 50 GeV between 300 GeV and 550 GeV, 100 GeV between 550 GeV and 750 GeV, while the last bin spans 750 GeV to 1200 GeV. Just one event with reconstructed $p_T = 1535$ GeV falls outside this region in the $\mu + \text{jets}$ sample, and none in the $e + \text{jets}$ sample.

The fourth step is to apply a bin-by-bin correction factor $f_{\text{ptcl!reco}}^i$, also referred to as efficiency correction, which restores the contribution of $t\bar{t}$ events that fulfill the particle-level selection but not the detector-level selection. This factor is defined as the ratio of the number of events that satisfy both the particle-level and detector-level selections to the number that meet the selection at particle level only. The distribution of the efficiency correction $f_{\text{ptcl!reco}}^i$ is shown in Fig. 4(a).

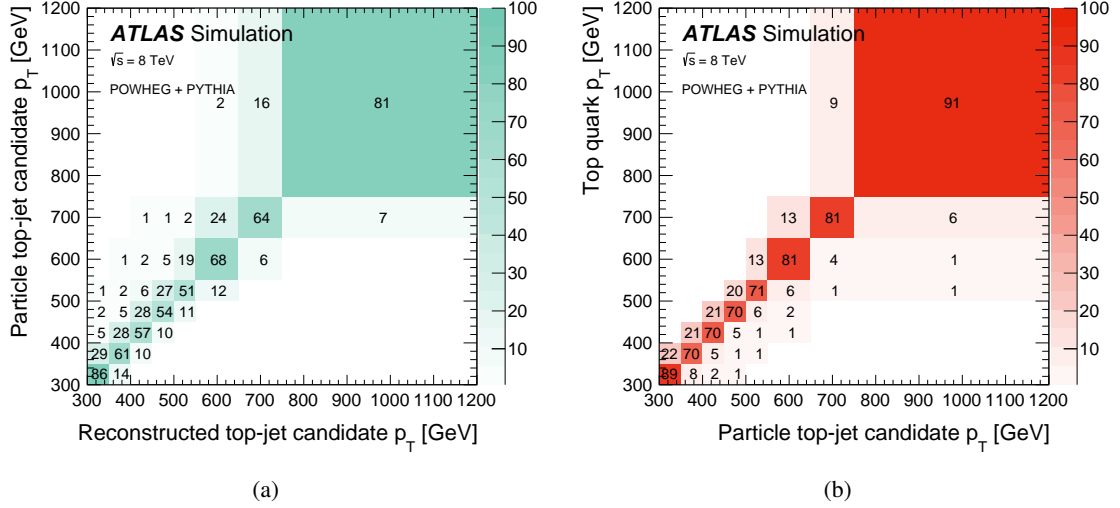


Figure 3: (a) Migration matrix between the particle-level $p_{T,\text{ptcl}}$ and reconstructed detector-level $p_{T,\text{reco}}$. (b) Migration matrix between the generated $p_{T,\text{parton}}$ and the particle-level $p_{T,\text{ptcl}}$. The unit of the matrix elements is the probability (expressed in percentage) for an event generated at a given value to be reconstructed at another value (each row adds up to 100%).

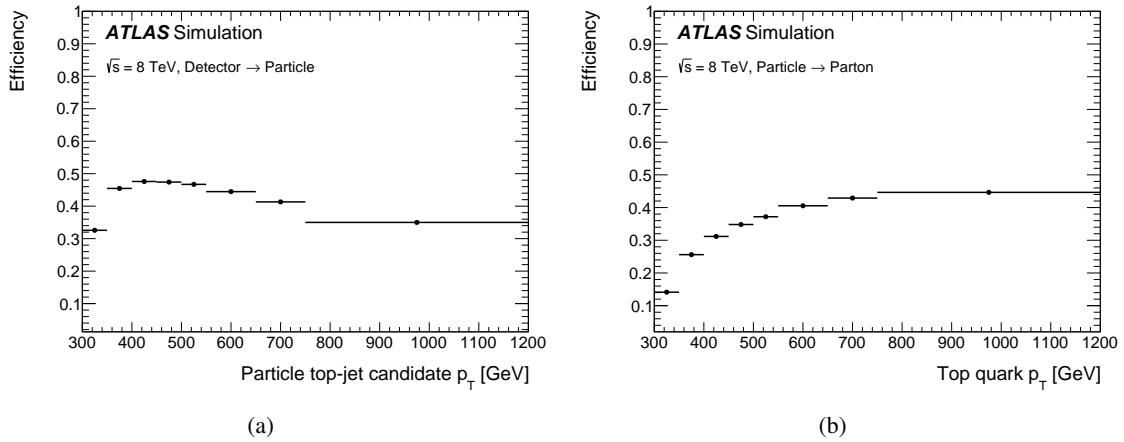


Figure 4: (a) Distribution of the correction factor $f_{\text{ptcl!reco}}$ as a function of $p_{T,\text{ptcl}}$. It represents the ratio of events that meet both the particle-level and detector-level to those that satisfy the particle-level selection requirements. (b) Distribution of the correction factor $f_{\text{parton!ptcl}}$ as a function of $p_{T,\text{parton}}$. It represents the ratio of events that meet both the parton-level and particle-level to those that satisfy the parton-level selection requirements.

The ability of the full correction procedure to recover a distribution that is significantly different from the nominal $t\bar{t}$ sample is tested. Simulated $t\bar{t}$ events are reweighted such that the $p_{T,\text{reco}}$ distribution matches the data. The corresponding $p_{T,\text{ptcl}}$ spectrum of the distorted $p_{T,\text{reco}}$ input spectrum is recovered with subpercent accuracy after unfolding.

The differential cross-section as a function of $p_{T,\text{parton}}$ is then derived according to:

$$\begin{aligned} \frac{d\sigma_{t\bar{t}}}{dp_{T,\text{parton}}}(p_{T,\text{parton}}^k) &= \frac{N_{\text{parton}}^k}{\mathcal{B}\Delta p_{T,\text{parton}}^k \mathcal{L}} \\ &= \frac{1}{\mathcal{B}\Delta p_{T,\text{parton}}^k \mathcal{L} f_{\text{parton!ptcl}}^k} \cdot \sum_j \hat{M}_{jk}^{-1} f_{\text{ptcl!parton}}^j N_{\text{ptcl}}^j. \end{aligned} \quad (3)$$

Similarly to Eq. (2), N_{ptcl}^j is the total number of events in bin j of $p_{T,\text{ptcl}}$ that enter the particle-level fiducial region described in Sec. 8.2, N_{parton}^k is the number of events in bin k of $p_{T,\text{parton}}$ in the full phase space, $\Delta p_{T,\text{parton}}^k$ is the size of bin k of the parton-level $p_{T,\text{parton}}$ (and of $p_{T,\text{ptcl}}$), \mathcal{L} is the total integrated luminosity of the data sample, and $\mathcal{B}=0.438$ [92] is the branching ratio for $t\bar{t}$ events with exactly one of the W bosons, from the decay of the $t\bar{t}$ pair, decaying to an electron or a muon or a τ lepton.

The corrections that are applied to the $p_{T,\text{ptcl}}$ variable are derived following steps similar to the ones described to derive $d\sigma_{t\bar{t}}/dp_{T,\text{ptcl}}$. They are also extracted from the nominal PowHEG+PYTHIA $t\bar{t}$ sample. First, the factor $f_{\text{ptcl!parton}}^j$ corrects the $p_{T,\text{ptcl}}$ spectrum for the $t\bar{t}$ events that pass the particle-level selection but fail the parton-level selection, shown in Fig. 2(b). Effects relating $p_{T,\text{parton}}$ to $p_{T,\text{ptcl}}$ are corrected with the same matrix unfolding procedure used for detector effects. This migration matrix \hat{M}_{jk} is shown in Fig. 3(b). A final correction factor $f_{\text{parton!ptcl}}^k$ is applied in bins of $p_{T,\text{parton}}$ to correct the result from the particle level to the partonic phase space, shown in Fig. 4(b).

To test the two-step derivation, the cross-section is also obtained by directly correcting the reconstructed distribution to parton level in a single step. The results are found to be consistent.

8.4. Propagation of statistical and systematic uncertainties

The propagation of statistical and systematic uncertainties is performed in the same way for both the particle-level and parton-level results. The impact of the data statistical uncertainty is evaluated by performing 1000 pseudoexperiments in which independent Poisson fluctuations in each $p_{T,\text{reco}}$ bin are assumed. The statistical uncertainty due to the limited size of the signal and background MC samples used to correct the data are estimated by performing 1000 pseudoexperiments using the bootstrap method [93], which builds 1000 statistically connected (co-varied) replicas of individual simulated signal or background spectra and derives the associated corrections.

For each systematic uncertainty arising from detector modeling, background modeling, and the electroweak correction factor, a varied $p_{T,\text{reco}}$ distribution is obtained and unfolded using corrections extracted from the nominal signal and background samples. The correlation between each systematic uncertainty's effect on the signal and background spectra is taken into account. For the $t\bar{t}$ generator,

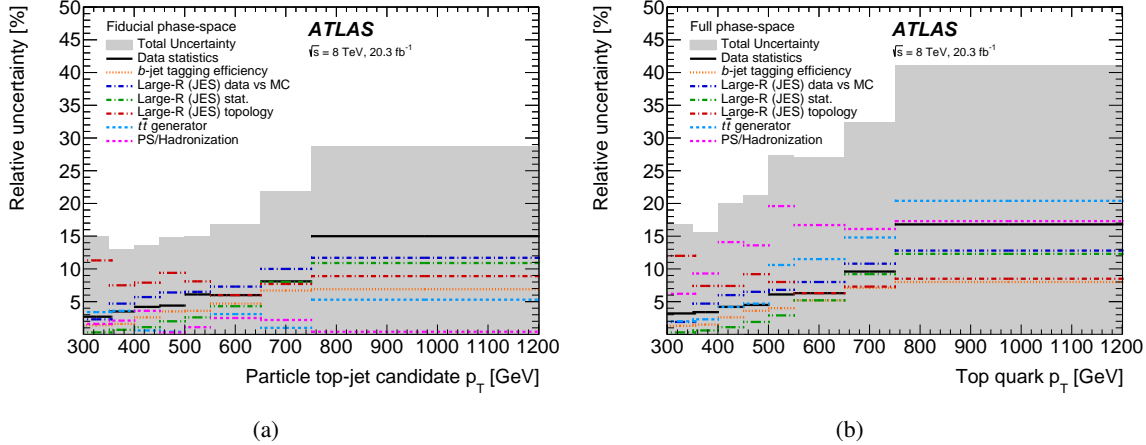


Figure 5: Relative uncertainties on (a) the particle-level differential cross section $d\sigma_{t\bar{t}}/dp_{T,\text{ptcl}}^i$ and (b) the parton-level differential cross section $d\sigma_{t\bar{t}}/dp_{T,\text{parton}}^i$. The total uncertainty (band) is shown along with the effect of the dominant uncertainties. The components “Large- R (JES) stat.” and “Large- R (JES) data vs MC” are, respectively, the statistical uncertainty and the systematic uncertainty associated with the difference in jet response between data and MC simulation when balancing p_T in photon+jet events.

parton shower, and ISR/FSR uncertainties, a systematic uncertainty variation is defined as the difference between the generated and unfolded cross-section of a given generator, with unfolding corrections extracted with an alternative generator (or alternative generator setting). The PDF uncertainty is computed by unfolding the nominal sample with correction factors extracted by reweighting the nominal sample at the hard-process level for each variation of the PDF.

Figure 5 shows the effect of the statistical and systematic uncertainties on $d\sigma_{t\bar{t}}/dp_{T,\text{ptcl}}^i$ and $d\sigma_{t\bar{t}}/dp_{T,\text{parton}}^i$. The total uncertainty generally increases with the measured p_T and ranges from 13% to 29% for the particle-level cross-section, and from 15% to 41% for the parton-level cross-section. The dominant uncertainty for the particle-level cross-section is the large- R jet energy scale, in particular its components due to the topology uncertainty at low p_T and the uncertainty from p_T balance in photon+jet events at high p_T . The experimental uncertainties have a comparable size at parton level. However, the reported parton-level cross-section has significantly larger systematic uncertainties than the particle-level cross-section since it is affected by larger $t\bar{t}$ modeling uncertainties. The parton shower or generator uncertainties are dominant for nearly all p_T bins of the parton-level cross-section, which illustrates the benefit of defining a particle-level cross-section in a fiducial region closely following the detector-level selection. A detailed breakdown of the systematic uncertainties is provided in Appendix A.

A covariance matrix including the effect of all uncertainties is calculated at particle level to make quantitative comparisons with theoretical predictions. This covariance matrix is obtained by summing two covariance matrices. The first covariance matrix incorporates uncertainties from detector and background modeling by performing 250,000 pseudoexperiments. In each pseudoexperiment, the data $p_{T,\text{reco}}$ distribution is varied following a Poisson distribution. Gaussian-distributed shifts are coherently added for each systematic uncertainty effect by scaling each Poisson-fluctuated bin with the relative variation from the associated systematic uncertainty effect. Differential cross-sections are obtained by unfolding each varied $p_{T,\text{reco}}$ distribution with the nominal corrections, and the results are

used to compute a covariance matrix.

The second covariance matrix is obtained by summing four separate covariance matrices corresponding to the effects of $t\bar{t}$ generator, parton shower, ISR/FSR, and PDF uncertainties. The standard deviations of the covariance matrices are derived by scaling the measured cross-section with the appropriate relative systematic uncertainty. The bin-to-bin correlation value is set to unity for the generator, parton shower, and ISR/FSR matrices, while it is set to 0.5 for the PDF matrix. This value is motivated by the fraction of the bins in which a single PDF set dominates in the determination of the envelopes used for their respective estimates. The procedure for these signal modeling uncertainties is needed because these effects cannot be represented by a variation at the detector level, and so cannot be included in the pseudoexperiment formalism used to build the first covariance matrix.

The correlation matrix derived from the particle-level covariance matrix is shown in Table 3. Agreement between the measured differential cross-sections and various predictions is quantified by calculating χ^2 values employing the covariance matrix and by inferring corresponding p -values. The χ^2 are evaluated using:

$$\chi^2 = V^T \cdot \text{Cov}^{-1} \cdot V,$$

where V is the vector of differences between measured differential cross-section values and predictions, and Cov^{-1} is the inverse of the covariance matrix.

$p_{T,\text{ptcl}}$ [GeV]	300–350	350–400	400–450	450–500	500–550	550–650	650–750	750–1200
300–350	1.00	0.83	0.79	0.79	0.72	0.63	0.58	0.51
350–400	0.83	1.00	0.83	0.80	0.76	0.74	0.67	0.60
400–450	0.79	0.83	1.00	0.87	0.79	0.78	0.77	0.63
450–500	0.79	0.80	0.87	1.00	0.89	0.76	0.77	0.66
500–550	0.72	0.76	0.79	0.89	1.00	0.84	0.75	0.62
550–650	0.63	0.74	0.78	0.76	0.84	1.00	0.89	0.71
650–750	0.58	0.67	0.77	0.77	0.75	0.89	1.00	0.87
750–1200	0.51	0.60	0.63	0.66	0.62	0.71	0.87	1.00

Table 3: Correlation matrix between the bins of the particle-level differential cross-section as a function of $p_{T,\text{ptcl}}$.

9. Results and interpretation

The unfolding procedure is applied to the observed top-jet candidate p_T distribution. The cross-sections are provided in Table 4 and Fig. 6 for the particle-level cross-section, and in Table 5 and Fig. 7 for the parton-level cross-section. The higher efficiency of reconstruction techniques for highly boosted top quarks allows measurement of the top quark p_T spectrum up to 1200 GeV. The differential cross-section is measured over two orders of magnitude. The measured differential cross-sections are compared to the predictions from ALPGEN+HERWIG, MC@NLO+HERWIG, POWHEG+HERWIG, and POWHEG+PYTHIA $t\bar{t}$ samples normalized to the NNLO+NNLL inclusive cross-section. The electroweak corrections are not applied to the Powheg+Pythia prediction in these figures in order to compare it on an equal footing with the other generators. All generators produce a top quark p_T spectrum that is harder than the one observed, with a difference that generally increases with p_T . The MC prediction

$p_{\text{T,ptcl}} [\text{GeV}]$	$\frac{d\sigma_{t\bar{t}}}{dp_{\text{T,ptcl}}} \left[\frac{\text{fb}}{\text{GeV}} \right]$	Statistical [%]	Systematic [%]
300 – 350	4.97	± 2.7	± 15
350 – 400	3.09	± 3.5	± 13
400 – 450	1.73	± 4.2	± 13
450 – 500	1.08	± 4.4	± 14
500 – 550	0.56	± 6.1	± 14
550 – 650	0.27	± 6.0	± 16
650 – 750	0.097	± 8.1	± 20
750 – 1200	0.012	± 15	± 24

Table 4: Fiducial particle-level differential cross-section, with statistical and systematic uncertainties, as a function of the top-jet candidate p_{T} .

$p_{\text{T,parton}} [\text{GeV}]$	$\frac{d\sigma_{t\bar{t}}}{dp_{\text{T,ptcl}}} \left[\frac{\text{fb}}{\text{GeV}} \right]$	Statistical [%]	Systematic [%]
300 – 350	60.1	± 3.2	± 16
350 – 400	26.2	± 3.4	± 15
400 – 450	11.8	± 4.2	± 20
450 – 500	6.27	± 4.5	± 21
500 – 550	3.06	± 6.1	± 27
550 – 650	1.21	± 6.3	± 26
650 – 750	0.375	± 9.6	± 31
750 – 1200	0.043	± 17	± 38

Table 5: Parton-level differential cross-section, with statistical and systematic uncertainties, as a function of the hadronically decaying top quark p_{T} .

to data ratio is approximately the same at both the particle and parton levels for Powheg+Pythia, which was used to extract the unfolding corrections. However, it changes significantly when going from particle level to parton level for the other MC generators, in particular for Powheg+Herwig, and Alpgen+Herwig, due to the different parton-level corrections in these MC generators. The level of agreement is better at parton level than at particle level because the parton level is affected by larger systematic uncertainties.

The χ^2 and p -values that quantify the level of agreement between the particle-level predictions and data are listed in Table 6. Within uncertainties, the differences are not significant for Powheg+Pythia, Powheg+Herwig and MC@NLO+Herwig, for which p -values of 0.11 (for Powheg+Pythia without electroweak corrections), 0.41, and 0.14 are obtained, respectively. Only the prediction of Alpgen+Herwig is significantly disfavored by the data at the particle level with a p -value of $5.9 \cdot 10^{-5}$.

The measured differential cross-sections are compared in Fig. 8 to the predictions of Powheg+Pythia with and without the electroweak corrections applied. The electroweak corrections lead to a slightly softer p_{T} spectrum, increasing the particle-level p -value from 0.11 to 0.28 without and with the corrections, respectively. The measured differential cross-sections are also compared in Fig. 9 to Powheg+Pythia predictions using either the HERAPDF [94] or CT10 PDF sets, and two different values of the Powheg h_{damp} parameter, the nominal value $h_{\text{damp}} = m_{\text{top}}$ and one with $h_{\text{damp}} = \infty$, which increases the amount of hard radiation and yields a lower p -value of 0.05. Better agreement with data is obtained when using the HERAPDF set instead of CT10, which reduces the difference between

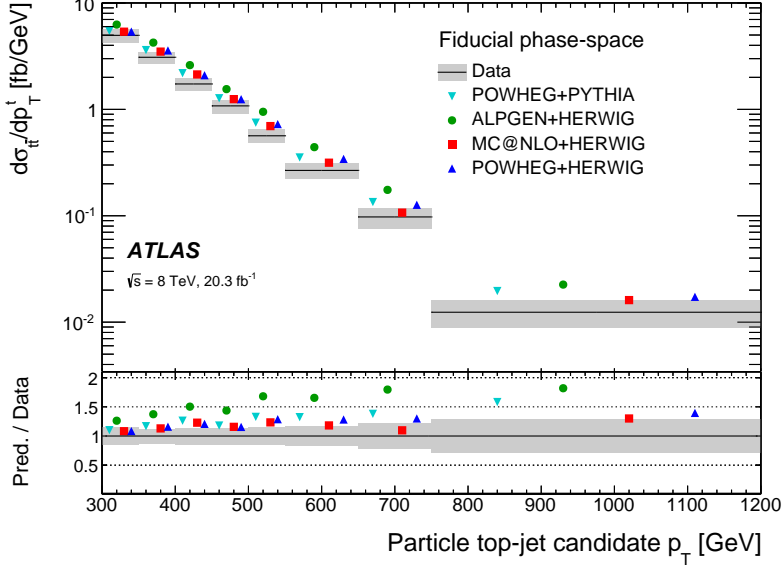


Figure 6: Fiducial particle-level differential cross-section as a function of the hadronic top-jet candidate p_T . POWHEG+PYTHIA, POWHEG+HERWIG, MC@NLO+HERWIG, and ALPGEN+HERWIG predictions are compared with the final results. MC samples are normalized to the NNLO+NNLL inclusive cross-section $\sigma_{t\bar{t}} = 253$ pb. No electroweak corrections are applied to the predictions. The lower part of the figure shows the ratio of the MC prediction to the data. The shaded area includes the total statistical plus systematic uncertainties. The points of the various predictions are spaced along the horizontal axis for presentation only; they correspond to the same p_T range.

MC generator	PDF	χ^2	p -value
POWHEG+PYTHIA $h_{\text{damp}} = m_{\text{top}} + \text{Electroweak corr.}$	CT10	9.8	0.28
POWHEG+PYTHIA $h_{\text{damp}} = m_{\text{top}}$	CT10	13.0	0.11
POWHEG+PYTHIA $h_{\text{damp}} = \infty$	CT10	15.6	0.05
POWHEG+PYTHIA $h_{\text{damp}} = m_{\text{top}}$	HERAPDF	9.4	0.31
POWHEG+PYTHIA $h_{\text{damp}} = \infty$	HERAPDF	10.9	0.21
POWHEG+HERWIG	CT10	8.2	0.41
MC@NLO+HERWIG	CT10	12.3	0.14
ALPGEN+HERWIG	CTEQ6	33.1	$5.9 \cdot 10^{-5}$

Table 6: Values of χ^2 and a p -value, computed for 8 degrees of freedom, obtained from the covariance matrix of the measured cross-section for various predictions. Electroweak corrections are applied only to the first prediction.

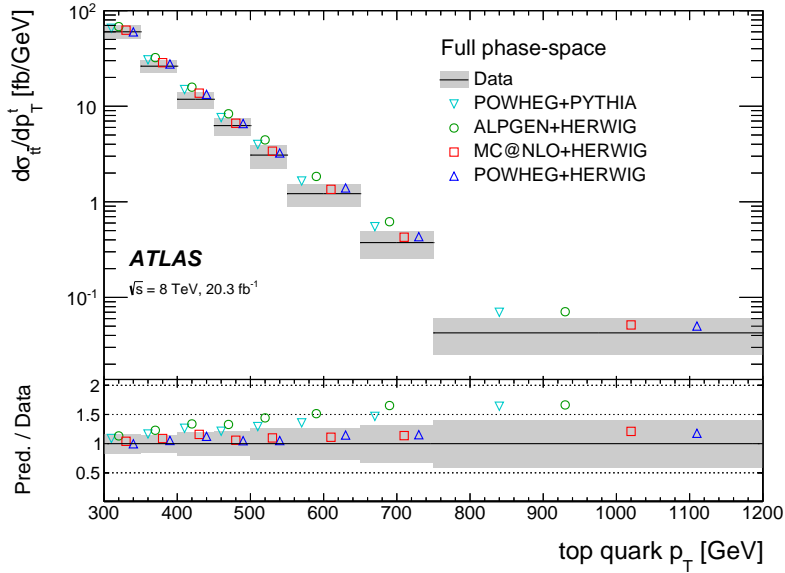


Figure 7: Parton-level differential cross-section as a function of the hadronically decaying top quark p_T . POWHEG+PYTHIA, POWHEG+HERWIG, MC@NLO+HERWIG, and ALPGEN+HERWIG predictions are compared with the final results. MC samples are normalized to the NNLO+NLL inclusive cross-section $\sigma_{t\bar{t}} = 253$ pb. No electroweak corrections are applied to the predictions. The lower part of the figure shows the ratio of the MC prediction to the data. The shaded area includes the total statistical plus systematic uncertainties. The points of the various predictions are spaced along the horizontal axis for presentation only; they correspond to the same p_T range.

data and MC simulation by up to about 20%. The Powheg+Pythia prediction that provides the best description of the data is the one that simultaneously employs the HERAPDF set and $h_{\text{damp}} = m_{\text{top}}$, corresponding to a p -value of 0.31 at particle level.

The measured parton-level cross-section is compared to the prediction of the parton-level NLO MCFM generator [95], which is interfaced with Applgrid [96] to convolve the perturbative coefficients with the strong coupling and the PDF. The inclusive cross-section computed by MCFM is used to normalize the prediction and no electroweak corrections are applied. Several PDF sets are compared: CT10, MSTW, NNPDF, and HERAPDF. The renormalization scale μ_R and factorization scale μ_F are dynamic: $\mu_R = \mu_F = \sqrt{m_{\text{top}}^2 + \hat{p}_{T,\text{top}}^2}$, where $\hat{p}_{T,\text{top}}$ is the average p_T of the two top quarks in the event. The uncertainties on the prediction include the PDF uncertainties estimated according to the prescription of each set and variations of the strong coupling constant, μ_F , and μ_R . The predictions are compared to the measured parton-level cross-section in Fig. 10. All predictions are in good agreement with the measured cross-section within the quoted uncertainties, which are dominated by systematic uncertainties correlated between p_T bins.

10. Conclusions

The differential $t\bar{t}$ production cross-section in $\sqrt{s} = 8$ TeV pp collisions has been measured as a function of the hadronically decaying top quark p_T in a high- p_T regime, using a dataset corresponding to

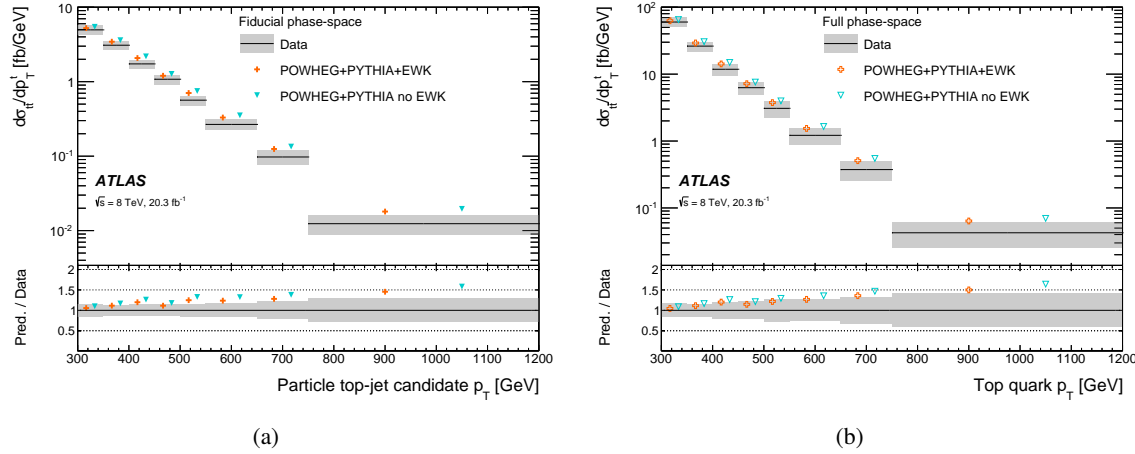


Figure 8: (a) Fiducial particle-level differential cross-section as a function of the hadronic top-jet candidate p_T and (b) parton-level differential cross-section as a function of the hadronically decaying top quark p_T , both compared to the PowHEG+PYTHIA predictions with and without electroweak corrections applied. MC samples are normalized to the NNLO+NNLL inclusive cross-section $\sigma_{\bar{t}t} = 253$ pb. The lower part of the figure shows the ratio of the MC prediction to the data. The shaded area includes the total statistical plus systematic uncertainties. The points of the various predictions are spaced along the horizontal axis for presentation only; they correspond to the same p_T range.

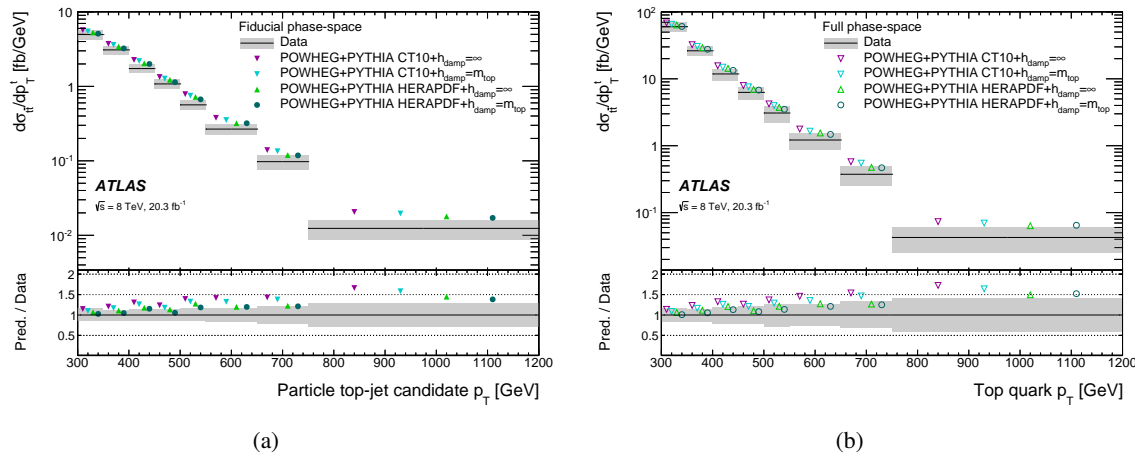


Figure 9: (a) Fiducial particle-level differential cross-section as a function of the hadronic top-jet candidate p_T and (b) parton-level differential cross-section as a function of the hadronically decaying top quark p_T , both compared to PowHEG+PYTHIA predictions using either the HERAPDF or CT10 PDF sets, and the PowHEG h_{damp} parameter set to ∞ or m_{top} . MC samples are normalized to the NNLO+NNLL inclusive cross-section $\sigma_{t\bar{t}} = 253$ pb. No electroweak corrections are applied to the predictions. The lower part of the figure shows the ratio of the MC prediction to the data. The shaded area includes the total statistical plus systematic uncertainties. The points of the various predictions are spaced along the horizontal axis for presentation only; they correspond to the same p_T range.

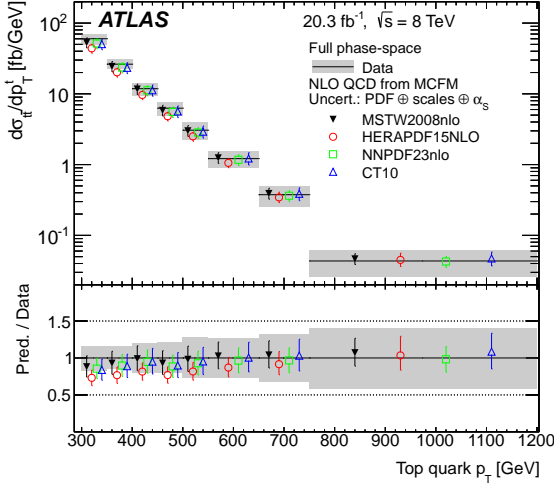


Figure 10: Parton-level differential cross-section as a function of the hadronically decaying top quark p_T . MCFM predictions with various PDF sets are also shown. The lower part of the figure shows the ratio of the MC prediction to the data. The shaded area includes the total statistical plus systematic uncertainties. The uncertainty on the predictions include the PDF uncertainties and variations of α_S , μ_F , μ_R .

an integrated luminosity of 20.3 fb^{-1} collected by the ATLAS detector at the LHC. Boosted hadronically decaying top quarks with $p_T > 300 \text{ GeV}$ are reconstructed within large- R jets and identified using jet substructure techniques. The measured p_T spectrum is extended in this analysis relative to previous measurements. A particle-level cross-section is measured in a fiducial region that closely follows the event selection. The measurement uncertainty ranges from 13% to 29% and is generally dominated by the uncertainty on the jet energy scale of large- R jets. A parton-level cross-section is also reported, with larger systematic uncertainties due to its greater reliance on $t\bar{t}$ MC generators to correct the data. The measured cross-sections are compared to the predictions of several NLO and LO matrix-element generators normalized to NNLO+NNLL QCD calculations, and using various PDF sets. Previous measurements suggest that the top quark p_T spectrum is well predicted at low p_T by NLO and matrix-element MC generators, both in normalization and shape, but that their predictions exceed the data at high p_T . The current analysis, focused on the boosted topology and extended to higher p_T values, also observes such a trend. However, a statistical analysis shows that the measurements are compatible with the majority of MC generator predictions within the quoted uncertainties.

Acknowledgments

We thank CERN for the very successful operation of the LHC, as well as the support staff from our institutions without whom ATLAS could not be operated efficiently.

We acknowledge the support of ANPCyT, Argentina; YerPhI, Armenia; ARC, Australia; BMWFW and FWF, Austria; ANAS, Azerbaijan; SSTC, Belarus; CNPq and FAPESP, Brazil; NSERC, NRC and CFI, Canada; CERN; CONICYT, Chile; CAS, MOST and NSFC, China; COLCIENCIAS, Colombia; MSMT CR, MPO CR and VSC CR, Czech Republic; DNRF, DNSRC and Lundbeck Foundation, Denmark; IN2P3-CNRS, CEA-DSM/IRFU, France; GNSF, Georgia; BMBF, HGF, and MPG, Germany; GSRT, Greece; RGC, Hong Kong SAR, China; ISF, I-CORE and Benoziyo Center, Israel;

INFN, Italy; MEXT and JSPS, Japan; CNRST, Morocco; FOM and NWO, Netherlands; RCN, Norway; MNiSW and NCN, Poland; FCT, Portugal; MNE/IFA, Romania; MES of Russia and NRC KI, Russian Federation; JINR; MESTD, Serbia; MSSR, Slovakia; ARRS and MIZŠ, Slovenia; DST/NRF, South Africa; MINECO, Spain; SRC and Wallenberg Foundation, Sweden; SERI, SNSF and Cantons of Bern and Geneva, Switzerland; MOST, Taiwan; TAEK, Turkey; STFC, United Kingdom; DOE and NSF, United States of America. In addition, individual groups and members have received support from BCKDF, the Canada Council, CANARIE, CRC, Compute Canada, FQRNT, and the Ontario Innovation Trust, Canada; EPLANET, ERC, FP7, Horizon 2020 and Marie Skłodowska-Curie Actions, European Union; Investissements d’Avenir Labex and Idex, ANR, Region Auvergne and Fondation Partager le Savoir, France; DFG and AvH Foundation, Germany; Herakleitos, Thales and Aristeia programmes co-financed by EU-ESF and the Greek NSRF; BSF, GIF and Minerva, Israel; BRF, Norway; the Royal Society and Leverhulme Trust, United Kingdom.

The crucial computing support from all WLCG partners is acknowledged gratefully, in particular from CERN and the ATLAS Tier-1 facilities at TRIUMF (Canada), NDGF (Denmark, Norway, Sweden), CC-IN2P3 (France), KIT/GridKA (Germany), INFN-CNAF (Italy), NL-T1 (Netherlands), PIC (Spain), ASGC (Taiwan), RAL (UK) and BNL (USA) and in the Tier-2 facilities worldwide.

A. Detailed tables of systematic uncertainties

Tables 7 and 8 report the detailed breakdown of the systematic uncertainties as a percentage of the measured differential cross sections.

$d\sigma_{t\bar{t}}/dp_{T,\text{ptcl}}$ Uncertainties [%] / Bins [GeV]	300–350	350–400	400–450	450–500	500–550	550–650	650–750	750–1200
Large- R jet p_T resolution	3.9/–4.0	–3.9/3.9	2.6/–2.6	1.3/–1.3	–/–	0.7/–0.7	2.6/–2.6	1.6/–1.5
Large- R jet mass resolution	–0.5/0.5	–0.2/0.2	–0.2/0.2	–0.2/0.2	–0.3/0.3	–0.3/0.3	–0.7/0.7	–0.7/0.7
Large- R jet $\sqrt{d_{12}}$ scale	1.0/–1.0	1.1/–1.0	0.8/–1.1	0.8/–1.3	0.9/–1.3	1.0/–1.4	1.4/–1.8	1.8/–2.5
Large- R jet mass scale	4.0/–4.5	2.5/–2.5	2.1/–2.0	1.7/–2.1	1.4/–1.6	1.3/–1.4	1.7/–2.2	2.2/–3.0
Large- R jet (JES) data vs MC	1.6/–2.3	4.7/–4.6	5.5/–5.7	6.4/–6.1	6.5/–6.0	7.3/–7.1	10.0/–9.6	11.7/–11.4
Large- R jet (JES) validation of $\Delta\phi$ cut	–/–	–/–	0.1/–0.2	0.3/–	–/–0.2	–/–0.3	0.5/–0.4	0.8/–0.5
Large- R jet (JES) cut on subleading small- R jet	0.9/–0.8	0.5/–1.0	1.2/–0.9	1.3/–1.0	1.3/–1.6	1.9/–2.7	2.8/–2.8	2.8/–2.9
Large- R jet (JES) photon purity	0.2/–	–/–	–/–	–/–	–0.1/–	–0.2/–	–/–	–/–0.4
Large- R jet (JES) photon energy scale	1.0/–0.9	1.7/–2.0	2.6/–2.4	2.9/–2.8	3.0/–3.2	3.0/–3.7	4.4/–3.9	5.6/–4.4
Large- R jet (JES) generator	0.8/–0.9	1.0/–1.1	1.3/–1.2	1.3/–0.8	0.5/–1.1	0.9/–1.6	1.5/–1.2	1.6/–1.2
Large- R jet (JES) out of cone and underlying events	0.2/–0.2	0.2/–	–/–0.3	0.2/–	–/–0.4	–/–0.6	0.5/–0.4	0.1/–0.4
Large- R jet (JES) JER	0.1/–	–/–	–/–	–/–	–/–0.2	–/–0.2	0.5/–0.4	0.4/–0.9
Large- R jet (JES) definition of small- R jet inside large- R jet	–/0.2	0.6/–1.0	1.5/–1.4	1.7/–1.2	1.3/–1.5	1.3/–2.3	2.2/–2.3	2.9/–2.5
Large- R jet (JES) cut on leading small- R jet	0.2/–0.2	0.4/–0.3	0.3/–0.3	–/–0.1	–/–	–/–0.2	0.1/–0.4	–/–0.7
Large- R jet (JES) statistics	0.3/–0.1	–/–0.7	1.1/–0.6	1.9/–2.0	2.1/–2.6	4.0/–4.3	8.0/–7.9	10.9/–10.7
Large- R jet (JES) correlation with JMS	1.1/–0.9	1.8/–2.1	2.6/–2.0	2.9/–2.7	2.2/–3.3	2.9/–3.5	4.0/–3.3	4.2/–3.8
Large- R jet (JES) interpolation	–/–	–/–	–/–	–/–	–0.1/–	–0.5/0.2	–0.7/0.6	–0.6/–
Large- R jet (JES) topology	11.3/–11.3	7.5/–5.9	7.8/–7.9	9.4/–8.3	8.1/–7.6	6.0/–5.9	7.7/–7.6	8.9/–8.7
Large- R jet (JES) pileup offset μ	–0.3/0.3	–0.2/0.2	–0.8/0.6	–0.3/0.2	–0.2/0.2	–0.8/0.4	–1.3/1.0	–1.1/1.6
Large- R jet (JES) pileup offset N_{PV}	–/0.2	–0.1/–	–0.2/0.1	–0.2/0.4	–0.5/–	–0.4/–	–0.5/0.5	–0.4/0.2
Small- R jet JES	0.4/–0.7	0.8/–1.3	1.5/–1.8	1.8/–1.6	1.7/–1.9	1.8/–3.0	2.3/–2.8	3.1/–3.1
Small- R jet reconstruction efficiency	–/–	–/–	–/–	–/–	–/–	–0.1/0.1	–/–	–/–
Small- R jet energy resolution	–0.2/0.2	–0.8/0.8	–/–	–0.7/0.7	–1.3/1.3	–0.8/0.7	–/–0.1	–1.5/1.4
Small- R jet JVF	–/0.2	–/0.4	–/0.2	–/0.2	–/0.2	–/0.2	–/0.5	–/0.5
b-tagging b-jet efficiency	1.4/–1.1	1.6/–1.4	2.6/–2.5	3.5/–3.4	3.6/–3.4	4.6/–4.7	5.8/–6.7	5.6/–6.9
b-tagging c-jet efficiency	0.6/–0.6	0.6/–0.6	–/–	–0.2/0.2	–0.8/0.8	–1.6/1.6	–2.3/2.2	–1.9/1.9
b-tagging light-jet efficiency	0.3/–0.3	0.3/–0.3	0.4/–0.4	0.6/–0.6	0.7/–0.6	0.8/–0.8	–1.0/0.8	–4.7/4.0
e efficiency	0.6/–0.6	0.6/–0.6	0.6/–0.6	0.6/–0.6	0.6/–0.6	0.7/–0.7	0.6/–0.6	0.6/–0.6
e energy resolution	–0.2/–	–/–	–0.2/–	–/–	–0.2/–	–0.4/–	–/–	–/–
e energy scale	–0.7/0.3	–0.9/0.6	–1.1/0.6	–1.2/0.8	–1.3/1.1	–1.3/0.7	–1.0/0.9	–0.9/1.1
μ efficiency	0.9/–0.9	0.9/–0.9	0.9/–1.0	0.8/–1.0	0.9/–1.0	1.1/–0.9	1.0/–0.8	1.2/–0.9
μ ID momentum resolution	–/–	–/–	–/–	–0.1/–	–/–	–0.2/–	–/–	–0.2/–
μ MS momentum resolution	–/–	–/–	–/–	–/–	–/–	0.2/–	0.1/–	–/–
μ momentum scale	–/–	–/–	–/–	–/–	–/–0.1	–/–	–/–0.1	–/–0.3
E_T^{miss} unassociated cells resolution	–/–	0.1/–	0.1/–	–0.2/–	–0.2/–	–/–	–/–	–/–0.3
E_T^{miss} unassociated cells scale	0.2/–	–/–	–/–0.1	–/0.1	–/–	–0.2/–	–/–	–0.2/–
Luminosity	2.8/–2.8	2.8/–2.8	2.9/–2.9	2.9/–2.9	2.9/–2.9	2.9/–2.9	2.9/–2.9	2.9/–2.9
W+jet	0.4/–0.4	0.2/–0.2	0.2/–0.2	0.2/–0.2	0.4/–0.4	0.9/–0.9	2.7/–2.7	5.4/–5.5
Single top	1.3/–1.3	0.6/–0.6	1.6/–1.6	1.5/–1.5	2.8/–2.8	4.4/–4.4	4.4/–4.4	3.9/–3.9
Z+jets	0.3/–0.3	0.2/–0.2	0.2/–0.2	0.4/–0.4	0.5/–0.5	0.7/–0.7	0.4/–0.4	0.3/–0.3
Multijet	–0.1/–	–0.1/0.1	–/–	0.2/–0.2	–/–	–0.3/0.3	–0.1/0.1	–0.1/0.1
Diboson	0.2/–0.2	0.2/–0.2	0.4/–0.4	0.2/–0.2	0.3/–0.3	0.4/–0.4	0.6/–0.6	0.7/–0.7
MC Signal statistics	0.5/–0.5	0.7/–0.7	0.9/–0.9	0.9/–0.9	1.3/–1.3	1.0/–1.0	1.1/–1.1	1.7/–1.7
MC Background statistics	0.5/–0.5	0.5/–0.5	0.7/–0.7	0.8/–0.8	1.2/–1.2	1.4/–1.4	1.8/–1.8	3.1/–3.1
$t\bar{t}$ generator	3.4/–3.4	3.6/–3.6	0.6/–0.6	0.4/–0.4	–/–	3.1/–3.1	1.0/–1.0	5.3/–5.3
PS/Hadronization	1.6/–1.6	2.1/–2.1	3.6/–3.6	0.3/–0.3	1.1/–1.1	2.5/–2.5	2.2/–2.2	0.4/–0.4
ISR/FSR	–4.0/4.0	–4.0/4.0	–3.6/3.6	–3.6/3.6	–3.6/3.6	–3.6/3.6	–5.5/5.5	–5.5/5.5
PDF	–/–	–/–	–/–	0.8/–0.8	0.8/–0.8	1.2/–1.2	1.2/–1.2	1.2/–1.2

Table 7: The individual systematic uncertainties calculated as a percentage of the differential cross-section $d\sigma_{t\bar{t}}/dp_{T,\text{ptcl}}$ in each bin.

$d\sigma_{t\bar{t}}/dp_{T,\text{parton}}$	Uncertainties [%] / Bins [GeV]	300–350	350–400	400–450	450–500	500–550	550–650	650–750	750–1200
Large- R jet p_T resolution	4.7/–4.8	–4.5/4.1	1.6/–1.7	2.0/–2.0	0.4/–0.3	0.7/–0.7	2.0/–2.0	2.3/–2.2	
Large- R jet mass resolution	–0.5/0.5	–0.2/0.2	–0.2/0.2	–0.2/0.2	–0.2/0.2	–0.4/0.4	–0.7/0.6	–0.8/0.8	
Large- R jet $\sqrt{d_{12}}$ scale	1.0/–1.0	1.1/–1.0	0.8/–1.1	0.8/–1.2	0.8/–1.3	1.0/–1.5	1.5/–2.0	1.9/–2.6	
Large- R jet mass scale	4.3/–4.8	2.5/–2.5	1.9/–1.8	1.6/–1.9	1.2/–1.5	1.2/–1.4	1.6/–2.1	2.0/–2.8	
Large- R jet (JES) data vs MC	1.1/–1.9	4.7/–4.6	5.9/–6.0	6.5/–6.2	6.8/–6.3	8.0/–7.6	10.8/–10.4	12.8/–12.5	
Large- R jet (JES) validation of $\Delta\phi$ cut	– / –	– / –	0.1/–0.2	0.2/ –	– / –0.1	– / –0.3	0.6/–0.4	0.9/–0.6	
Large- R jet (JES) cut on subleading small- R jet	0.9/–0.8	0.5/–1.0	1.1/–0.9	1.3/–1.0	1.4/–1.7	2.1/–2.8	2.9/–3.2	3.2/–3.3	
Large- R jet (JES) photon purity	0.2/ –	– / –	– / –	– / –	–0.1/ –	–0.2/ –	– / –0.2	– / –0.3	
Large- R jet (JES) photon energy scale	0.9/–0.7	1.6/–2.0	2.7/–2.5	3.0/–2.9	3.0/–3.4	3.4/–3.9	4.8/–4.3	6.0/–4.7	
Large- R jet (JES) generator	0.8/–0.9	1.0/–1.1	1.4/–1.2	1.2/–0.9	0.7/–1.1	0.9/–1.5	1.4/–1.4	1.8/–1.2	
Large- R jet (JES) out of cone and underlying events	0.2/–0.2	0.2/ –	0.1/–0.3	0.2/ –	– / –0.3	– / –0.6	0.3/–0.5	0.3/–0.5	
Large- R jet (JES) JER	0.1/ –	– / –	– / –	– / –	– / –0.1	0.1/–0.3	0.5/–0.6	0.6/–0.9	
Large- R jet (JES) definition of small- R jet inside large- R jet	–0.2/0.4	0.5/–1.0	1.6/–1.6	1.8/–1.3	1.4/–1.6	1.5/–2.3	2.4/–2.6	3.2/–2.8	
Large- R jet (JES) cut on leading small- R jet	0.2/–0.2	0.4/–0.3	0.3/–0.3	– / –0.1	– / –	– / –0.2	– / –0.5	– / –0.7	
Large- R jet (JES) statistics	0.3/ –	– / –0.6	1.1/–0.6	1.9/–1.8	2.4/–2.9	4.8/–5.2	9.1/–9.2	12.3/–12.3	
Large- R jet (JES) correlation with JMS	0.9/–0.8	1.7/–2.1	2.7/–2.2	2.9/–2.7	2.5/–3.4	3.0/–3.7	4.1/–3.7	4.7/–3.9	
Large- R jet (JES) interpolation	– / –	– / –	– / –	– / –0.1	–0.2/ –	–0.5/0.2	–0.8/0.4	–0.8/0.2	
Large- R jet (JES) topology	11.8/–12.0	7.4/–5.7	7.4/–7.3	9.2/–8.4	8.0/–7.5	6.3/–6.2	7.3/–7.2	8.5/–8.4	
Large- R jet (JES) pileup offset μ	–0.3/0.3	–0.2/0.2	–0.8/0.6	–0.4/0.3	–0.3/0.1	–0.8/0.4	–1.3/1.2	–1.4/1.8	
Large- R jet (JES) pileup offset N_{PV}	– / 0.2	–0.1/ –	–0.2/0.1	–0.2/0.3	–0.5/ –	–0.5/ –	–0.5/0.3	–0.5/0.4	
Small- R jet JES	0.6/–0.8	0.8/–1.3	1.6/–1.9	2.0/–1.7	1.8/–2.0	1.9/–3.0	2.5/–3.3	3.3/–3.5	
Small- R jet reconstruction efficiency	– / –	– / –	– / –	– / –	– / –	–0.1/0.1	– / –	– / –	
Small- R jet energy resolution	–0.1/0.1	–0.8/0.8	–0.1/0.1	–0.6/0.6	–1.2/1.2	–0.9/0.8	–0.6/0.5	–1.1/1.0	
Small- R jet JVF	0.2/ –	– /0.4	– /0.3	– /0.2	– /0.2	– /0.3	– /0.5	– /0.6	
b -tagging b -jet efficiency	1.3/–1.0	1.5/–1.3	2.6/–2.5	3.6/–3.5	4.0/–3.8	5.0/–5.2	6.1/–7.1	6.5/–8.0	
b -tagging c -jet efficiency	0.7/–0.7	0.6/–0.6	– / –	–0.3/0.3	–1.0/1.0	–1.9/1.9	–2.5/2.4	–2.6/2.5	
b -tagging light-jet efficiency	0.3/–0.3	0.2/–0.2	0.4/–0.4	0.6/–0.6	0.9/–0.8	0.4/–0.5	–2.0/1.6	–4.9/4.0	
e efficiency	0.6/–0.6	0.6/–0.6	0.6/–0.6	0.6/–0.6	0.7/–0.7	0.7/–0.7	0.6/–0.6	0.6/–0.6	
e energy resolution	–0.2/ –	– / –	–0.1/ –	–0.1/ –	–0.1/0.1	–0.3/ –	–0.1/ –	– / –	
e energy scale	–0.6/0.3	–0.9/0.6	–1.1/0.6	–1.2/0.8	–1.3/1.0	–1.3/0.9	–1.0/0.9	–0.9/1.1	
μ efficiency	0.9/–0.9	0.9/–0.9	0.9/–1.0	0.9/–1.0	0.9/–1.0	1.1/–0.9	1.1/–0.8	1.2/–0.8	
μ ID momentum resolution	– / –	– / –	– / –	–0.1/ –	– / –	– /0.1	– / –	–0.2/ –	
μ MS momentum resolution	– / –	– / –	– / –	– / –	– / –	0.2/ –	0.1/ –	– / –	
μ momentum scale	– / –	– / –	– / –	– / –	– / –	– / –	– / –0.2	– / –0.3	
E_T^{miss} unassociated cells resolution	– / –	0.1/ –	0.2/ –	–0.2/ –	–0.2/ –	– / –	– / –	– / –0.3	
E_T^{miss} unassociated cells scale	0.3/ –	– / –	– / –0.1	– / –	– / –	–0.2/ –	–0.2/ –	–0.2/ –	
Luminosity	2.9/–2.9	2.8/–2.8	2.9/–2.9	2.9/–2.9	2.9/–2.9	2.9/–2.9	2.9/–2.9	2.9/–2.9	
W+jet	0.4/–0.4	0.2/–0.2	0.2/–0.2	0.2/–0.2	0.4/–0.3	1.3/–1.3	3.6/–3.7	5.8/–6.1	
Single top	1.4/–1.4	0.6/–0.6	1.4/–1.4	1.6/–1.6	3.0/–3.0	4.6/–4.6	5.0/–5.0	4.7/–4.7	
Z+jets	0.3/–0.3	0.2/–0.2	0.2/–0.2	0.4/–0.4	0.5/–0.5	0.7/–0.7	0.5/–0.5	0.3/–0.3	
Multijet	–0.1/0.1	–0.1/0.1	– / –	0.2/–0.2	– / –	–0.3/0.2	–0.2/0.2	–0.2/0.2	
Diboson	0.2/–0.2	0.2/–0.2	0.4/–0.4	0.3/–0.3	0.3/–0.3	0.5/–0.5	0.7/–0.7	0.8/–0.8	
MC Signal statistics	0.8/–0.8	0.9/–0.9	1.2/–1.2	1.1/–1.1	1.7/–1.7	1.4/–1.4	1.5/–1.5	2.9/–2.9	
MC Background statistics	0.6/–0.6	0.6/–0.6	0.7/–0.7	0.8/–0.8	1.1/–1.1	1.4/–1.4	2.0/–2.0	3.1/–3.1	
$t\bar{t}$ generator	2.0/–2.0	2.3/–2.3	4.2/–4.2	4.7/–4.7	10.6/–10.6	11.5/–11.5	14.8/–14.8	20.4/–20.4	
PS/Hadronization	6.2/–6.2	9.3/–9.3	14.1/–14.1	13.6/–13.6	19.6/–19.6	16.7/–16.7	16.1/–16.1	17.3/–17.3	
ISR/FSR	–4.1/4.1	–4.1/4.1	–5.6/5.6	–5.6/5.6	–5.6/5.6	–5.6/5.6	–6.5/6.5	–6.5/6.5	
PDF	0.3/–0.3	0.3/–0.3	0.3/–0.3	1.2/–1.2	1.2/–1.2	2.2/–2.2	2.2/–2.2	2.2/–2.2	

Table 8: The individual systematic uncertainties calculated as a percentage of the differential cross-section $d\sigma_{t\bar{t}}/dp_{T,\text{parton}}$ in each bin.

References

- [1] D. Atwood, A. Kagan and T. Rizzo,
Constraining anomalous top quark couplings at the Tevatron, Phys. Rev. **D 52** (1995) 6264, arXiv:[hep-ph/9407408 \[hep-ph\]](#).
- [2] C. Englert et al., *Constraining the Intrinsic Structure of Top-Quarks*, Phys. Lett. **B 721** (2013) 261, arXiv:[1210.2570 \[hep-ph\]](#).
- [3] ATLAS Collaboration, *Measurement of the $t\bar{t}$ production cross-section using $e\mu$ events with b -tagged jets in pp collisions at $\sqrt{s} = 7$ and 8 TeV with the ATLAS detector*, Eur. Phys. J. **C 74** (2014) 3109, arXiv:[1406.5375 \[hep-ex\]](#).
- [4] CMS collaboration, *Measurement of the $t\bar{t}$ production cross section in the dilepton channel in pp collisions at $\sqrt{s} = 7$ TeV*, JHEP **11** (2012) 067, arXiv:[1208.2671 \[hep-ex\]](#).
- [5] CMS Collaboration, *Measurement of the $t\bar{t}$ production cross section in the dilepton channel in pp collisions at $\sqrt{s} = 8$ TeV*, JHEP **02** (2014) 024, arXiv:[1312.7582 \[hep-ex\]](#).
- [6] M. Cacciari et al., *Top-pair production at hadron colliders with next-to-next-to-leading logarithmic soft-gluon resummation*, Phys. Lett. **B 710** (2012) 612, arXiv:[1111.5869 \[hep-ph\]](#).
- [7] M. Beneke et al., *Hadronic top-quark pair production with NNLL threshold resummation*, Nucl.Phys. **B 855** (2012) 695, arXiv:[1109.1536 \[hep-ph\]](#).
- [8] P. Baernreuther, M. Czakon and A. Mitov, *Percent Level Precision Physics at the Tevatron: Next-to-Next-to-Leading order QCD Corrections to $q\bar{q} \rightarrow t\bar{t} + X$* , Phys. Rev. Lett. **109** (2012) 132001, arXiv:[1204.5201 \[hep-ph\]](#).
- [9] M. Czakon and A. Mitov, *NNLO corrections to top-pair production at hadron colliders: the all-fermionic scattering channels*, JHEP **12** (2012) 054, arXiv:[1207.0236 \[hep-ph\]](#).
- [10] M. Czakon and A. Mitov, *NNLO corrections to top pair production at hadron colliders: the quark-gluon reaction*, JHEP **01** (2013) 080, arXiv:[1210.6832 \[hep-ph\]](#).
- [11] M. Czakon, P. Fiedler and A. Mitov, *Total Top-Quark Pair-Production Cross Section at Hadron Colliders Through $O(\alpha_S^4)$* , Phys. Rev. Lett. **110** (2013) 252004, arXiv:[1303.6254 \[hep-ph\]](#).
- [12] ATLAS Collaboration, *Measurements of top quark pair relative differential cross-sections with ATLAS in pp collisions at $\sqrt{s} = 7$ TeV*, Eur. Phys. J. **C 73** (2013) 2261, arXiv:[1207.5644 \[hep-ex\]](#).
- [13] ATLAS Collaboration, *Measurements of normalized differential cross sections for $t\bar{t}$ production in pp collisions at $\sqrt{s} = 7$ TeV using the ATLAS detector*, Phys. Rev. **D 90** (2014) 072004, arXiv:[1407.0371 \[hep-ex\]](#).
- [14] ATLAS Collaboration, *Differential top-antitop cross-section measurements as a function of observables constructed from final-state particles using pp collisions at $\sqrt{s} = 7$ TeV in the ATLAS detector*, JHEP **06** (2015) 100, arXiv:[1502.05923 \[hep-ex\]](#).
- [15] CMS Collaboration, *Measurement of differential top-quark pair production cross sections in pp collisions at $\sqrt{s} = 7$ TeV*, Eur. Phys. J. **C 73** (2013) 2339, arXiv:[1211.2220 \[hep-ex\]](#).

- [16] CMS Collaboration, *Measurement of the differential cross section for top quark pair production in pp collisions at $\sqrt{s} = 8$ TeV*, Eur. Phys. J. **C75**.11 (2015) 542, arXiv:1505.04480 [hep-ex].
- [17] ATLAS Collaboration, *Prospects for top anti-top resonance searches using early ATLAS data*, ATL-PHYS-PUB-2010-008, <https://cdsweb.cern.ch/record/1278454> (2010).
- [18] ATLAS Collaboration, *A search for ttbar resonances in the lepton plus jets final state with ATLAS using 4.7 fb^{-1} of pp collisions at $\sqrt{s} = 7$ TeV*, Phys. Rev. D **88** (2013) 012004, arXiv:1305.2756 [hep-ex].
- [19] ATLAS Collaboration, *Search for resonances decaying into top-quark pairs using fully hadronic decays in pp collisions with ATLAS at $\sqrt{s} = 7$ TeV*, JHEP **01** (2013) 116, arXiv:1211.2202 [hep-ex].
- [20] ATLAS Collaboration, *A search for t̄t resonances using lepton-plus-jets events in proton-proton collisions at $\sqrt{s} = 8$ TeV with the ATLAS detector*, JHEP **08** (2015) 148, arXiv:1505.07018 [hep-ex].
- [21] CMS Collaboration, *Search for Anomalous t̄t Production in the Highly-Boosted All-Hadronic Final State*, JHEP **09** (2012) 029, [Erratum: JHEP 03 (2014) 132], arXiv:1204.2488 [hep-ex].
- [22] ATLAS Collaboration, *The ATLAS Experiment at the CERN Large Hadron Collider*, JINST **3** (2008) S08003.
- [23] ATLAS Collaboration, *Improved luminosity determination in pp collisions at $\sqrt{s} = 7$ TeV using the ATLAS detector at the LHC*, Eur. Phys. J. C **73** (2013) 2518, arXiv:1302.4393 [hep-ex].
- [24] GEANT4 Collaboration, S. Agostinelli et al., *GEANT4: A simulation toolkit*, Nucl. Instrum. Meth. **A506** (2003) 250.
- [25] ATLAS Collaboration, *The ATLAS Simulation Infrastructure*, Eur. Phys. J. C**70** (2010) 823–874, arXiv:1005.4568 [physics.ins-det].
- [26] ATLAS Collaboration, *Performance of the Fast ATLAS Tracking Simulation (FATRAS) and the ATLAS Fast Calorimeter Simulation (FastCaloSim) with single particles*, ATL-SOFT-PUB-2014-001, <https://cdsweb.cern.ch/record/1669341> (2014).
- [27] S. Frixione, P. Nason and C. Oleari, *Matching NLO QCD computations with Parton Shower simulations: the POWHEG method*, JHEP **11** (2007) 070, arXiv:0709.2092 [hep-ph].
- [28] S. Alioli et al., *A general framework for implementing NLO calculations in shower Monte Carlo programs: the POWHEG BOX*, JHEP **06** (2010) 043, arXiv:1002.2581 [hep-ph].
- [29] H.-L. Lai et al., *New parton distributions for collider physics*, Phys. Rev. D **82** (2010) 074024, arXiv:1007.2241 [hep-ph].
- [30] T. Sjöstrand, S. Mrenna and P. Z. Skands, *PYTHIA 6.4 Physics and Manual*, JHEP **05** (2006) 026, arXiv:hep-ph/0603175 [hep-ph].
- [31] P. Skands, *Tuning Monte Carlo Generators: The Perugia Tunes*, Phys. Rev. D **82** (2010) 074018, update available on arXiv, arXiv:1005.3457 [hep-ph].

- [32] J. Pumplin et al.,
New generation of parton distributions with uncertainties from global QCD analysis,
JHEP **07** (2002) 012, arXiv:[hep-ph/0201195 \[hep-ph\]](#).
- [33] M. Aliev et al., *HATHOR: HAdronic Top and Heavy quarks crOss section calculatoR*,
Comput. Phys. Commun. **182** (2011) 1034, arXiv:[1007.1327 \[hep-ph\]](#).
- [34] J. H. Kühn, A. Scharf and P. Uwer,
Electroweak corrections to top-quark pair production in quark-antiquark annihilation,
Eur. Phys. J. C **45** (2006) 139, arXiv:[hep-ph/0508092 \[hep-ph\]](#).
- [35] J. H. Kühn, A. Scharf and P. Uwer,
Electroweak effects in top-quark pair production at hadron colliders,
Eur. Phys. J. C **51** (2007) 37, arXiv:[hep-ph/0610335 \[hep-ph\]](#).
- [36] J. H. Kühn, A. Scharf and P. Uwer,
Weak interactions in top-quark pair production at hadron colliders: An update,
Phys. Rev. D **91** (2015) 014020, arXiv:[1305.5773 \[hep-ph\]](#).
- [37] S. Frixione and B. R. Webber, *The MC@NLO 3.4 Event Generator* (2008),
arXiv:[0812.0770 \[hep-ph\]](#).
- [38] G. Corcella et al., *HERWIG 6: An Event generator for hadron emission reactions with interfering gluons (including supersymmetric processes)*,
JHEP **01** (2001) 010, arXiv:[hep-ph/0011363 \[hep-ph\]](#).
- [39] J. M. Butterworth, J. R. Forshaw and M. H. Seymour,
Multiparton interactions in photoproduction at HERA, **Z. Phys. C** **72** (1996) 637–646, arXiv:[hep-ph/9601371 \[hep-ph\]](#).
- [40] ATLAS Collaboration, *New ATLAS event generator tunes to 2010 data*,
ATL-PHYS-PUB-2011-008 (2011), URL: <https://cds.cern.ch/record/1345343>.
- [41] M. L. Mangano et al.,
ALPGEN, a generator for hard multiparton processes in hadronic collisions,
JHEP **07** (2003) 001, arXiv:[hep-ph/0206293 \[hep-ph\]](#).
- [42] M. L. Mangano et al., *Matching matrix elements and shower evolution for top-quark production in hadronic collisions*,
JHEP **01** (2007) 013, arXiv:[hep-ph/0611129 \[hep-ph\]](#).
- [43] B. P. Kersevan and E. Richter-Was, *The Monte Carlo event generator AcerMC version 2.0 with interfaces to PYTHIA 6.2 and HERWIG 6.5*,
Comput. Phys. Commun. **184** (2013) 919–985, arXiv:[hep-ph/0405247 \[hep-ph\]](#).
- [44] ATLAS Collaboration, *Measurement of $t\bar{t}$ production with a veto on additional central jet activity in pp collisions at $\sqrt{s} = 7$ TeV using the ATLAS detector*,
Eur. Phys. J. C **72** (2012) 2043, arXiv:[1203.5015 \[hep-ex\]](#).
- [45] ATLAS Collaboration,
Measurement of jet shapes in top-quark pair events at $\sqrt{s} = 7$ TeV using the ATLAS detector,
Eur. Phys. J. C **73**.12 (2013) 2676, arXiv:[1307.5749 \[hep-ex\]](#).
- [46] ATLAS Collaboration, *Monte Carlo generator comparisons to ATLAS measurements constraining QCD radiation in top anti-top final states*, ATL-PHYS-PUB-2013-005 (2013), URL: <http://cds.cern.ch/record/1532067>.

- [47] ATLAS Collaboration, *Comparison of Monte Carlo generator predictions to ATLAS measurements of top pair production at 7 TeV*, ATL-PHYS-PUB-2015-002 (2015), URL: <http://cds.cern.ch/record/1981319>.
- [48] M. Czakon and A. Mitov, *Top++: A Program for the Calculation of the Top-Pair Cross-Section at Hadron Colliders*, *Comput. Phys. Commun.* **185** (2014) 2930, arXiv:[1112.5675 \[hep-ph\]](https://arxiv.org/abs/1112.5675).
- [49] R. Hamberg, W. van Neerven and T. Matsuura, *A Complete calculation of the order α_s^2 correction to the Drell-Yan K factor*, *Nucl. Phys. B* **359** (1991) 343.
- [50] R. Gavin et al., *W Physics at the LHC with FEWZ 2.1*, *Comput. Phys. Commun.* **184** (2013) 208, arXiv:[1201.5896 \[hep-ph\]](https://arxiv.org/abs/1201.5896).
- [51] S. Alioli et al., *NLO single-top production matched with shower in POWHEG: s- and t-channel contributions*, *JHEP* **09** (2009) 111, [Erratum: JHEP 02 (2010) 011], arXiv:[0907.4076 \[hep-ph\]](https://arxiv.org/abs/0907.4076).
- [52] R. Frederix, E. Re and P. Torrielli, *Single-top t-channel hadroproduction in the four-flavour scheme with POWHEG and aMC@NLO*, *JHEP* **09** (2012) 130, arXiv:[1207.5391 \[hep-ph\]](https://arxiv.org/abs/1207.5391).
- [53] E. Re, *Single-top Wt-channel production matched with parton showers using the POWHEG method*, *Eur. Phys. J. C* **71** (2011) 1547, arXiv:[1009.2450 \[hep-ph\]](https://arxiv.org/abs/1009.2450).
- [54] S. Frixione et al., *Single-top hadroproduction in association with a W boson*, *JHEP* **07** (2008) 029, arXiv:[0805.3067 \[hep-ph\]](https://arxiv.org/abs/0805.3067).
- [55] N. Kidonakis, *Next-to-next-to-leading-order collinear and soft gluon corrections for t-channel single top quark production*, *Phys. Rev. D* **83** (2011) 091503, arXiv:[1103.2792 \[hep-ph\]](https://arxiv.org/abs/1103.2792).
- [56] N. Kidonakis, *Two-loop soft anomalous dimensions for single top quark associated production with a W^- or H^-* , *Phys. Rev. D* **82** (2010) 054018, arXiv:[1005.4451 \[hep-ph\]](https://arxiv.org/abs/1005.4451).
- [57] N. Kidonakis, *Next-to-next-to-leading logarithm resummation for s-channel single top quark production*, *Phys. Rev. D* **81** (2010) 054028, arXiv:[1001.5034 \[hep-ph\]](https://arxiv.org/abs/1001.5034).
- [58] T. Gleisberg et al., *Event generation with SHERPA 1.1*, *JHEP* **02** (2009) 007, arXiv:[0811.4622 \[hep-ph\]](https://arxiv.org/abs/0811.4622).
- [59] J. M. Campbell, R. K. Ellis and C. Williams, *Vector boson pair production at the LHC*, *JHEP* **07** (2011) 018, arXiv:[1105.0020 \[hep-ph\]](https://arxiv.org/abs/1105.0020).
- [60] M. Cacciari, G. P. Salam and G. Soyez, *The Anti- k_t jet clustering algorithm*, *JHEP* **04** (2008) 063, arXiv:[0802.1189 \[hep-ph\]](https://arxiv.org/abs/0802.1189).
- [61] M. Cacciari, G. P. Salam and G. Soyez, *FastJet User Manual*, *Eur. Phys. J. C* **72** (2012) 1896, arXiv:[1111.6097 \[hep-ph\]](https://arxiv.org/abs/1111.6097).
- [62] W. Lampl et al., *Calorimeter clustering algorithms: description and performance*, ATL-LARG-PUB-2008-002, <https://cdsweb.cern.ch/record/1099735> (2008).
- [63] ATLAS Collaboration, *Jet energy measurement with the ATLAS detector in proton-proton collisions at $\sqrt{s} = 7$ TeV*, *Eur. Phys. J. C* **73** (2013) 2304, arXiv:[1112.6426 \[hep-ex\]](https://arxiv.org/abs/1112.6426).

- [64] ATLAS Collaboration, *Data-driven determination of the energy scale and resolution of jets reconstructed in the ATLAS calorimeters using dijet and multijet events at $\sqrt{s} = 8$ TeV*, ATLAS-CONF-2015-017, <https://cdsweb.cern.ch/record/2008678> (2015).
- [65] D. Krohn, J. Thaler and L.-T. Wang, *Jet Trimming*, JHEP **02** (2010) 084, arXiv:[0912.1342 \[hep-ph\]](#).
- [66] M. Cacciari, G. P. Salam and G. Soyez, *The Catchment Area of Jets*, JHEP **04** (2008) 005, arXiv:[0802.1188 \[hep-ph\]](#).
- [67] M. Cacciari and G. P. Salam, *Pileup subtraction using jet areas*, Phys. Lett. **B 659** (2008) 119, arXiv:[0707.1378 \[hep-ph\]](#).
- [68] S. D. Ellis and D. E. Soper, *Successive combination jet algorithm for hadron collisions*, Phys. Rev. **D 48** (1993) 3160, arXiv:[hep-ph/9305266 \[hep-ph\]](#).
- [69] S. Catani et al., *Longitudinally invariant k_\perp clustering algorithms for hadron hadron collisions*, Nucl. Phys. **B 406** (1993) 187.
- [70] ATLAS Collaboration, *Jet energy measurement and its systematic uncertainty in proton-proton collisions at $\sqrt{s} = 7$ TeV with the ATLAS detector*, Eur. Phys. J. **C 75** (2015) 17, arXiv:[1406.0076 \[hep-ex\]](#).
- [71] ATLAS Collaboration, *Performance of jet substructure techniques for large- R jets in proton-proton collisions at $\sqrt{s} = 7$ TeV using the ATLAS detector*, JHEP **09** (2013) 076, arXiv:[1306.4945 \[hep-ex\]](#).
- [72] ATLAS Collaboration, *Identification of high transverse momentum top quarks in pp collisions at $\sqrt{s} = 8$ TeV with the ATLAS detector*, ATLAS-CONF-2015-036, <https://cds.cern.ch/record/2043862> (2015).
- [73] ATLAS Collaboration, *Calibration of the performance of b-tagging for c and light-flavour jets in the 2012 ATLAS data*, ATLAS-CONF-2014-046, <https://cdsweb.cern.ch/record/1741020> (2014).
- [74] ATLAS Collaboration, *Electron reconstruction and identification efficiency measurements with the ATLAS detector using the 2011 LHC proton-proton collision data*, Eur. Phys. J. **C74** (2014) 2941, arXiv:[1404.2240 \[hep-ex\]](#).
- [75] ATLAS Collaboration, *Measurement of the muon reconstruction performance of the ATLAS detector using 2011 and 2012 LHC proton–proton collision data*, Eur. Phys. J. **C 74** (2014) 3130, arXiv:[1407.3935 \[hep-ex\]](#).
- [76] K. Rehermann and B. Tweedie, *Efficient Identification of Boosted Semileptonic Top Quarks at the LHC*, JHEP **03** (2011) 059, arXiv:[1007.2221 \[hep-ph\]](#).
- [77] ATLAS Collaboration, *Performance of Missing Transverse Momentum Reconstruction in Proton-Proton Collisions at 7 TeV with ATLAS*, Eur. Phys. J. **C 72** (2012) 1844, arXiv:[1108.5602 \[hep-ex\]](#).
- [78] ATLAS Collaboration, *Measurement of the charge asymmetry in top quark pair production in pp collisions at $\sqrt{s} = 7$ TeV using the ATLAS detector*, Eur. Phys. J. **C72** (2012) 2039, arXiv:[1203.4211 \[hep-ex\]](#).

- [79] ATLAS Collaboration, *Estimation of non-prompt and fake lepton backgrounds in final states with top quarks produced in proton-proton collisions at $\sqrt{s} = 8$ TeV with the ATLAS detector*, ATLAS-CONF-2014-058, <https://cdsweb.cern.ch/record/1951336> (2014).
- [80] ATLAS Collaboration, *Jet mass and substructure of inclusive jets in $\sqrt{s} = 7$ TeV pp collisions with the ATLAS experiment*, JHEP **05** (2012) 128, arXiv:1203.4606 [hep-ex].
- [81] ATLAS Collaboration, *Jet energy resolution in proton-proton collisions at $\sqrt{s} = 7$ TeV recorded in 2010 with the ATLAS detector*, Eur. Phys. J. **C73** (2013) 2306, arXiv:1210.6210 [hep-ex].
- [82] ATLAS Collaboration, *Single hadron response measurement and calorimeter jet energy scale uncertainty with the ATLAS detector at the LHC*, Eur. Phys. J. **C73** (2013) 2305, arXiv:1203.1302 [hep-ex].
- [83] ATLAS Collaboration, *Jet energy resolution in proton-proton collisions at $\sqrt{s} = 7$ TeV recorded in 2010 with the ATLAS detector*, Eur. Phys. J. **C73** (2013) 2306, arXiv:1210.6210 [hep-ex].
- [84] ATLAS Collaboration, *Calibration of b-tagging using dileptonic top pair events in a combinatorial likelihood approach with the ATLAS experiment*, ATLAS-CONF-2014-004, <https://cdsweb.cern.ch/record/1664335> (2014).
- [85] ATLAS Collaboration, *Measurement of the b-tag Efficiency in a Sample of Jets Containing Muons with 5 fb^{-1} of Data from the ATLAS Detector*, ATLAS-CONF-2012-043, <https://cdsweb.cern.ch/record/1435197> (2012).
- [86] ATLAS Collaboration, *Measurement of the Mistag Rate of b-tagging algorithms with 5 fb^{-1} of Data Collected by the ATLAS Detector*, ATLAS-CONF-2012-040, <https://cdsweb.cern.ch/record/1435194> (2012).
- [87] ATLAS Collaboration, *Electron performance measurements with the ATLAS detector using the 2010 LHC proton-proton collision data*, Eur. Phys. J. **C72** (2012) 1909, arXiv:1110.3174 [hep-ex].
- [88] M. Botje et al., *The PDF4LHC Working Group Interim Recommendations* (2011), arXiv:1101.0538 [hep-ph].
- [89] A. Martin et al., *Parton distributions for the LHC*, Eur. Phys. J. **C63** (2009) 189, arXiv:0901.0002 [hep-ph].
- [90] R. D. Ball et al., *Parton distributions with LHC data*, Nucl. Phys. **B867** (2013) 244, arXiv:1207.1303 [hep-ph].
- [91] A. Hoecker and V. Kartvelishvili, *SVD approach to data unfolding*, Nucl. Instrum. Meth. **A372** (1996) 469, arXiv:hep-ph/9509307 [hep-ph].
- [92] Particle Data Group, K.A. Olive et al., *Review of Particle Physics*, Chin. Phys. **C38** (2014) 090001.
- [93] B. Efron, *Bootstrap Methods: Another Look at the Jackknife*, Ann. Statist. **7** (1979) 1.
- [94] H1 and ZEUS Collaborations, F. D. Aaron et al., *Combined Measurement and QCD Analysis of the Inclusive $e^\pm p$ Scattering Cross Sections at HERA*, JHEP **01** (2010) 109, arXiv:0911.0884 [hep-ex].
- [95] J. M. Campbell and R. K. Ellis, *MCFM for the Tevatron and the LHC*, Nucl. Phys. Proc. Suppl. **205** (2010) 10, arXiv:1007.3492 [hep-ph].

- [96] T. Carli et al., *A posteriori inclusion of parton density functions in NLO QCD final-state calculations at hadron colliders: The APPLGRID Project*, *Eur. Phys. J. C* **66** (2010) 503, arXiv:[0911.2985 \[hep-ph\]](https://arxiv.org/abs/0911.2985).

The ATLAS Collaboration

G. Aad⁸⁵, B. Abbott¹¹³, J. Abdallah¹⁵¹, O. Abdinov¹¹, R. Aben¹⁰⁷, M. Abolins⁹⁰, O.S. AbouZeid¹⁵⁸, H. Abramowicz¹⁵³, H. Abreu¹⁵², R. Abreu¹¹⁶, Y. Abulaiti^{146a,146b}, B.S. Acharya^{164a,164b,a}, L. Adamczyk^{38a}, D.L. Adams²⁵, J. Adelman¹⁰⁸, S. Adomeit¹⁰⁰, T. Adye¹³¹, A.A. Affolder⁷⁴, T. Agatonovic-Jovin¹³, J. Agricola⁵⁴, J.A. Aguilar-Saavedra^{126a,126f}, S.P. Ahlen²², F. Ahmadov^{65,b}, G. Aielli^{133a,133b}, H. Akerstedt^{146a,146b}, T.P.A. Åkesson⁸¹, A.V. Akimov⁹⁶, G.L. Alberghi^{20a,20b}, J. Albert¹⁶⁹, S. Albrand⁵⁵, M.J. Alconada Verzini⁷¹, M. Aleksi³⁰, I.N. Aleksandrov⁶⁵, C. Alexa^{26b}, G. Alexander¹⁵³, T. Alexopoulos¹⁰, M. Alhroob¹¹³, G. Alimonti^{91a}, L. Alio⁸⁵, J. Alison³¹, S.P. Alkire³⁵, B.M.M. Allbrooke¹⁴⁹, P.P. Allport¹⁸, A. Aloisio^{104a,104b}, A. Alonso³⁶, F. Alonso⁷¹, C. Alpigiani¹³⁸, A. Altheimer³⁵, B. Alvarez Gonzalez³⁰, D. Álvarez Piqueras¹⁶⁷, M.G. Alviggi^{104a,104b}, B.T. Amadio¹⁵, K. Amako⁶⁶, Y. Amaral Coutinho^{24a}, C. Amelung²³, D. Amidei⁸⁹, S.P. Amor Dos Santos^{126a,126c}, A. Amorim^{126a,126b}, S. Amoroso⁴⁸, N. Amram¹⁵³, G. Amundsen²³, C. Anastopoulos¹³⁹, L.S. Anzu⁴⁹, N. Andari¹⁰⁸, T. Andeen³⁵, C.F. Anders^{58b}, G. Anders³⁰, J.K. Anders⁷⁴, K.J. Anderson³¹, A. Andreazza^{91a,91b}, V. Andrei^{58a}, S. Angelidakis⁹, I. Angelozzi¹⁰⁷, P. Anger⁴⁴, A. Angerami³⁵, F. Anghinolfi³⁰, A.V. Anisenkov^{109,c}, N. Anjos¹², A. Annovi^{124a,124b}, M. Antonelli⁴⁷, A. Antonov⁹⁸, J. Antos^{144b}, F. Anulli^{132a}, M. Aoki⁶⁶, L. Aperio Bella¹⁸, G. Arabidze⁹⁰, Y. Arai⁶⁶, J.P. Araque^{126a}, A.T.H. Arce⁴⁵, F.A. Arduh⁷¹, J.-F. Arguin⁹⁵, S. Argyropoulos⁶³, M. Arik^{19a}, A.J. Armbruster³⁰, O. Arnaez³⁰, H. Arnold⁴⁸, M. Arratia²⁸, O. Arslan²¹, A. Artamonov⁹⁷, G. Artoni²³, S. Artz⁸³, S. Asai¹⁵⁵, N. Asbah⁴², A. Ashkenazi¹⁵³, B. Åsman^{146a,146b}, L. Asquith¹⁴⁹, K. Assamagan²⁵, R. Astalos^{144a}, M. Atkinson¹⁶⁵, N.B. Atlay¹⁴¹, K. Augsten¹²⁸, M. Aurousseau^{145b}, G. Avolio³⁰, B. Axen¹⁵, M.K. Ayoub¹¹⁷, G. Azuelos^{95,d}, M.A. Baak³⁰, A.E. Baas^{58a}, M.J. Baca¹⁸, C. Bacci^{134a,134b}, H. Bachacou¹³⁶, K. Bachas¹⁵⁴, M. Backes³⁰, M. Backhaus³⁰, P. Bagiacchi^{132a,132b}, P. Bagnaia^{132a,132b}, Y. Bai^{33a}, T. Bain³⁵, J.T. Baines¹³¹, O.K. Baker¹⁷⁶, E.M. Baldin^{109,c}, P. Balek¹²⁹, T. Balestri¹⁴⁸, F. Balli⁸⁴, W.K. Balunas¹²², E. Banas³⁹, Sw. Banerjee^{173,e}, A.A.E. Bannoura¹⁷⁵, L. Barak³⁰, E.L. Barberio⁸⁸, D. Barberis^{50a,50b}, M. Barbero⁸⁵, T. Barillari¹⁰¹, M. Barisonzi^{164a,164b}, T. Barklow¹⁴³, N. Barlow²⁸, S.L. Barnes⁸⁴, B.M. Barnett¹³¹, R.M. Barnett¹⁵, Z. Barnovska⁵, A. Baroncelli^{134a}, G. Barone²³, A.J. Barr¹²⁰, F. Barreiro⁸², J. Barreiro Guimarães da Costa^{33a}, R. Bartoldus¹⁴³, A.E. Barton⁷², P. Bartos^{144a}, A. Basalaev¹²³, A. Bassalat¹¹⁷, A. Basye¹⁶⁵, R.L. Bates⁵³, S.J. Batista¹⁵⁸, J.R. Batley²⁸, M. Battaglia¹³⁷, M. Bause^{132a,132b}, F. Bauer¹³⁶, H.S. Bawa^{143,f}, J.B. Beacham¹¹¹, M.D. Beattie⁷², T. Beau⁸⁰, P.H. Beauchemin¹⁶¹, R. Beccherle^{124a,124b}, P. Bechtle²¹, H.P. Beck^{17,g}, K. Becker¹²⁰, M. Becker⁸³, M. Beckingham¹⁷⁰, C. Becot¹¹⁷, A.J. Beddall^{19b}, A. Beddall^{19b}, V.A. Bednyakov⁶⁵, C.P. Bee¹⁴⁸, L.J. Beemster¹⁰⁷, T.A. Beermann³⁰, M. Begel²⁵, J.K. Behr¹²⁰, C. Belanger-Champagne⁸⁷, W.H. Bell⁴⁹, G. Bella¹⁵³, L. Bellagamba^{20a}, A. Bellerive²⁹, M. Bellomo⁸⁶, K. Belotskiy⁹⁸, O. Beltramello³⁰, O. Benary¹⁵³, D. Benchekroun^{135a}, M. Bender¹⁰⁰, K. Bendtz^{146a,146b}, N. Benekos¹⁰, Y. Benhammou¹⁵³, E. Benhar Noccioli⁴⁹, J.A. Benitez Garcia^{159b}, D.P. Benjamin⁴⁵, J.R. Bensinger²³, S. Bentvelsen¹⁰⁷, L. Beresford¹²⁰, M. Beretta⁴⁷, D. Berge¹⁰⁷, E. Bergeaas Kuutmann¹⁶⁶, N. Berger⁵, F. Berghaus¹⁶⁹, J. Beringer¹⁵, C. Bernard²², N.R. Bernard⁸⁶, C. Bernius¹¹⁰, F.U. Bernlochner²¹, T. Berry⁷⁷, P. Berta¹²⁹, C. Bertella⁸³, G. Bertoli^{146a,146b}, F. Bertolucci^{124a,124b}, C. Bertsche¹¹³, D. Bertsche¹¹³, M.I. Besana^{91a}, G.J. Besjes³⁶, O. Bessidskaia Bylund^{146a,146b}, M. Bessner⁴², N. Besson¹³⁶, C. Betancourt⁴⁸, S. Bethke¹⁰¹, A.J. Bevan⁷⁶, W. Bhimji¹⁵, R.M. Bianchi¹²⁵, L. Bianchini²³, M. Bianco³⁰, O. Biebel¹⁰⁰, D. Biedermann¹⁶, N.V. Biesuz^{124a,124b}, M. Biglietti^{134a}, J. Bilbao De Mendizabal⁴⁹, H. Bilokon⁴⁷, M. Bindi⁵⁴, S. Binet¹¹⁷, A. Bingul^{19b}, C. Bini^{132a,132b}, S. Biondi^{20a,20b}, D.M. Bjergaard⁴⁵, C.W. Black¹⁵⁰, J.E. Black¹⁴³, K.M. Black²², D. Blackburn¹³⁸, R.E. Blair⁶, J.-B. Blanchard¹³⁶,

J.E. Blanco⁷⁷, T. Blazek^{144a}, I. Bloch⁴², C. Blocker²³, W. Blum^{83,*}, U. Blumenschein⁵⁴,
 S. Blunier^{32a}, G.J. Bobbink¹⁰⁷, V.S. Bobrovnikov^{109,c}, S.S. Bocchetta⁸¹, A. Bocci⁴⁵, C. Bock¹⁰⁰,
 M. Boehler⁴⁸, J.A. Bogaerts³⁰, D. Bogavac¹³, A.G. Bogdanchikov¹⁰⁹, C. Bohm^{146a}, V. Boisvert⁷⁷,
 T. Bold^{38a}, V. Boldea^{26b}, A.S. Boldyrev⁹⁹, M. Bomben⁸⁰, M. Bona⁷⁶, M. Boonekamp¹³⁶,
 A. Borisov¹³⁰, G. Borissov⁷², S. Borroni⁴², J. Bortfeldt¹⁰⁰, V. Bortolotto^{60a,60b,60c}, K. Bos¹⁰⁷,
 D. Boscherini^{20a}, M. Bosman¹², J. Boudreau¹²⁵, J. Bouffard², E.V. Bouhova-Thacker⁷²,
 D. Boumediene³⁴, C. Bourdarios¹¹⁷, N. Bousson¹¹⁴, S.K. Boutle⁵³, A. Boveia³⁰, J. Boyd³⁰,
 I.R. Boyko⁶⁵, I. Bozic¹³, J. Bracinik¹⁸, A. Brandt⁸, G. Brandt⁵⁴, O. Brandt^{58a}, U. Bratzler¹⁵⁶,
 B. Brau⁸⁶, J.E. Brau¹¹⁶, H.M. Braun^{175,*}, W.D. Breaden Madden⁵³, K. Brendlinger¹²²,
 A.J. Brennan⁸⁸, L. Brenner¹⁰⁷, R. Brenner¹⁶⁶, S. Bressler¹⁷², T.M. Bristow⁴⁶, D. Britton⁵³,
 D. Britzger⁴², F.M. Brochu²⁸, I. Brock²¹, R. Brock⁹⁰, J. Bronner¹⁰¹, G. Brooijmans³⁵, T. Brooks⁷⁷,
 W.K. Brooks^{32b}, J. Brosamer¹⁵, E. Brost¹¹⁶, P.A. Bruckman de Renstrom³⁹, D. Bruncko^{144b},
 R. Bruneliere⁴⁸, A. Bruni^{20a}, G. Bruni^{20a}, M. Bruschi^{20a}, N. Bruscino²¹, L. Bryngemark⁸¹,
 T. Buanes¹⁴, Q. Buat¹⁴², P. Buchholz¹⁴¹, A.G. Buckley⁵³, I.A. Budagov⁶⁵, F. Buehrer⁴⁸, L. Bugge¹¹⁹,
 M.K. Bugge¹¹⁹, O. Bulekov⁹⁸, D. Bullock⁸, H. Burckhart³⁰, S. Burdin⁷⁴, C.D. Burgard⁴⁸,
 B. Burghgrave¹⁰⁸, S. Burke¹³¹, I. Burmeister⁴³, E. Busato³⁴, D. Büscher⁴⁸, V. Büscher⁸³,
 P. Bussey⁵³, J.M. Butler²², A.I. Butt³, C.M. Buttar⁵³, J.M. Butterworth⁷⁸, P. Butti¹⁰⁷, W. Buttinger²⁵,
 A. Buzatu⁵³, A.R. Buzykaev^{109,c}, S. Cabrera Urbán¹⁶⁷, D. Caforio¹²⁸, V.M. Cairo^{37a,37b}, O. Cakir^{4a},
 N. Calace⁴⁹, P. Calafiura¹⁵, A. Calandri¹³⁶, G. Calderini⁸⁰, P. Calfayan¹⁰⁰, L.P. Caloba^{24a},
 D. Calvet³⁴, S. Calvet³⁴, R. Camacho Toro³¹, S. Camarda⁴², P. Camarri^{133a,133b}, D. Cameron¹¹⁹,
 R. Caminal Armadans¹⁶⁵, S. Campana³⁰, M. Campanelli⁷⁸, A. Campoverde¹⁴⁸, V. Canale^{104a,104b},
 A. Canepa^{159a}, M. Cano Bret^{33e}, J. Cantero⁸², R. Cantrill^{126a}, T. Cao⁴⁰, M.D.M. Capeans Garrido³⁰,
 I. Caprini^{26b}, M. Caprini^{26b}, M. Capua^{37a,37b}, R. Caputo⁸³, R.M. Carbone³⁵, R. Cardarelli^{133a},
 F. Cardillo⁴⁸, T. Carli³⁰, G. Carlino^{104a}, L. Carminati^{91a,91b}, S. Caron¹⁰⁶, E. Carquin^{32a},
 G.D. Carrillo-Montoya³⁰, J.R. Carter²⁸, J. Carvalho^{126a,126c}, D. Casadei⁷⁸, M.P. Casado¹²,
 M. Casolino¹², D.W. Casper¹⁶³, E. Castaneda-Miranda^{145a}, A. Castelli¹⁰⁷, V. Castillo Gimenez¹⁶⁷,
 N.F. Castro^{126a,h}, P. Catastini⁵⁷, A. Catinaccio³⁰, J.R. Catmore¹¹⁹, A. Cattai³⁰, J. Caudron⁸³,
 V. Cavaliere¹⁶⁵, D. Cavalli^{91a}, M. Cavalli-Sforza¹², V. Cavasinni^{124a,124b}, F. Ceradini^{134a,134b},
 L. Cerdà Alberich¹⁶⁷, B.C. Cerio⁴⁵, K. Cerny¹²⁹, A.S. Cerqueira^{24b}, A. Cerri¹⁴⁹, L. Cerrito⁷⁶,
 F. Cerutti¹⁵, M. Cerv³⁰, A. Cervelli¹⁷, S.A. Cetin^{19c}, A. Chafaq^{135a}, D. Chakraborty¹⁰⁸,
 I. Chalupkova¹²⁹, Y.L. Chan^{60a}, P. Chang¹⁶⁵, J.D. Chapman²⁸, D.G. Charlton¹⁸, C.C. Chau¹⁵⁸,
 C.A. Chavez Barajas¹⁴⁹, S. Che¹¹¹, S. Cheatham¹⁵², A. Chegwidden⁹⁰, S. Chekanov⁶,
 S.V. Chekulaev^{159a}, G.A. Chelkov^{65,i}, M.A. Chelstowska⁸⁹, C. Chen⁶⁴, H. Chen²⁵, K. Chen¹⁴⁸,
 L. Chen^{33d,j}, S. Chen^{33c}, S. Chen¹⁵⁵, X. Chen^{33f}, Y. Chen⁶⁷, H.C. Cheng⁸⁹, Y. Cheng³¹,
 A. Cheplakov⁶⁵, E. Cheremushkina¹³⁰, R. Cherkaoui El Moursli^{135e}, V. Chernyatin^{25,*}, E. Cheu⁷,
 L. Chevalier¹³⁶, V. Chiarella⁴⁷, G. Chiarelli^{124a,124b}, G. Chiodini^{73a}, A.S. Chisholm¹⁸,
 R.T. Chislett⁷⁸, A. Chitan^{26b}, M.V. Chizhov⁶⁵, K. Choi⁶¹, S. Chouridou⁹, B.K.B. Chow¹⁰⁰,
 V. Christodoulou⁷⁸, D. Chromek-Burckhardt³⁰, J. Chudoba¹²⁷, A.J. Chuinard⁸⁷, J.J. Chwastowski³⁹,
 L. Chytka¹¹⁵, G. Ciapetti^{132a,132b}, A.K. Ciftci^{4a}, D. Cinca⁵³, V. Cindro⁷⁵, I.A. Cioara²¹, A. Ciocio¹⁵,
 F. Cirotto^{104a,104b}, Z.H. Citron¹⁷², M. Ciubancan^{26b}, A. Clark⁴⁹, B.L. Clark⁵⁷, P.J. Clark⁴⁶,
 R.N. Clarke¹⁵, C. Clement^{146a,146b}, Y. Coadou⁸⁵, M. Cobal^{164a,164c}, A. Coccaro⁴⁹, J. Cochran⁶⁴,
 L. Coffey²³, J.G. Cogan¹⁴³, L. Colasurdo¹⁰⁶, B. Cole³⁵, S. Cole¹⁰⁸, A.P. Colijn¹⁰⁷, J. Collot⁵⁵,
 T. Colombo^{58c}, G. Compostella¹⁰¹, P. Conde Muñoz^{126a,126b}, E. Coniavitis⁴⁸, S.H. Connell^{145b},
 I.A. Connolly⁷⁷, V. Consorti⁴⁸, S. Constantinescu^{26b}, C. Conta^{121a,121b}, G. Conti³⁰, F. Conventi^{104a,k},
 M. Cooke¹⁵, B.D. Cooper⁷⁸, A.M. Cooper-Sarkar¹²⁰, T. Cornelissen¹⁷⁵, M. Corradi^{132a,132b},
 F. Corriveau^{87,l}, A. Corso-Radu¹⁶³, A. Cortes-Gonzalez¹², G. Cortiana¹⁰¹, G. Costa^{91a},
 M.J. Costa¹⁶⁷, D. Costanzo¹³⁹, D. Côté⁸, G. Cottin²⁸, G. Cowan⁷⁷, B.E. Cox⁸⁴, K. Cranmer¹¹⁰,

G. Cree²⁹, S. Crépé-Renaudin⁵⁵, F. Crescioli⁸⁰, W.A. Cribbs^{146a,146b}, M. Crispin Ortuzar¹²⁰,
 M. Cristinziani²¹, V. Croft¹⁰⁶, G. Crosetti^{37a,37b}, T. Cuhadar Donszelmann¹³⁹, J. Cummings¹⁷⁶,
 M. Curatolo⁴⁷, J. Cúth⁸³, C. Cuthbert¹⁵⁰, H. Czirr¹⁴¹, P. Czodrowski³, S. D'Auria⁵³, M. D'Onofrio⁷⁴,
 M.J. Da Cunha Sargedas De Sousa^{126a,126b}, C. Da Via⁸⁴, W. Dabrowski^{38a}, A. Dafinca¹²⁰, T. Dai⁸⁹,
 O. Dale¹⁴, F. Dallaire⁹⁵, C. Dallapiccola⁸⁶, M. Dam³⁶, J.R. Dandoy³¹, N.P. Dang⁴⁸, A.C. Daniells¹⁸,
 M. Danninger¹⁶⁸, M. Dano Hoffmann¹³⁶, V. Dao⁴⁸, G. Darbo^{50a}, S. Darmora⁸, J. Dassoulas³,
 A. Dattagupta⁶¹, W. Davey²¹, C. David¹⁶⁹, T. Davidek¹²⁹, E. Davies^{120,m}, M. Davies¹⁵³,
 P. Davison⁷⁸, Y. Davygora^{58a}, E. Dawe⁸⁸, I. Dawson¹³⁹, R.K. Daya-Ishmukhametova⁸⁶, K. De⁸,
 R. de Asmundis^{104a}, A. De Benedetti¹¹³, S. De Castro^{20a,20b}, S. De Cecco⁸⁰, N. De Groot¹⁰⁶,
 P. de Jong¹⁰⁷, H. De la Torre⁸², F. De Lorenzi⁶⁴, D. De Pedis^{132a}, A. De Salvo^{132a}, U. De Sanctis¹⁴⁹,
 A. De Santo¹⁴⁹, J.B. De Vivie De Regie¹¹⁷, W.J. Dearnaley⁷², R. Debbe²⁵, C. Debenedetti¹³⁷,
 D.V. Dedovich⁶⁵, I. Deigaard¹⁰⁷, J. Del Peso⁸², T. Del Prete^{124a,124b}, D. Delgove¹¹⁷, F. Deliot¹³⁶,
 C.M. Delitzsch⁴⁹, M. Deliyergiyev⁷⁵, A. Dell'Acqua³⁰, L. Dell'Asta²², M. Dell'Orso^{124a,124b},
 M. Della Pietra^{104a,k}, D. della Volpe⁴⁹, M. Delmastro⁵, P.A. Delsart⁵⁵, C. Deluca¹⁰⁷,
 D.A. DeMarco¹⁵⁸, S. Demers¹⁷⁶, M. Demichev⁶⁵, A. Demilly⁸⁰, S.P. Denisov¹³⁰, D. Derendarz³⁹,
 J.E. Derkaoui^{135d}, F. Derue⁸⁰, P. Dervan⁷⁴, K. Desch²¹, C. Deterre⁴², K. Dette⁴³, P.O. Deviveiros³⁰,
 A. Dewhurst¹³¹, S. Dhaliwal²³, A. Di Ciaccio^{133a,133b}, L. Di Ciaccio⁵, A. Di Domenico^{132a,132b},
 C. Di Donato^{132a,132b}, A. Di Girolamo³⁰, B. Di Girolamo³⁰, A. Di Mattia¹⁵², B. Di Micco^{134a,134b},
 R. Di Nardo⁴⁷, A. Di Simone⁴⁸, R. Di Sipio¹⁵⁸, D. Di Valentino²⁹, C. Diaconu⁸⁵, M. Diamond¹⁵⁸,
 F.A. Dias⁴⁶, M.A. Diaz^{32a}, E.B. Diehl⁸⁹, J. Dietrich¹⁶, S. Diglio⁸⁵, A. Dimitrievska¹³,
 J. Dingfelder²¹, P. Dita^{26b}, S. Dita^{26b}, F. Dittus³⁰, F. Djama⁸⁵, T. Djobava^{51b}, J.I. Djuvsland^{58a},
 M.A.B. do Vale^{24c}, D. Dobos³⁰, M. Dobre^{26b}, C. Doglioni⁸¹, T. Dohmae¹⁵⁵, J. Dolejsi¹²⁹,
 Z. Dolezal¹²⁹, B.A. Dolgoshein^{98,*}, M. Donadelli^{24d}, S. Donati^{124a,124b}, P. Dondero^{121a,121b},
 J. Donini³⁴, J. Dopke¹³¹, A. Doria^{104a}, M.T. Dova⁷¹, A.T. Doyle⁵³, E. Drechsler⁵⁴, M. Dris¹⁰,
 Y. Du^{33d}, E. Dubreuil³⁴, E. Duchovni¹⁷², G. Duckeck¹⁰⁰, O.A. Ducu^{26b,85}, D. Duda¹⁰⁷,
 A. Dudarev³⁰, L. Duflot¹¹⁷, L. Duguid⁷⁷, M. Dührssen³⁰, M. Dunford^{58a}, H. Duran Yildiz^{4a},
 M. Düren⁵², A. Durglishvili^{51b}, D. Duschinger⁴⁴, B. Dutta⁴², M. Dyndal^{38a}, C. Eckardt⁴²,
 K.M. Ecker¹⁰¹, R.C. Edgar⁸⁹, W. Edson², N.C. Edwards⁴⁶, W. Ehrenfeld²¹, T. Eifert³⁰, G. Eigen¹⁴,
 K. Einsweiler¹⁵, T. Ekelof¹⁶⁶, M. El Kacimi^{135c}, M. Ellert¹⁶⁶, S. Elles⁵, F. Ellinghaus¹⁷⁵,
 A.A. Elliot¹⁶⁹, N. Ellis³⁰, J. Elmsheuser¹⁰⁰, M. Elsing³⁰, D. Emelyanov¹³¹, Y. Enari¹⁵⁵,
 O.C. Endner⁸³, M. Endo¹¹⁸, J. Erdmann⁴³, A. Ereditato¹⁷, G. Ernis¹⁷⁵, J. Ernst², M. Ernst²⁵,
 S. Errede¹⁶⁵, E. Ertel⁸³, M. Escalier¹¹⁷, H. Esch⁴³, C. Escobar¹²⁵, B. Esposito⁴⁷, A.I. Etienne¹³⁶,
 E. Etzion¹⁵³, H. Evans⁶¹, A. Ezhilov¹²³, F. Fabbri^{20a,20b}, L. Fabbri^{20a,20b}, G. Facini³¹,
 R.M. Fakhrutdinov¹³⁰, S. Falciano^{132a}, R.J. Falla⁷⁸, J. Faltova¹²⁹, Y. Fang^{33a}, M. Fanti^{91a,91b},
 A. Farbin⁸, A. Farilla^{134a}, T. Farooque¹², S. Farrell¹⁵, S.M. Farrington¹⁷⁰, P. Farthouat³⁰, F. Fassi^{135e},
 P. Fassnacht³⁰, D. Fassouliotis⁹, M. Faucci Giannelli⁷⁷, A. Favareto^{50a,50b}, L. Fayard¹¹⁷,
 O.L. Fedin^{123,n}, W. Fedorko¹⁶⁸, S. Feigl³⁰, L. Feligioni⁸⁵, C. Feng^{33d}, E.J. Feng³⁰, H. Feng⁸⁹,
 A.B. Fenyuk¹³⁰, L. Feremenga⁸, P. Fernandez Martinez¹⁶⁷, S. Fernandez Perez³⁰, J. Ferrando⁵³,
 A. Ferrari¹⁶⁶, P. Ferrari¹⁰⁷, R. Ferrari^{121a}, D.E. Ferreira de Lima⁵³, A. Ferrer¹⁶⁷, D. Ferrere⁴⁹,
 C. Ferretti⁸⁹, A. Ferretto Parodi^{50a,50b}, M. Fiascaris³¹, F. Fiedler⁸³, A. Filipčič⁷⁵, M. Filipuzzi⁴²,
 F. Filthaut¹⁰⁶, M. Fincke-Keeler¹⁶⁹, K.D. Finelli¹⁵⁰, M.C.N. Fiolhais^{126a,126c}, L. Fiorini¹⁶⁷,
 A. Firan⁴⁰, A. Fischer², C. Fischer¹², J. Fischer¹⁷⁵, W.C. Fisher⁹⁰, N. Flaschel⁴², I. Fleck¹⁴¹,
 P. Fleischmann⁸⁹, G.T. Fletcher¹³⁹, G. Fletcher⁷⁶, R.R.M. Fletcher¹²², T. Flick¹⁷⁵, A. Floderus⁸¹,
 L.R. Flores Castillo^{60a}, M.J. Flowerdew¹⁰¹, A. Formica¹³⁶, A. Forti⁸⁴, D. Fournier¹¹⁷, H. Fox⁷²,
 S. Fracchia¹², P. Francavilla⁸⁰, M. Franchini^{20a,20b}, D. Francis³⁰, L. Franconi¹¹⁹, M. Franklin⁵⁷,
 M. Frate¹⁶³, M. Fraternali^{121a,121b}, D. Freeborn⁷⁸, S.T. French²⁸, S.M. Fressard-Batraneanu³⁰,
 F. Friedrich⁴⁴, D. Froidevaux³⁰, J.A. Frost¹²⁰, C. Fukunaga¹⁵⁶, E. Fullana Torregrosa⁸³,

B.G. Fulsom¹⁴³, T. Fusayasu¹⁰², J. Fuster¹⁶⁷, C. Gabaldon⁵⁵, O. Gabizon¹⁷⁵, A. Gabrielli^{20a,20b}, A. Gabrielli¹⁵, G.P. Gach¹⁸, S. Gadatsch³⁰, S. Gadomski⁴⁹, G. Gagliardi^{50a,50b}, P. Gagnon⁶¹, C. Galea¹⁰⁶, B. Galhardo^{126a,126c}, E.J. Gallas¹²⁰, B.J. Gallop¹³¹, P. Gallus¹²⁸, G. Galster³⁶, K.K. Gan¹¹¹, J. Gao^{33b,85}, Y. Gao⁴⁶, Y.S. Gao^{143,f}, F.M. Garay Walls⁴⁶, F. Garberson¹⁷⁶, C. García¹⁶⁷, J.E. García Navarro¹⁶⁷, M. Garcia-Sciveres¹⁵, R.W. Gardner³¹, N. Garelli¹⁴³, V. Garonne¹¹⁹, C. Gatti⁴⁷, A. Gaudiello^{50a,50b}, G. Gaudio^{121a}, B. Gaur¹⁴¹, L. Gauthier⁹⁵, P. Gauzzi^{132a,132b}, I.L. Gavrilenko⁹⁶, C. Gay¹⁶⁸, G. Gaycken²¹, E.N. Gazis¹⁰, P. Ge^{33d}, Z. Gecse¹⁶⁸, C.N.P. Gee¹³¹, Ch. Geich-Gimbel²¹, M.P. Geisler^{58a}, C. Gemme^{50a}, M.H. Genest⁵⁵, C. Geng^{33b,o}, S. Gentile^{132a,132b}, M. George⁵⁴, S. George⁷⁷, D. Gerbaudo¹⁶³, A. Gershon¹⁵³, S. Ghasemi¹⁴¹, H. Ghazlane^{135b}, B. Giacobbe^{20a}, S. Giagu^{132a,132b}, V. Giangiobbe¹², P. Giannetti^{124a,124b}, B. Gibbard²⁵, S.M. Gibson⁷⁷, M. Gignac¹⁶⁸, M. Gilchriese¹⁵, T.P.S. Gillam²⁸, D. Gillberg³⁰, G. Gilles³⁴, D.M. Gingrich^{3,d}, N. Giokaris⁹, M.P. Giordani^{164a,164c}, F.M. Giorgi^{20a}, F.M. Giorgi¹⁶, P.F. Giraud¹³⁶, P. Giromini⁴⁷, D. Giugni^{91a}, C. Giuliani¹⁰¹, M. Giuliani^{58b}, B.K. Gjelsten¹¹⁹, S. Gkaitatzis¹⁵⁴, I. Gkialas¹⁵⁴, E.L. Gkougkousis¹¹⁷, L.K. Gladilin⁹⁹, C. Glasman⁸², J. Glatzer³⁰, P.C.F. Glaysher⁴⁶, A. Glazov⁴², M. Goblirsch-Kolb¹⁰¹, J.R. Goddard⁷⁶, J. Godlewski³⁹, S. Goldfarb⁸⁹, T. Golling⁴⁹, D. Golubkov¹³⁰, A. Gomes^{126a,126b,126d}, R. Gonçalo^{126a}, J. Goncalves Pinto Firmino Da Costa¹³⁶, L. Gonella²¹, S. González de la Hoz¹⁶⁷, G. Gonzalez Parra¹², S. Gonzalez-Sevilla⁴⁹, L. Goossens³⁰, P.A. Gorbounov⁹⁷, H.A. Gordon²⁵, I. Gorelov¹⁰⁵, B. Gorini³⁰, E. Gorini^{73a,73b}, A. Gorišek⁷⁵, E. Gornicki³⁹, A.T. Goshaw⁴⁵, C. Gössling⁴³, M.I. Gostkin⁶⁵, D. Goujdami^{135c}, A.G. Goussiou¹³⁸, N. Govender^{145b}, E. Gozani¹⁵², H.M.X. Grabas¹³⁷, L. Gruber⁵⁴, I. Grabowska-Bold^{38a}, P.O.J. Gradin¹⁶⁶, P. Grafström^{20a,20b}, J. Gramling⁴⁹, E. Gramstad¹¹⁹, S. Grancagnolo¹⁶, V. Gratchev¹²³, H.M. Gray³⁰, E. Graziani^{134a}, Z.D. Greenwood^{79,p}, C. Grefe²¹, K. Gregersen⁷⁸, I.M. Gregor⁴², P. Grenier¹⁴³, J. Griffiths⁸, A.A. Grillo¹³⁷, K. Grimm⁷², S. Grinstein^{12,q}, Ph. Gris³⁴, J.-F. Grivaz¹¹⁷, S. Groh⁸³, J.P. Grohs⁴⁴, A. Grohsjean⁴², E. Gross¹⁷², J. Grosse-Knetter⁵⁴, G.C. Grossi⁷⁹, Z.J. Grout¹⁴⁹, L. Guan⁸⁹, J. Guenther¹²⁸, F. Guescini⁴⁹, D. Guest¹⁶³, O. Gueta¹⁵³, E. Guido^{50a,50b}, T. Guillemin¹¹⁷, S. Guindon², U. Gul⁵³, C. Gumpert³⁰, J. Guo^{33e}, Y. Guo^{33b,o}, S. Gupta¹²⁰, G. Gustavino^{132a,132b}, P. Gutierrez¹¹³, N.G. Gutierrez Ortiz⁷⁸, C. Gutschow⁴⁴, C. Guyot¹³⁶, C. Gwenlan¹²⁰, C.B. Gwilliam⁷⁴, A. Haas¹¹⁰, C. Haber¹⁵, H.K. Hadavand⁸, N. Haddad^{135e}, P. Haefner²¹, S. Hageböck²¹, Z. Hajduk³⁹, H. Hakobyan¹⁷⁷, M. Haleem⁴², J. Haley¹¹⁴, D. Hall¹²⁰, G. Halladjian⁹⁰, G.D. Hallewell⁸⁵, K. Hamacher¹⁷⁵, P. Hamal¹¹⁵, K. Hamano¹⁶⁹, A. Hamilton^{145a}, G.N. Hamity¹³⁹, P.G. Hamnett⁴², L. Han^{33b}, K. Hanagaki^{66,r}, K. Hanawa¹⁵⁵, M. Hance¹³⁷, B. Haney¹²², P. Hanke^{58a}, R. Hanna¹³⁶, J.B. Hansen³⁶, J.D. Hansen³⁶, M.C. Hansen²¹, P.H. Hansen³⁶, K. Hara¹⁶⁰, A.S. Hard¹⁷³, T. Harenberg¹⁷⁵, F. Hariri¹¹⁷, S. Harkusha⁹², R.D. Harrington⁴⁶, P.F. Harrison¹⁷⁰, F. Hartjes¹⁰⁷, M. Hasegawa⁶⁷, Y. Hasegawa¹⁴⁰, A. Hasib¹¹³, S. Hassani¹³⁶, S. Haug¹⁷, R. Hauser⁹⁰, L. Hauswald⁴⁴, M. Havranek¹²⁷, C.M. Hawkes¹⁸, R.J. Hawkings³⁰, A.D. Hawkins⁸¹, T. Hayashi¹⁶⁰, D. Hayden⁹⁰, C.P. Hays¹²⁰, J.M. Hays⁷⁶, H.S. Hayward⁷⁴, S.J. Haywood¹³¹, S.J. Head¹⁸, T. Heck⁸³, V. Hedberg⁸¹, L. Heelan⁸, S. Heim¹²², T. Heim¹⁷⁵, B. Heinemann¹⁵, L. Heinrich¹¹⁰, J. Hejbal¹²⁷, L. Helary²², S. Hellman^{146a,146b}, C. Helsens³⁰, J. Henderson¹²⁰, R.C.W. Henderson⁷², Y. Heng¹⁷³, C. Hengler⁴², S. Henkelmann¹⁶⁸, A. Henrichs¹⁷⁶, A.M. Henriques Correia³⁰, S. Henrot-Versille¹¹⁷, G.H. Herbert¹⁶, Y. Hernández Jiménez¹⁶⁷, G. Herten⁴⁸, R. Hertenberger¹⁰⁰, L. Hervas³⁰, G.G. Hesketh⁷⁸, N.P. Hessey¹⁰⁷, J.W. Hetherly⁴⁰, R. Hickling⁷⁶, E. Higón-Rodriguez¹⁶⁷, E. Hill¹⁶⁹, J.C. Hill²⁸, K.H. Hiller⁴², S.J. Hillier¹⁸, I. Hinchliffe¹⁵, E. Hines¹²², R.R. Hinman¹⁵, M. Hirose¹⁵⁷, D. Hirschbuehl¹⁷⁵, J. Hobbs¹⁴⁸, N. Hod¹⁰⁷, M.C. Hodgkinson¹³⁹, P. Hodgson¹³⁹, A. Hoecker³⁰, M.R. Hoeferkamp¹⁰⁵, F. Hoenig¹⁰⁰, M. Hohlfeld⁸³, D. Hohn²¹, T.R. Holmes¹⁵, M. Homann⁴³, T.M. Hong¹²⁵, W.H. Hopkins¹¹⁶, Y. Horii¹⁰³, A.J. Horton¹⁴², J.-Y. Hostachy⁵⁵, S. Hou¹⁵¹, A. Hoummada^{135a}, J. Howard¹²⁰, J. Howarth⁴², M. Hrabovsky¹¹⁵, I. Hristova¹⁶, J. Hrvnac¹¹⁷,

T. Hryn'ova⁵, A. Hrynevich⁹³, C. Hsu^{145c}, P.J. Hsu^{151,s}, S.-C. Hsu¹³⁸, D. Hu³⁵, Q. Hu^{33b}, X. Hu⁸⁹,
 Y. Huang⁴², Z. Hubacek¹²⁸, F. Hubaut⁸⁵, F. Huegging²¹, T.B. Huffman¹²⁰, E.W. Hughes³⁵,
 G. Hughes⁷², M. Huhtinen³⁰, T.A. Hülsing⁸³, N. Huseynov^{65,b}, J. Huston⁹⁰, J. Huth⁵⁷,
 G. Iacobucci⁴⁹, G. Iakovidis²⁵, I. Ibragimov¹⁴¹, L. Iconomidou-Fayard¹¹⁷, E. Ideal¹⁷⁶, Z. Idrissi^{135e},
 P. Iengo³⁰, O. Igonkina¹⁰⁷, T. Iizawa¹⁷¹, Y. Ikegami⁶⁶, M. Ikeno⁶⁶, Y. Ilchenko^{31,t}, D. Iliadis¹⁵⁴,
 N. Ilic¹⁴³, T. Ince¹⁰¹, G. Introzzi^{121a,121b}, P. Ioannou⁹, M. Iodice^{134a}, K. Iordanidou³⁵, V. Ippolito⁵⁷,
 A. Irles Quiles¹⁶⁷, C. Isaksson¹⁶⁶, M. Ishino⁶⁸, M. Ishitsuka¹⁵⁷, R. Ishmukhametov¹¹¹, C. Issever¹²⁰,
 S. Istin^{19a}, J.M. Iturbe Ponce⁸⁴, R. Iuppa^{133a,133b}, J. Ivarsson⁸¹, W. Iwanski³⁹, H. Iwasaki⁶⁶,
 J.M. Izen⁴¹, V. Izzo^{104a}, S. Jabbar³, B. Jackson¹²², M. Jackson⁷⁴, P. Jackson¹, M.R. Jaekel³⁰,
 V. Jain², K.B. Jakobi⁸³, K. Jakobs⁴⁸, S. Jakobsen³⁰, T. Jakoubek¹²⁷, J. Jakubek¹²⁸, D.O. Jamin¹¹⁴,
 D.K. Jana⁷⁹, E. Jansen⁷⁸, R. Jansky⁶², J. Janssen²¹, M. Janus⁵⁴, G. Jarlskog⁸¹, N. Javadov^{65,b},
 T. Javůrek⁴⁸, L. Jeanty¹⁵, J. Jejelava^{51a,u}, G.-Y. Jeng¹⁵⁰, D. Jennens⁸⁸, P. Jenni^{48,v}, J. Jentzsch⁴³,
 C. Jeske¹⁷⁰, S. Jézéquel⁵, H. Ji¹⁷³, J. Jia¹⁴⁸, H. Jiang⁶⁴, Y. Jiang^{33b}, S. Jiggins⁷⁸, J. Jimenez Pena¹⁶⁷,
 S. Jin^{33a}, A. Jinaru^{26b}, O. Jinnouchi¹⁵⁷, M.D. Joergensen³⁶, P. Johansson¹³⁹, K.A. Johns⁷,
 W.J. Johnson¹³⁸, K. Jon-And^{146a,146b}, G. Jones¹⁷⁰, R.W.L. Jones⁷², T.J. Jones⁷⁴, J. Jongmanns^{58a},
 P.M. Jorge^{126a,126b}, K.D. Joshi⁸⁴, J. Jovicevic^{159a}, X. Ju¹⁷³, A. Juste Rozas^{12,q}, M. Kaci¹⁶⁷,
 A. Kaczmarska³⁹, M. Kado¹¹⁷, H. Kagan¹¹¹, M. Kagan¹⁴³, S.J. Kahn⁸⁵, E. Kajomovitz⁴⁵,
 C.W. Kalderon¹²⁰, A. Kaluza⁸³, S. Kama⁴⁰, A. Kamenshchikov¹³⁰, N. Kanaya¹⁵⁵, S. Kaneti²⁸,
 V.A. Kantserov⁹⁸, J. Kanzaki⁶⁶, B. Kaplan¹¹⁰, L.S. Kaplan¹⁷³, A. Kapliy³¹, D. Kar^{145c},
 K. Karakostas¹⁰, A. Karamaoun³, N. Karastathis^{10,107}, M.J. Kareem⁵⁴, E. Karentzos¹⁰,
 M. Karnevskiy⁸³, S.N. Karpov⁶⁵, Z.M. Karpova⁶⁵, K. Karthik¹¹⁰, V. Kartvelishvili⁷²,
 A.N. Karyukhin¹³⁰, K. Kasahara¹⁶⁰, L. Kashif¹⁷³, R.D. Kass¹¹¹, A. Kastanas¹⁴, Y. Kataoka¹⁵⁵,
 C. Kato¹⁵⁵, A. Katre⁴⁹, J. Katzy⁴², K. Kawade¹⁰³, K. Kawagoe⁷⁰, T. Kawamoto¹⁵⁵, G. Kawamura⁵⁴,
 S. Kazama¹⁵⁵, V.F. Kazanin^{109,c}, R. Keeler¹⁶⁹, R. Kehoe⁴⁰, J.S. Keller⁴², J.J. Kempster⁷⁷,
 H. Keoshkerian⁸⁴, O. Kepka¹²⁷, B.P. Kerševan⁷⁵, S. Kersten¹⁷⁵, R.A. Keyes⁸⁷, F. Khalil-zada¹¹,
 H. Khandanyan^{146a,146b}, A. Khanov¹¹⁴, A.G. Kharlamov^{109,c}, T.J. Khoo²⁸, V. Khovanskiy⁹⁷,
 E. Khramov⁶⁵, J. Khubua^{51b,w}, S. Kido⁶⁷, H.Y. Kim⁸, S.H. Kim¹⁶⁰, Y.K. Kim³¹, N. Kimura¹⁵⁴,
 O.M. Kind¹⁶, B.T. King⁷⁴, M. King¹⁶⁷, S.B. King¹⁶⁸, J. Kirk¹³¹, A.E. Kiryunin¹⁰¹, T. Kishimoto⁶⁷,
 D. Kisielewska^{38a}, F. Kiss⁴⁸, K. Kiuchi¹⁶⁰, O. Kivernyk¹³⁶, E. Kladiva^{144b}, M.H. Klein³⁵, M. Klein⁷⁴,
 U. Klein⁷⁴, K. Kleinknecht⁸³, P. Klimek^{146a,146b}, A. Klimentov²⁵, R. Klingenberg⁴³, J.A. Klinger¹³⁹,
 T. Klioutchnikova³⁰, E.-E. Kluge^{58a}, P. Kluit¹⁰⁷, S. Kluth¹⁰¹, J. Knapik³⁹, E. Kneringer⁶²,
 E.B.F.G. Knoops⁸⁵, A. Knue⁵³, A. Kobayashi¹⁵⁵, D. Kobayashi¹⁵⁷, T. Kobayashi¹⁵⁵, M. Kobel⁴⁴,
 M. Kocian¹⁴³, P. Kodys¹²⁹, T. Koffas²⁹, E. Koffeman¹⁰⁷, L.A. Kogan¹²⁰, S. Kohlmann¹⁷⁵,
 Z. Kohout¹²⁸, T. Kohriki⁶⁶, T. Koi¹⁴³, H. Kolanoski¹⁶, M. Kolb^{58b}, I. Koletsou⁵, A.A. Komar^{96,*},
 Y. Komori¹⁵⁵, T. Kondo⁶⁶, N. Kondrashova⁴², K. Köneke⁴⁸, A.C. König¹⁰⁶, T. Kono^{66,x},
 R. Konoplich^{110,y}, N. Konstantinidis⁷⁸, R. Kopeliansky¹⁵², S. Koperny^{38a}, L. Köpke⁸³, A.K. Kopp⁴⁸,
 K. Korcyl³⁹, K. Kordas¹⁵⁴, A. Korn⁷⁸, A.A. Korol^{109,c}, I. Korolkov¹², E.V. Korolkova¹³⁹,
 O. Kortner¹⁰¹, S. Kortner¹⁰¹, T. Kosek¹²⁹, V.V. Kostyukhin²¹, V.M. Kotov⁶⁵, A. Kotwal⁴⁵,
 A. Kourkoumeli-Charalampidi¹⁵⁴, C. Kourkoumelis⁹, V. Kouskoura²⁵, A. Koutsman^{159a},
 R. Kowalewski¹⁶⁹, T.Z. Kowalski^{38a}, W. Kozanecki¹³⁶, A.S. Kozhin¹³⁰, V.A. Kramarenko⁹⁹,
 G. Kramberger⁷⁵, D. Krasnopevtsev⁹⁸, M.W. Krasny⁸⁰, A. Krasznahorkay³⁰, J.K. Kraus²¹,
 A. Kravchenko²⁵, S. Kreiss¹¹⁰, M. Kretz^{58c}, J. Kretzschmar⁷⁴, K. Kreutzfeldt⁵², P. Krieger¹⁵⁸,
 K. Krizka³¹, K. Kroeninger⁴³, H. Kroha¹⁰¹, J. Kroll¹²², J. Kroseberg²¹, J. Krstic¹³, U. Kruchonak⁶⁵,
 H. Krüger²¹, N. Krumnack⁶⁴, A. Kruse¹⁷³, M.C. Kruse⁴⁵, M. Kruskal²², T. Kubota⁸⁸, H. Kucuk⁷⁸,
 S. Kuday^{4b}, S. Kuehn⁴⁸, A. Kugel^{58c}, F. Kuger¹⁷⁴, A. Kuhl¹³⁷, T. Kuhl⁴², V. Kukhtin⁶⁵, R. Kukla¹³⁶,
 Y. Kulchitsky⁹², S. Kuleshov^{32b}, M. Kuna^{132a,132b}, T. Kunigo⁶⁸, A. Kupco¹²⁷, H. Kurashige⁶⁷,
 Y.A. Kurochkin⁹², V. Kus¹²⁷, E.S. Kuwertz¹⁶⁹, M. Kuze¹⁵⁷, J. Kvita¹¹⁵, T. Kwan¹⁶⁹,

D. Kyriazopoulos¹³⁹, A. La Rosa¹³⁷, J.L. La Rosa Navarro^{24d}, L. La Rotonda^{37a,37b}, C. Lacasta¹⁶⁷, F. Lacava^{132a,132b}, J. Lacey²⁹, H. Lacker¹⁶, D. Lacour⁸⁰, V.R. Lacuesta¹⁶⁷, E. Ladygin⁶⁵, R. Lafaye⁵, B. Laforge⁸⁰, T. Lagouri¹⁷⁶, S. Lai⁵⁴, L. Lambourne⁷⁸, S. Lammers⁶¹, C.L. Lampen⁷, W. Lampl⁷, E. Lançon¹³⁶, U. Landgraf⁴⁸, M.P.J. Landon⁷⁶, V.S. Lang^{58a}, J.C. Lange¹², A.J. Lankford¹⁶³, F. Lanni²⁵, K. Lantzsch²¹, A. Lanza^{121a}, S. Laplace⁸⁰, C. Lapoire³⁰, J.F. Laporte¹³⁶, T. Lari^{91a}, F. Lasagni Manghi^{20a,20b}, M. Lassnig³⁰, P. Laurelli⁴⁷, W. Lavrijsen¹⁵, A.T. Law¹³⁷, P. Laycock⁷⁴, T. Lazovich⁵⁷, O. Le Dortz⁸⁰, E. Le Guirriec⁸⁵, E. Le Menedeu¹², M. LeBlanc¹⁶⁹, T. LeCompte⁶, F. Ledroit-Guillon⁵⁵, C.A. Lee^{145a}, S.C. Lee¹⁵¹, L. Lee¹, G. Lefebvre⁸⁰, M. Lefebvre¹⁶⁹, F. Legger¹⁰⁰, C. Leggett¹⁵, A. Lehan⁷⁴, G. Lehmann Miotto³⁰, X. Lei⁷, W.A. Leight²⁹, A. Leisos^{154,z}, A.G. Leister¹⁷⁶, M.A.L. Leite^{24d}, R. Leitner¹²⁹, D. Lellouch¹⁷², B. Lemmer⁵⁴, K.J.C. Leney⁷⁸, T. Lenz²¹, B. Lenzi³⁰, R. Leone⁷, S. Leone^{124a,124b}, C. Leonidopoulos⁴⁶, S. Leontsinis¹⁰, C. Leroy⁹⁵, C.G. Lester²⁸, M. Levchenko¹²³, J. Levêque⁵, D. Levin⁸⁹, L.J. Levinson¹⁷², M. Levy¹⁸, A. Lewis¹²⁰, A.M. Leyko²¹, M. Leyton⁴¹, B. Li^{33b,aa}, H. Li¹⁴⁸, H.L. Li³¹, L. Li⁴⁵, L. Li^{33e}, S. Li⁴⁵, X. Li⁸⁴, Y. Li^{33c,ab}, Z. Liang¹³⁷, H. Liao³⁴, B. Libert^{133a}, A. Liblong¹⁵⁸, P. Lichard³⁰, K. Lie¹⁶⁵, J. Liebal²¹, W. Liebig¹⁴, C. Limbach²¹, A. Limosani¹⁵⁰, S.C. Lin^{151,ac}, T.H. Lin⁸³, F. Linde¹⁰⁷, B.E. Lindquist¹⁴⁸, J.T. Linnemann⁹⁰, E. Lipeles¹²², A. Lipniacka¹⁴, M. Lisovyi^{58b}, T.M. Liss¹⁶⁵, D. Lissauer²⁵, A. Lister¹⁶⁸, A.M. Litke¹³⁷, B. Liu^{151,ad}, D. Liu¹⁵¹, H. Liu⁸⁹, J. Liu⁸⁵, J.B. Liu^{33b}, K. Liu⁸⁵, L. Liu¹⁶⁵, M. Liu⁴⁵, M. Liu^{33b}, Y. Liu^{33b}, M. Livan^{121a,121b}, A. Lleres⁵⁵, J. Llorente Merino⁸², S.L. Lloyd⁷⁶, F. Lo Sterzo¹⁵¹, E. Lobodzinska⁴², P. Loch⁷, W.S. Lockman¹³⁷, F.K. Loebinger⁸⁴, A.E. Loevschall-Jensen³⁶, K.M. Loew²³, A. Loginov¹⁷⁶, T. Lohse¹⁶, K. Lohwasser⁴², M. Lokajicek¹²⁷, B.A. Long²², J.D. Long¹⁶⁵, R.E. Long⁷², K.A.Looper¹¹¹, L. Lopes^{126a}, D. Lopez Mateos⁵⁷, B. Lopez Paredes¹³⁹, I. Lopez Paz¹², J. Lorenz¹⁰⁰, N. Lorenzo Martinez⁶¹, M. Losada¹⁶², P.J. Lösel¹⁰⁰, X. Lou^{33a}, A. Lounis¹¹⁷, J. Love⁶, P.A. Love⁷², H. Lu^{60a}, N. Lu⁸⁹, H.J. Lubatti¹³⁸, C. Luci^{132a,132b}, A. Lucotte⁵⁵, C. Luedtke⁴⁸, F. Luehring⁶¹, W. Lukas⁶², L. Luminari^{132a}, O. Lundberg^{146a,146b}, B. Lund-Jensen¹⁴⁷, D. Lynn²⁵, R. Lysak¹²⁷, E. Lytken⁸¹, H. Ma²⁵, L.L. Ma^{33d}, G. Maccarrone⁴⁷, A. Macchiolo¹⁰¹, C.M. Macdonald¹³⁹, B. Maćek⁷⁵, J. Machado Miguens^{122,126b}, D. Macina³⁰, D. Madaffari⁸⁵, R. Madar³⁴, H.J. Maddocks⁷², W.F. Mader⁴⁴, A. Madsen⁴², J. Maeda⁶⁷, S. Maeland¹⁴, T. Maeno²⁵, A. Maevskiy⁹⁹, E. Magradze⁵⁴, K. Mahboubi⁴⁸, J. Mahlstedt¹⁰⁷, C. Maiani¹³⁶, C. Maidantchik^{24a}, A.A. Maier¹⁰¹, T. Maier¹⁰⁰, A. Maio^{126a,126b,126d}, S. Majewski¹¹⁶, Y. Makida⁶⁶, N. Makovec¹¹⁷, B. Malaescu⁸⁰, Pa. Malecki³⁹, V.P. Maleev¹²³, F. Malek⁵⁵, U. Mallik⁶³, D. Malon⁶, C. Malone¹⁴³, S. Maltezos¹⁰, V.M. Malyshev¹⁰⁹, S. Malyukov³⁰, J. Mamuzic⁴², G. Mancini⁴⁷, B. Mandelli³⁰, L. Mandelli^{91a}, I. Mandić⁷⁵, R. Mandrysch⁶³, J. Maneira^{126a,126b}, L. Manhaes de Andrade Filho^{24b}, J. Manjarres Ramos^{159b}, A. Mann¹⁰⁰, A. Manousakis-Katsikakis⁹, B. Mansoulie¹³⁶, R. Mantifel⁸⁷, M. Mantoani⁵⁴, L. Mapelli³⁰, L. March^{145c}, G. Marchiori⁸⁰, M. Marcisovsky¹²⁷, C.P. Marino¹⁶⁹, M. Marjanovic¹³, D.E. Marley⁸⁹, F. Marroquim^{24a}, S.P. Marsden⁸⁴, Z. Marshall¹⁵, L.F. Marti¹⁷, S. Marti-Garcia¹⁶⁷, B. Martin⁹⁰, T.A. Martin¹⁷⁰, V.J. Martin⁴⁶, B. Martin dit Latour¹⁴, M. Martinez^{12,q}, S. Martin-Haugh¹³¹, V.S. Martoiu^{26b}, A.C. Martyniuk⁷⁸, M. Marx¹³⁸, F. Marzano^{132a}, A. Marzin³⁰, L. Masetti⁸³, T. Mashimo¹⁵⁵, R. Mashinistov⁹⁶, J. Masił⁸⁴, A.L. Maslennikov^{109,c}, I. Massa^{20a,20b}, L. Massa^{20a,20b}, P. Mastrandrea⁵, A. Mastroberardino^{37a,37b}, T. Masubuchi¹⁵⁵, P. Mättig¹⁷⁵, J. Mattmann⁸³, J. Maurer^{26b}, S.J. Maxfield⁷⁴, D.A. Maximov^{109,c}, R. Mazini¹⁵¹, S.M. Mazza^{91a,91b}, G. Mc Goldrick¹⁵⁸, S.P. Mc Kee⁸⁹, A. McCarn⁸⁹, R.L. McCarthy¹⁴⁸, T.G. McCarthy²⁹, N.A. McCubbin¹³¹, K.W. McFarlane^{56,*}, J.A. McFayden⁷⁸, G. Mchedlidze⁵⁴, S.J. McMahon¹³¹, R.A. McPherson^{169,l}, M. Medinnis⁴², S. Meehan¹³⁸, S. Mehlhase¹⁰⁰, A. Mehta⁷⁴, K. Meier^{58a}, C. Meineck¹⁰⁰, B. Meirose⁴¹, B.R. Mellado Garcia^{145c}, F. Meloni¹⁷, A. Mengarelli^{20a,20b}, S. Menke¹⁰¹, E. Meoni¹⁶¹, K.M. Mercurio⁵⁷, S. Mergelmeyer²¹, P. Mermod⁴⁹, L. Merola^{104a,104b}, C. Meroni^{91a}, F.S. Merritt³¹, A. Messina^{132a,132b}, J. Metcalfe⁶,

A.S. Mete¹⁶³, C. Meyer⁸³, C. Meyer¹²², J.-P. Meyer¹³⁶, J. Meyer¹⁰⁷, H. Meyer Zu Theenhausen^{58a}, R.P. Middleton¹³¹, S. Miglioranzo^{164a,164c}, L. Mijović²¹, G. Mikenberg¹⁷², M. Mikestikova¹²⁷, M. Mikuž⁷⁵, M. Milesi⁸⁸, A. Milic³⁰, D.W. Miller³¹, C. Mills⁴⁶, A. Milov¹⁷², D.A. Milstead^{146a,146b}, A.A. Minaenko¹³⁰, Y. Minami¹⁵⁵, I.A. Minashvili⁶⁵, A.I. Mincer¹¹⁰, B. Mindur^{38a}, M. Mineev⁶⁵, Y. Ming¹⁷³, L.M. Mir¹², K.P. Mistry¹²², T. Mitani¹⁷¹, J. Mitrevski¹⁰⁰, V.A. Mitsou¹⁶⁷, A. Miucci⁴⁹, P.S. Miyagawa¹³⁹, J.U. Mjörnmark⁸¹, T. Moa^{146a,146b}, K. Mochizuki⁸⁵, S. Mohapatra³⁵, W. Mohr⁴⁸, S. Molander^{146a,146b}, R. Moles-Valls²¹, R. Monden⁶⁸, M.C. Mondragon⁹⁰, K. Mönig⁴², C. Monini⁵⁵, J. Monk³⁶, E. Monnier⁸⁵, A. Montalbano¹⁴⁸, J. Montejo Berlingen³⁰, F. Monticelli⁷¹, S. Monzani^{132a,132b}, R.W. Moore³, N. Morange¹¹⁷, D. Moreno¹⁶², M. Moreno Llácer⁵⁴, P. Morettini^{50a}, D. Mori¹⁴², T. Mori¹⁵⁵, M. Morii⁵⁷, M. Morinaga¹⁵⁵, V. Morisbak¹¹⁹, S. Moritz⁸³, A.K. Morley¹⁵⁰, G. Mornacchi³⁰, J.D. Morris⁷⁶, S.S. Mortensen³⁶, A. Morton⁵³, L. Morvaj¹⁰³, M. Mosidze^{51b}, J. Moss¹⁴³, K. Motohashi¹⁵⁷, R. Mount¹⁴³, E. Mountricha²⁵, S.V. Mouraviev^{96,*}, E.J.W. Moyse⁸⁶, S. Muanza⁸⁵, R.D. Mudd¹⁸, F. Mueller¹⁰¹, J. Mueller¹²⁵, R.S.P. Mueller¹⁰⁰, T. Mueller²⁸, D. Muenstermann⁴⁹, P. Mullen⁵³, G.A. Mullier¹⁷, F.J. Munoz Sanchez⁸⁴, J.A. Murillo Quijada¹⁸, W.J. Murray^{170,131}, H. Musheghyan⁵⁴, E. Musto¹⁵², A.G. Myagkov^{130,ae}, M. Myska¹²⁸, B.P. Nachman¹⁴³, O. Nackenhorst⁴⁹, J. Nadal⁵⁴, K. Nagai¹²⁰, R. Nagai¹⁵⁷, Y. Nagai⁸⁵, K. Nagano⁶⁶, A. Nagarkar¹¹¹, Y. Nagasaka⁵⁹, K. Nagata¹⁶⁰, M. Nagel¹⁰¹, E. Nagy⁸⁵, A.M. Nairz³⁰, Y. Nakahama³⁰, K. Nakamura⁶⁶, T. Nakamura¹⁵⁵, I. Nakano¹¹², H. Namasivayam⁴¹, R.F. Naranjo Garcia⁴², R. Narayan³¹, D.I. Narrias Villar^{58a}, T. Naumann⁴², G. Navarro¹⁶², R. Nayyar⁷, H.A. Neal⁸⁹, P.Yu. Nechaeva⁹⁶, T.J. Neep⁸⁴, P.D. Nef¹⁴³, A. Negri^{121a,121b}, M. Negrini^{20a}, S. Nektarijevic¹⁰⁶, C. Nellist¹¹⁷, A. Nelson¹⁶³, S. Nemecek¹²⁷, P. Nemethy¹¹⁰, A.A. Nepomuceno^{24a}, M. Nessi^{30,af}, M.S. Neubauer¹⁶⁵, M. Neumann¹⁷⁵, R.M. Neves¹¹⁰, P. Nevski²⁵, P.R. Newman¹⁸, D.H. Nguyen⁶, R.B. Nickerson¹²⁰, R. Nicolaïdou¹³⁶, B. Nicquevert³⁰, J. Nielsen¹³⁷, N. Nikiforou³⁵, A. Nikiforov¹⁶, V. Nikolaenko^{130,ae}, I. Nikolic-Audit⁸⁰, K. Nikolopoulos¹⁸, J.K. Nilsen¹¹⁹, P. Nilsson²⁵, Y. Ninomiya¹⁵⁵, A. Nisati^{132a}, R. Nisius¹⁰¹, T. Nobe¹⁵⁵, L. Nodulman⁶, M. Nomachi¹¹⁸, I. Nomidis²⁹, T. Nooney⁷⁶, S. Norberg¹¹³, M. Nordberg³⁰, O. Novgorodova⁴⁴, S. Nowak¹⁰¹, M. Nozaki⁶⁶, L. Nozka¹¹⁵, K. Ntekas¹⁰, G. Nunes Hanninger⁸⁸, T. Nunnemann¹⁰⁰, E. Nurse⁷⁸, F. Nuti⁸⁸, F. O'grady⁷, D.C. O'Neil¹⁴², V. O'Shea⁵³, F.G. Oakham^{29,d}, H. Oberlack¹⁰¹, T. Obermann²¹, J. Ocariz⁸⁰, A. Ochi⁶⁷, I. Ochoa³⁵, J.P. Ochoa-Ricoux^{32a}, S. Oda⁷⁰, S. Odaka⁶⁶, H. Ogren⁶¹, A. Oh⁸⁴, S.H. Oh⁴⁵, C.C. Ohm¹⁵, H. Ohman¹⁶⁶, H. Oide³⁰, W. Okamura¹¹⁸, H. Okawa¹⁶⁰, Y. Okumura³¹, T. Okuyama⁶⁶, A. Olariu^{26b}, S.A. Olivares Pino⁴⁶, D. Oliveira Damazio²⁵, A. Olszewski³⁹, J. Olszowska³⁹, A. Onofre^{126a,126e}, K. Onogi¹⁰³, P.U.E. Onyisi^{31,t}, C.J. Oram^{159a}, M.J. Oreglia³¹, Y. Oren¹⁵³, D. Orestano^{134a,134b}, N. Orlando¹⁵⁴, C. Oropeza Barrera⁵³, R.S. Orr¹⁵⁸, B. Osculati^{50a,50b}, R. Ospanov⁸⁴, G. Otero y Garzon²⁷, H. Otono⁷⁰, M. Ouchrif^{135d}, F. Ould-Saada¹¹⁹, A. Ourau¹³⁶, K.P. Oussoren¹⁰⁷, Q. Ouyang^{33a}, A. Ovcharova¹⁵, M. Owen⁵³, R.E. Owen¹⁸, V.E. Ozcan^{19a}, N. Ozturk⁸, K. Pachal¹⁴², A. Pacheco Pages¹², C. Padilla Aranda¹², M. Pagáčová⁴⁸, S. Pagan Griso¹⁵, E. Paganis¹³⁹, F. Paige²⁵, P. Pais⁸⁶, K. Pajchel¹¹⁹, G. Palacino^{159b}, S. Palestini³⁰, M. Palka^{38b}, D. Pallin³⁴, A. Palma^{126a,126b}, Y.B. Pan¹⁷³, E.St. Panagiotopoulou¹⁰, C.E. Pandini⁸⁰, J.G. Panduro Vazquez⁷⁷, P. Pani^{146a,146b}, S. Panitkin²⁵, D. Pantea^{26b}, L. Paolozzi⁴⁹, Th.D. Papadopoulou¹⁰, K. Papageorgiou¹⁵⁴, A. Paramonov⁶, D. Paredes Hernandez¹⁷⁶, M.A. Parker²⁸, K.A. Parker¹³⁹, F. Parodi^{50a,50b}, J.A. Parsons³⁵, U. Parzefall⁴⁸, E. Pasqualucci^{132a}, S. Passaggio^{50a}, F. Pastore^{134a,134b,*}, Fr. Pastore⁷⁷, G. Pásztor²⁹, S. Pataraia¹⁷⁵, N.D. Patel¹⁵⁰, J.R. Pater⁸⁴, T. Pauly³⁰, J. Pearce¹⁶⁹, B. Pearson¹¹³, L.E. Pedersen³⁶, M. Pedersen¹¹⁹, S. Pedraza Lopez¹⁶⁷, R. Pedro^{126a,126b}, S.V. Peleganchuk^{109,c}, D. Pelikan¹⁶⁶, O. Penc¹²⁷, C. Peng^{33a}, H. Peng^{33b}, B. Penning³¹, J. Penwell⁶¹, D.V. Perepelitsa²⁵, E. Perez Codina^{159a}, M.T. Pérez García-Estañ¹⁶⁷, L. Perini^{91a,91b}, H. Pernegger³⁰, S. Perrella^{104a,104b}, R. Peschke⁴², V.D. Peshekhanov⁶⁵, K. Peters³⁰, R.F.Y. Peters⁸⁴, B.A. Petersen³⁰, T.C. Petersen³⁶,

E. Petit⁴², A. Petridis¹, C. Petridou¹⁵⁴, P. Petroff¹¹⁷, E. Petrolo^{132a}, F. Petrucci^{134a,134b},
 N.E. Pettersson¹⁵⁷, R. Pezoa^{32b}, P.W. Phillips¹³¹, G. Piacquadio¹⁴³, E. Pianori¹⁷⁰, A. Picazio⁴⁹,
 E. Piccaro⁷⁶, M. Piccinini^{20a,20b}, M.A. Pickering¹²⁰, R. Piegaia²⁷, D.T. Pignotti¹¹¹, J.E. Pilcher³¹,
 A.D. Pilkinson⁸⁴, A.W.J. Pin⁸⁴, J. Pina^{126a,126b,126d}, M. Pinamonti^{164a,164c,ag}, J.L. Pinfold³,
 A. Pingel³⁶, S. Pires⁸⁰, H. Pirumov⁴², M. Pitt¹⁷², C. Pizio^{91a,91b}, L. Plazak^{144a}, M.-A. Pleier²⁵,
 V. Pleskot¹²⁹, E. Plotnikova⁶⁵, P. Plucinski^{146a,146b}, D. Pluth⁶⁴, R. Poettgen^{146a,146b}, L. Poggioli¹¹⁷,
 D. Pohl²¹, G. Polesello^{121a}, A. Poley⁴², A. Policicchio^{37a,37b}, R. Polifka¹⁵⁸, A. Polini^{20a},
 C.S. Pollard⁵³, V. Polychronakos²⁵, K. Pommès³⁰, L. Pontecorvo^{132a}, B.G. Pope⁹⁰,
 G.A. Popeneiciu^{26c}, D.S. Popovic¹³, A. Poppleton³⁰, S. Pospisil¹²⁸, K. Potamianos¹⁵, I.N. Potrap⁶⁵,
 C.J. Potter¹⁴⁹, C.T. Potter¹¹⁶, G. Pouland³⁰, J. Poveda³⁰, V. Pozdnyakov⁶⁵, M.E. Pozo Astigarraga³⁰,
 P. Pralavorio⁸⁵, A. Pranko¹⁵, S. Prasad³⁰, S. Prell⁶⁴, D. Price⁸⁴, L.E. Price⁶, M. Primavera^{73a},
 S. Prince⁸⁷, M. Proissl⁴⁶, K. Prokofiev^{60c}, F. Prokoshin^{32b}, E. Protopapadaki¹³⁶, S. Protopopescu²⁵,
 J. Proudfoot⁶, M. Przybycien^{38a}, E. Ptacek¹¹⁶, D. Puddu^{134a,134b}, E. Pueschel⁸⁶, D. Puldon¹⁴⁸,
 M. Purohit^{25,ah}, P. Puzo¹¹⁷, J. Qian⁸⁹, G. Qin⁵³, Y. Qin⁸⁴, A. Quadt⁵⁴, D.R. Quarrie¹⁵,
 W.B. Quayle^{164a,164b}, M. Queitsch-Maitland⁸⁴, D. Quilty⁵³, S. Raddum¹¹⁹, V. Radeka²⁵,
 V. Radescu⁴², S.K. Radhakrishnan¹⁴⁸, P. Radloff¹¹⁶, P. Rados⁸⁸, F. Ragusa^{91a,91b}, G. Rahal¹⁷⁸,
 S. Rajagopalan²⁵, M. Rammensee³⁰, C. Rangel-Smith¹⁶⁶, F. Rauscher¹⁰⁰, S. Rave⁸³,
 T. Ravenscroft⁵³, M. Raymond³⁰, A.L. Read¹¹⁹, N.P. Readioff⁷⁴, D.M. Rebuzzi^{121a,121b},
 A. Redelbach¹⁷⁴, G. Redlinger²⁵, R. Reece¹³⁷, K. Reeves⁴¹, L. Rehnisch¹⁶, J. Reichert¹²²,
 H. Reisin²⁷, C. Rembser³⁰, H. Ren^{33a}, A. Renaud¹¹⁷, M. Rescigno^{132a}, S. Resconi^{91a},
 O.L. Rezanova^{109,c}, P. Reznicek¹²⁹, R. Rezvani⁹⁵, R. Richter¹⁰¹, S. Richter⁷⁸, E. Richter-Was^{38b},
 O. Ricken²¹, M. Ridel⁸⁰, P. Rieck¹⁶, C.J. Riegel¹⁷⁵, J. Rieger⁵⁴, O. Rifki¹¹³, M. Rijssenbeek¹⁴⁸,
 A. Rimoldi^{121a,121b}, L. Rinaldi^{20a}, B. Ristic⁴⁹, E. Ritsch³⁰, I. Riu¹², F. Rizatdinova¹¹⁴, E. Rizvi⁷⁶,
 S.H. Robertson^{87,l}, A. Robichaud-Veronneau⁸⁷, D. Robinson²⁸, J.E.M. Robinson⁴², A. Robson⁵³,
 C. Roda^{124a,124b}, S. Roe³⁰, O. Røhne¹¹⁹, A. Romaniouk⁹⁸, M. Romano^{20a,20b}, S.M. Romano Saez³⁴,
 E. Romero Adam¹⁶⁷, N. Rompotis¹³⁸, M. Ronzani⁴⁸, L. Roos⁸⁰, E. Ros¹⁶⁷, S. Rosati^{132a},
 K. Rosbach⁴⁸, P. Rose¹³⁷, O. Rosenthal¹⁴¹, V. Rossetti^{146a,146b}, E. Rossi^{104a,104b}, L.P. Rossi^{50a},
 J.H.N. Rosten²⁸, R. Rosten¹³⁸, M. Rotaru^{26b}, I. Roth¹⁷², J. Rothberg¹³⁸, D. Rousseau¹¹⁷,
 C.R. Royon¹³⁶, A. Rozanov⁸⁵, Y. Rozen¹⁵², X. Ruan^{145c}, F. Rubbo¹⁴³, I. Rubinskiy⁴², V.I. Rud⁹⁹,
 C. Rudolph⁴⁴, M.S. Rudolph¹⁵⁸, F. Rühr⁴⁸, A. Ruiz-Martinez³⁰, Z. Rurikova⁴⁸, N.A. Rusakovich⁶⁵,
 A. Ruschke¹⁰⁰, H.L. Russell¹³⁸, J.P. Rutherford⁷, N. Ruthmann³⁰, Y.F. Ryabov¹²³, M. Rybar¹⁶⁵,
 G. Rybkin¹¹⁷, N.C. Ryder¹²⁰, A. Ryzhov¹³⁰, A.F. Saavedra¹⁵⁰, G. Sabato¹⁰⁷, S. Sacerdoti²⁷,
 A. Saddique³, H.F-W. Sadrozinski¹³⁷, R. Sadykov⁶⁵, F. Safai Tehrani^{132a}, P. Saha¹⁰⁸,
 M. Sahinsoy^{58a}, M. Saimpert¹³⁶, T. Saito¹⁵⁵, H. Sakamoto¹⁵⁵, Y. Sakurai¹⁷¹, G. Salamanna^{134a,134b},
 A. Salamon^{133a}, J.E. Salazar Loyola^{32b}, M. Saleem¹¹³, D. Salek¹⁰⁷, P.H. Sales De Bruin¹³⁸,
 D. Salihagic¹⁰¹, A. Salnikov¹⁴³, J. Salt¹⁶⁷, D. Salvatore^{37a,37b}, F. Salvatore¹⁴⁹, A. Salvucci^{60a},
 A. Salzburger³⁰, D. Sammel⁴⁸, D. Sampsonidis¹⁵⁴, A. Sanchez^{104a,104b}, J. Sánchez¹⁶⁷,
 V. Sanchez Martinez¹⁶⁷, H. Sandaker¹¹⁹, R.L. Sandbach⁷⁶, H.G. Sander⁸³, M.P. Sanders¹⁰⁰,
 M. Sandhoff¹⁷⁵, C. Sandoval¹⁶², R. Sandstroem¹⁰¹, D.P.C. Sankey¹³¹, M. Sannino^{50a,50b},
 A. Sansoni⁴⁷, C. Santoni³⁴, R. Santonico^{133a,133b}, H. Santos^{126a}, I. Santoyo Castillo¹⁴⁹, K. Sapp¹²⁵,
 A. Sapronov⁶⁵, J.G. Saraiva^{126a,126d}, B. Sarrazin²¹, O. Sasaki⁶⁶, Y. Sasaki¹⁵⁵, K. Sato¹⁶⁰,
 G. Sauvage^{5,*}, E. Sauvan⁵, G. Savage⁷⁷, P. Savard^{158,d}, C. Sawyer¹³¹, L. Sawyer^{79,p}, J. Saxon³¹,
 C. Sbarra^{20a}, A. Sbrizzi^{20a,20b}, T. Scanlon⁷⁸, D.A. Scannicchio¹⁶³, M. Scarcella¹⁵⁰,
 V. Scarfone^{37a,37b}, J. Schaarschmidt¹⁷², P. Schacht¹⁰¹, D. Schaefer³⁰, R. Schaefer⁴², J. Schaeffer⁸³,
 S. Schaepe²¹, S. Schaetzel^{58b}, U. Schäfer⁸³, A.C. Schaffer¹¹⁷, D. Schaile¹⁰⁰, R.D. Schamberger¹⁴⁸,
 V. Scharf^{58a}, V.A. Schegelsky¹²³, D. Scheirich¹²⁹, M. Schernau¹⁶³, C. Schiavi^{50a,50b}, C. Schillo⁴⁸,
 M. Schioppa^{37a,37b}, S. Schlenker³⁰, K. Schmieden³⁰, C. Schmitt⁸³, S. Schmitt^{58b}, S. Schmitt⁴²,

S. Schmitz⁸³, B. Schneider^{159a}, Y.J. Schnellbach⁷⁴, U. Schnoor⁴⁴, L. Schoeffel¹³⁶, A. Schoening^{58b},
 B.D. Schoenrock⁹⁰, E. Schopf²¹, A.L.S. Schorlemmer⁵⁴, M. Schott⁸³, D. Schouten^{159a},
 J. Schovancova⁸, S. Schramm⁴⁹, M. Schreyer¹⁷⁴, N. Schuh⁸³, M.J. Schultens²¹,
 H.-C. Schultz-Coulon^{58a}, H. Schulz¹⁶, M. Schumacher⁴⁸, B.A. Schumm¹³⁷, Ph. Schune¹³⁶,
 C. Schwanenberger⁸⁴, A. Schwartzman¹⁴³, T.A. Schwarz⁸⁹, Ph. Schwegler¹⁰¹, H. Schweiger⁸⁴,
 Ph. Schwemling¹³⁶, R. Schwienhorst⁹⁰, J. Schwindling¹³⁶, T. Schwindt²¹, E. Scifo¹¹⁷, G. Sciolla²³,
 F. Scuri^{124a,124b}, F. Scutti²¹, J. Searcy⁸⁹, G. Sedov⁴², E. Sedykh¹²³, P. Seema²¹, S.C. Seidel¹⁰⁵,
 A. Seiden¹³⁷, F. Seifert¹²⁸, J.M. Seixas^{24a}, G. Sekhniaidze^{104a}, K. Sekhon⁸⁹, S.J. Sekula⁴⁰,
 D.M. Seliverstov^{123,*}, N. Semprini-Cesari^{20a,20b}, C. Serfon³⁰, L. Serin¹¹⁷, L. Serkin^{164a,164b},
 T. Serre⁸⁵, M. Sessa^{134a,134b}, R. Seuster^{159a}, H. Severini¹¹³, T. Sfiligoj⁷⁵, F. Sforza³⁰, A. Sfyrla³⁰,
 E. Shabalina⁵⁴, M. Shamim¹¹⁶, L.Y. Shan^{33a}, R. Shang¹⁶⁵, J.T. Shank²², M. Shapiro¹⁵,
 P.B. Shatalov⁹⁷, K. Shaw^{164a,164b}, S.M. Shaw⁸⁴, A. Shcherbakova^{146a,146b}, C.Y. Shehu¹⁴⁹,
 P. Sherwood⁷⁸, L. Shi^{151,ai}, S. Shimizu⁶⁷, C.O. Shimmin¹⁶³, M. Shimojima¹⁰², M. Shiyakova⁶⁵,
 A. Shmeleva⁹⁶, D. Shoaleh Saadi⁹⁵, M.I. Shochet³¹, S. Shojaii^{91a,91b}, S. Shrestha¹¹¹, E. Shulga⁹⁸,
 M.A. Shupe⁷, P. Sicho¹²⁷, P.E. Sidebo¹⁴⁷, O. Sidiropoulou¹⁷⁴, D. Sidorov¹¹⁴, A. Sidoti^{20a,20b},
 F. Siegert⁴⁴, Dj. Sijacki¹³, J. Silva^{126a,126d}, Y. Silver¹⁵³, S.B. Silverstein^{146a}, V. Simak¹²⁸, O. Simard⁵,
 Lj. Simic¹³, S. Simion¹¹⁷, E. Simioni⁸³, B. Simmons⁷⁸, D. Simon³⁴, M. Simon⁸³, P. Sinervo¹⁵⁸,
 N.B. Sinev¹¹⁶, M. Sioli^{20a,20b}, G. Siragusa¹⁷⁴, A.N. Sisakyan^{65,*}, S.Yu. Sivoklokov⁹⁹,
 J. Sjölin^{146a,146b}, T.B. Sjursen¹⁴, M.B. Skinner⁷², H.P. Skottowe⁵⁷, P. Skubic¹¹³, M. Slater¹⁸,
 T. Slavicek¹²⁸, M. Slawinska¹⁰⁷, K. Sliwa¹⁶¹, V. Smakhtin¹⁷², B.H. Smart⁴⁶, L. Smestad¹⁴,
 S.Yu. Smirnov⁹⁸, Y. Smirnov⁹⁸, L.N. Smirnova^{99,aj}, O. Smirnova⁸¹, M.N.K. Smith³⁵, R.W. Smith³⁵,
 M. Smizanska⁷², K. Smolek¹²⁸, A.A. Snesarev⁹⁶, G. Snidero⁷⁶, S. Snyder²⁵, R. Sobie^{169,l},
 F. Socher⁴⁴, A. Soffer¹⁵³, D.A. Soh^{151,ai}, G. Sokhrannyi⁷⁵, C.A. Solans³⁰, M. Solar¹²⁸, J. Solc¹²⁸,
 E.Yu. Soldatov⁹⁸, U. Soldevila¹⁶⁷, A.A. Solodkov¹³⁰, A. Soloshenko⁶⁵, O.V. Solovyanov¹³⁰,
 V. Solovyev¹²³, P. Sommer⁴⁸, H.Y. Song^{33b,aa}, N. Soni¹, A. Sood¹⁵, A. Sopczak¹²⁸, B. Sopko¹²⁸,
 V. Sopko¹²⁸, V. Sorin¹², D. Sosa^{58b}, M. Sosebee⁸, C.L. Sotropoulou^{124a,124b}, R. Soualah^{164a,164c},
 A.M. Soukharov^{109,c}, D. South⁴², B.C. Sowden⁷⁷, S. Spagnolo^{73a,73b}, M. Spalla^{124a,124b},
 M. Spangenberg¹⁷⁰, F. Spanò⁷⁷, W.R. Spearman⁵⁷, D. Sperlich¹⁶, F. Spettel¹⁰¹, R. Spighi^{20a},
 G. Spigo³⁰, L.A. Spiller⁸⁸, M. Spousta¹²⁹, R.D. St. Denis^{53,*}, A. Stabile^{91a}, S. Staerz³⁰,
 J. Stahlman¹²², R. Stamen^{58a}, S. Stamm¹⁶, E. Stanecka³⁹, R.W. Stanek⁶, C. Stanescu^{134a},
 M. Stanescu-Bellu⁴², M.M. Stanitzki⁴², S. Stapnes¹¹⁹, E.A. Starchenko¹³⁰, J. Stark⁵⁵, P. Staroba¹²⁷,
 P. Starovoitov^{58a}, R. Staszewski³⁹, P. Steinberg²⁵, B. Stelzer¹⁴², H.J. Stelzer³⁰,
 O. Stelzer-Chilton^{159a}, H. Stenzel⁵², G.A. Stewart⁵³, J.A. Stillings²¹, M.C. Stockton⁸⁷, M. Stoebe⁸⁷,
 G. Stoica^{26b}, P. Stolte⁵⁴, S. Stonjek¹⁰¹, A.R. Stradling⁸, A. Straessner⁴⁴, M.E. Stramaglia¹⁷,
 J. Strandberg¹⁴⁷, S. Strandberg^{146a,146b}, A. Strandlie¹¹⁹, E. Strauss¹⁴³, M. Strauss¹¹³, P. Strizenec^{144b},
 R. Ströhmer¹⁷⁴, D.M. Strom¹¹⁶, R. Stroynowski⁴⁰, A. Strubig¹⁰⁶, S.A. Stucci¹⁷, B. Stugu¹⁴,
 N.A. Styles⁴², D. Su¹⁴³, J. Su¹²⁵, R. Subramaniam⁷⁹, A. Succurro¹², S. Suchek^{58a}, Y. Sugaya¹¹⁸,
 M. Suk¹²⁸, V.V. Sulin⁹⁶, S. Sultansoy^{4c}, T. Sumida⁶⁸, S. Sun⁵⁷, X. Sun^{33a}, J.E. Sundermann⁴⁸,
 K. Suruliz¹⁴⁹, G. Susinno^{37a,37b}, M.R. Sutton¹⁴⁹, S. Suzuki⁶⁶, M. Svatos¹²⁷, M. Swiatlowski³¹,
 I. Sykora^{144a}, T. Sykora¹²⁹, D. Ta⁴⁸, C. Taccini^{134a,134b}, K. Tackmann⁴², J. Taenzer¹⁵⁸, A. Taffard¹⁶³,
 R. Tafirout^{159a}, N. Taiblum¹⁵³, H. Takai²⁵, R. Takashima⁶⁹, H. Takeda⁶⁷, T. Takeshita¹⁴⁰,
 Y. Takubo⁶⁶, M. Talby⁸⁵, A.A. Talyshев^{109,c}, J.Y.C. Tam¹⁷⁴, K.G. Tan⁸⁸, J. Tanaka¹⁵⁵, R. Tanaka¹¹⁷,
 S. Tanaka⁶⁶, B.B. Tannenwald¹¹¹, S. Tapia Araya^{32b}, S. Tapprogge⁸³, S. Tarem¹⁵², F. Tarrade²⁹,
 G.F. Tartarelli^{91a}, P. Tas¹²⁹, M. Tasevsky¹²⁷, T. Tashiro⁶⁸, E. Tassi^{37a,37b}, A. Tavares Delgado^{126a,126b},
 Y. Tayalati^{135d}, A.C. Taylor¹⁰⁵, F.E. Taylor⁹⁴, G.N. Taylor⁸⁸, P.T.E. Taylor⁸⁸, W. Taylor^{159b},
 F.A. Teischinger³⁰, P. Teixeira-Dias⁷⁷, K.K. Temming⁴⁸, D. Temple¹⁴², H. Ten Kate³⁰, P.K. Teng¹⁵¹,
 J.J. Teoh¹¹⁸, F. Tepel¹⁷⁵, S. Terada⁶⁶, K. Terashi¹⁵⁵, J. Terron⁸², S. Terzo¹⁰¹, M. Testa⁴⁷,

R.J. Teuscher^{158,l}, T. Theveneaux-Pelzer³⁴, J.P. Thomas¹⁸, J. Thomas-Wilsker⁷⁷, E.N. Thompson³⁵, P.D. Thompson¹⁸, R.J. Thompson⁸⁴, A.S. Thompson⁵³, L.A. Thomsen¹⁷⁶, E. Thomson¹²², M. Thomson²⁸, R.P. Thun^{89,*}, M.J. Tibbetts¹⁵, R.E. Ticse Torres⁸⁵, V.O. Tikhomirov^{96,ak}, Yu.A. Tikhonov^{109,c}, S. Timoshenko⁹⁸, E. Tiouchichine⁸⁵, P. Tipton¹⁷⁶, S. Tisserant⁸⁵, K. Todome¹⁵⁷, T. Todorov^{5,*}, S. Todorova-Nova¹²⁹, J. Tojo⁷⁰, S. Tokár^{144a}, K. Tokushuku⁶⁶, K. Tollefson⁹⁰, E. Tolley⁵⁷, L. Tomlinson⁸⁴, M. Tomoto¹⁰³, L. Tompkins^{143,al}, K. Toms¹⁰⁵, E. Torrence¹¹⁶, H. Torres¹⁴², E. Torró Pastor¹³⁸, J. Toth^{85,am}, F. Touchard⁸⁵, D.R. Tovey¹³⁹, T. Trefzger¹⁷⁴, L. Tremblet³⁰, A. Tricoli³⁰, I.M. Trigger^{159a}, S. Trincaz-Duvoid⁸⁰, M.F. Tripiana¹², W. Trischuk¹⁵⁸, B. Trocmé⁵⁵, C. Troncon^{91a}, M. Trottier-McDonald¹⁵, M. Trovatelli¹⁶⁹, L. Truong^{164a,164c}, M. Trzebinski³⁹, A. Trzupek³⁹, C. Tsarouchas³⁰, J.C-L. Tseng¹²⁰, P.V. Tsiashka⁹², D. Tsionou¹⁵⁴, G. Tsipolitis¹⁰, N. Tsirintanis⁹, S. Tsiskaridze¹², V. Tsiskaridze⁴⁸, E.G. Tskhadadze^{51a}, K.M. Tsui^{60a}, I.I. Tsukerman⁹⁷, V. Tsulaia¹⁵, S. Tsuno⁶⁶, D. Tsybychev¹⁴⁸, A. Tudorache^{26b}, V. Tudorache^{26b}, A.N. Tuna⁵⁷, S.A. Tupputi^{20a,20b}, S. Turchikhin^{99,aj}, D. Turecek¹²⁸, R. Turra^{91a,91b}, A.J. Turvey⁴⁰, P.M. Tuts³⁵, A. Tykhonov⁴⁹, M. Tylmad^{146a,146b}, M. Tyndel¹³¹, I. Ueda¹⁵⁵, R. Ueno²⁹, M. Ughetto^{146a,146b}, F. Ukegawa¹⁶⁰, G. Unal³⁰, A. Undrus²⁵, G. Unel¹⁶³, F.C. Ungaro⁸⁸, Y. Unno⁶⁶, C. Unverdorben¹⁰⁰, J. Urban^{144b}, P. Urquijo⁸⁸, P. Urrejola⁸³, G. Usai⁸, A. Usanova⁶², L. Vacavant⁸⁵, V. Vacek¹²⁸, B. Vachon⁸⁷, C. Valderanis⁸³, N. Valencic¹⁰⁷, S. Valentini^{20a,20b}, A. Valero¹⁶⁷, L. Valery¹², S. Valkar¹²⁹, S. Vallecorsa⁴⁹, J.A. Valls Ferrer¹⁶⁷, W. Van Den Wollenberg¹⁰⁷, P.C. Van Der Deijl¹⁰⁷, R. van der Geer¹⁰⁷, H. van der Graaf¹⁰⁷, N. van Eldik¹⁵², P. van Gemmeren⁶, J. Van Nieuwkoop¹⁴², I. van Vulpen¹⁰⁷, M.C. van Woerden³⁰, M. Vanadia^{132a,132b}, W. Vandelli³⁰, R. Vanguri¹²², A. Vaniachine⁶, F. Vannucci⁸⁰, G. Vardanyan¹⁷⁷, R. Vari^{132a}, E.W. Varnes⁷, T. Varol⁴⁰, D. Varouchas⁸⁰, A. Vartapetian⁸, K.E. Varvell¹⁵⁰, F. Vazeille³⁴, T. Vazquez Schroeder⁸⁷, J. Veatch⁷, L.M. Veloce¹⁵⁸, F. Veloso^{126a,126c}, T. Velz²¹, S. Veneziano^{132a}, A. Ventura^{73a,73b}, D. Ventura⁸⁶, M. Venturi¹⁶⁹, N. Venturi¹⁵⁸, A. Venturini²³, V. Vercesi^{121a}, M. Verducci^{132a,132b}, W. Verkerke¹⁰⁷, J.C. Vermeulen¹⁰⁷, A. Vest⁴⁴, M.C. Vetterli^{142,d}, O. Viazlo⁸¹, I. Vichou¹⁶⁵, T. Vickey¹³⁹, O.E. Vickey Boeriu¹³⁹, G.H.A. Viehhauser¹²⁰, S. Viel¹⁵, R. Vigne⁶², M. Villa^{20a,20b}, M. Villaplana Perez^{91a,91b}, E. Vilucchi⁴⁷, M.G. Vincter²⁹, V.B. Vinogradov⁶⁵, I. Vivarelli¹⁴⁹, S. Vlachos¹⁰, D. Vladoiu¹⁰⁰, M. Vlasak¹²⁸, M. Vogel^{32a}, P. Vokac¹²⁸, G. Volpi^{124a,124b}, M. Volpi⁸⁸, H. von der Schmitt¹⁰¹, H. von Radziewski⁴⁸, E. von Toerne²¹, V. Vorobel¹²⁹, K. Vorobev⁹⁸, M. Vos¹⁶⁷, R. Voss³⁰, J.H. Vossebeld⁷⁴, N. Vranjes¹³, M. Vranjes Milosavljevic¹³, V. Vrba¹²⁷, M. Vreeswijk¹⁰⁷, R. Vuillermet³⁰, I. Vukotic³¹, Z. Vykydal¹²⁸, P. Wagner²¹, W. Wagner¹⁷⁵, H. Wahlberg⁷¹, S. Wahrmund⁴⁴, J. Wakabayashi¹⁰³, J. Walder⁷², R. Walker¹⁰⁰, W. Walkowiak¹⁴¹, C. Wang¹⁵¹, F. Wang¹⁷³, H. Wang¹⁵, H. Wang⁴⁰, J. Wang⁴², J. Wang¹⁵⁰, K. Wang⁸⁷, R. Wang⁶, S.M. Wang¹⁵¹, T. Wang²¹, T. Wang³⁵, X. Wang¹⁷⁶, C. Wanotayaroj¹¹⁶, A. Warburton⁸⁷, C.P. Ward²⁸, D.R. Wardrope⁷⁸, A. Washbrook⁴⁶, C. Wasicki⁴², P.M. Watkins¹⁸, A.T. Watson¹⁸, I.J. Watson¹⁵⁰, M.F. Watson¹⁸, G. Watts¹³⁸, S. Watts⁸⁴, B.M. Waugh⁷⁸, S. Webb⁸⁴, M.S. Weber¹⁷, S.W. Weber¹⁷⁴, J.S. Webster⁶, A.R. Weidberg¹²⁰, B. Weinert⁶¹, J. Weingarten⁵⁴, C. Weiser⁴⁸, H. Weits¹⁰⁷, P.S. Wells³⁰, T. Wenaus²⁵, T. Wengler³⁰, S. Wenig³⁰, N. Wermes²¹, M. Werner⁴⁸, P. Werner³⁰, M. Wessels^{58a}, J. Wetter¹⁶¹, K. Whalen¹¹⁶, A.M. Wharton⁷², A. White⁸, M.J. White¹, R. White^{32b}, S. White^{124a,124b}, D. Whiteson¹⁶³, F.J. Wickens¹³¹, W. Wiedenmann¹⁷³, M. Wielers¹³¹, P. Wienemann²¹, C. Wiglesworth³⁶, L.A.M. Wiik-Fuchs²¹, A. Wildauer¹⁰¹, H.G. Wilkens³⁰, H.H. Williams¹²², S. Williams¹⁰⁷, C. Willis⁹⁰, S. Willocq⁸⁶, A. Wilson⁸⁹, J.A. Wilson¹⁸, I. Wingerter-Seez⁵, F. Winklmeier¹¹⁶, B.T. Winter²¹, M. Wittgen¹⁴³, J. Wittkowski¹⁰⁰, S.J. Wollstadt⁸³, M.W. Wolter³⁹, H. Wolters^{126a,126c}, B.K. Wosiek³⁹, J. Wotschack³⁰, M.J. Woudstra⁸⁴, K.W. Wozniak³⁹, M. Wu⁵⁵, M. Wu³¹, S.L. Wu¹⁷³, X. Wu⁴⁹, Y. Wu⁸⁹, T.R. Wyatt⁸⁴, B.M. Wynne⁴⁶, S. Xella³⁶, D. Xu^{33a}, L. Xu²⁵, B. Yabsley¹⁵⁰, S. Yacoob^{145a}, R. Yakabe⁶⁷, M. Yamada⁶⁶, D. Yamaguchi¹⁵⁷, Y. Yamaguchi¹¹⁸, A. Yamamoto⁶⁶, S. Yamamoto¹⁵⁵,

T. Yamanaka¹⁵⁵, K. Yamauchi¹⁰³, Y. Yamazaki⁶⁷, Z. Yan²², H. Yang^{33e}, H. Yang¹⁷³, Y. Yang¹⁵¹, W-M. Yao¹⁵, Y.C. Yap⁸⁰, Y. Yasu⁶⁶, E. Yatsenko⁵, K.H. Yau Wong²¹, J. Ye⁴⁰, S. Ye²⁵, I. Yeletskikh⁶⁵, A.L. Yen⁵⁷, E. Yildirim⁴², K. Yorita¹⁷¹, R. Yoshida⁶, K. Yoshihara¹²², C. Young¹⁴³, C.J.S. Young³⁰, S. Youssef²², D.R. Yu¹⁵, J. Yu⁸, J.M. Yu⁸⁹, J. Yu¹¹⁴, L. Yuan⁶⁷, S.P.Y. Yuen²¹, A. Yurkewicz¹⁰⁸, I. Yusuff^{28,an}, B. Zabinski³⁹, R. Zaidan⁶³, A.M. Zaitsev^{130,ae}, J. Zaliekas¹⁴, A. Zaman¹⁴⁸, S. Zambito⁵⁷, L. Zanello^{132a,132b}, D. Zanzi⁸⁸, C. Zeitnitz¹⁷⁵, M. Zeman¹²⁸, A. Zemla^{38a}, J.C. Zeng¹⁶⁵, Q. Zeng¹⁴³, K. Zengel²³, O. Zenin¹³⁰, T. Ženiš^{144a}, D. Zerwas¹¹⁷, D. Zhang⁸⁹, F. Zhang¹⁷³, G. Zhang^{33b}, H. Zhang^{33c}, J. Zhang⁶, L. Zhang⁴⁸, R. Zhang^{33b,j}, X. Zhang^{33d}, Z. Zhang¹¹⁷, X. Zhao⁴⁰, Y. Zhao^{33d,117}, Z. Zhao^{33b}, A. Zhemchugov⁶⁵, J. Zhong¹²⁰, B. Zhou⁸⁹, C. Zhou⁴⁵, L. Zhou³⁵, L. Zhou⁴⁰, M. Zhou¹⁴⁸, N. Zhou^{33f}, C.G. Zhu^{33d}, H. Zhu^{33a}, J. Zhu⁸⁹, Y. Zhu^{33b}, X. Zhuang^{33a}, K. Zhukov⁹⁶, A. Zibell¹⁷⁴, D. Ziemska⁶¹, N.I. Zimine⁶⁵, C. Zimmermann⁸³, S. Zimmermann⁴⁸, Z. Zinonos⁵⁴, M. Zinser⁸³, M. Ziolkowski¹⁴¹, L. Živković¹³, G. Zobernig¹⁷³, A. Zoccoli^{20a,20b}, M. zur Nedden¹⁶, G. Zurzolo^{104a,104b}, L. Zwalski³⁰.

¹ Department of Physics, University of Adelaide, Adelaide, Australia

² Physics Department, SUNY Albany, Albany NY, United States of America

³ Department of Physics, University of Alberta, Edmonton AB, Canada

^{4 (a)} Department of Physics, Ankara University, Ankara; ^(b) Istanbul Aydin University, Istanbul; ^(c) Division of Physics, TOBB University of Economics and Technology, Ankara, Turkey

⁵ LAPP, CNRS/IN2P3 and Université Savoie Mont Blanc, Annecy-le-Vieux, France

⁶ High Energy Physics Division, Argonne National Laboratory, Argonne IL, United States of America

⁷ Department of Physics, University of Arizona, Tucson AZ, United States of America

⁸ Department of Physics, The University of Texas at Arlington, Arlington TX, United States of America

⁹ Physics Department, University of Athens, Athens, Greece

¹⁰ Physics Department, National Technical University of Athens, Zografou, Greece

¹¹ Institute of Physics, Azerbaijan Academy of Sciences, Baku, Azerbaijan

¹² Institut de Física d'Altes Energies and Departament de Física de la Universitat Autònoma de Barcelona, Barcelona, Spain

¹³ Institute of Physics, University of Belgrade, Belgrade, Serbia

¹⁴ Department for Physics and Technology, University of Bergen, Bergen, Norway

¹⁵ Physics Division, Lawrence Berkeley National Laboratory and University of California, Berkeley CA, United States of America

¹⁶ Department of Physics, Humboldt University, Berlin, Germany

¹⁷ Albert Einstein Center for Fundamental Physics and Laboratory for High Energy Physics, University of Bern, Bern, Switzerland

¹⁸ School of Physics and Astronomy, University of Birmingham, Birmingham, United Kingdom

^{19 (a)} Department of Physics, Bogazici University, Istanbul; ^(b) Department of Physics Engineering, Gaziantep University, Gaziantep; ^(c) Department of Physics, Dogus University, Istanbul, Turkey

^{20 (a)} INFN Sezione di Bologna; ^(b) Dipartimento di Fisica e Astronomia, Università di Bologna, Bologna, Italy

²¹ Physikalisches Institut, University of Bonn, Bonn, Germany

²² Department of Physics, Boston University, Boston MA, United States of America

²³ Department of Physics, Brandeis University, Waltham MA, United States of America

^{24 (a)} Universidade Federal do Rio De Janeiro COPPE/EE/IF, Rio de Janeiro; ^(b) Electrical Circuits Department, Federal University of Juiz de Fora (UFJF), Juiz de Fora; ^(c) Federal University of Sao

- Joao del Rei (UFSJ), Sao Joao del Rei; ^(d) Instituto de Fisica, Universidade de Sao Paulo, Sao Paulo, Brazil
²⁵ Physics Department, Brookhaven National Laboratory, Upton NY, United States of America
²⁶ ^(a) Transilvania University of Brasov, Brasov, Romania; ^(b) National Institute of Physics and Nuclear Engineering, Bucharest; ^(c) National Institute for Research and Development of Isotopic and Molecular Technologies, Physics Department, Cluj Napoca; ^(d) University Politehnica Bucharest, Bucharest; ^(e) West University in Timisoara, Timisoara, Romania
²⁷ Departamento de Física, Universidad de Buenos Aires, Buenos Aires, Argentina
²⁸ Cavendish Laboratory, University of Cambridge, Cambridge, United Kingdom
²⁹ Department of Physics, Carleton University, Ottawa ON, Canada
³⁰ CERN, Geneva, Switzerland
³¹ Enrico Fermi Institute, University of Chicago, Chicago IL, United States of America
³² ^(a) Departamento de Física, Pontificia Universidad Católica de Chile, Santiago; ^(b) Departamento de Física, Universidad Técnica Federico Santa María, Valparaíso, Chile
³³ ^(a) Institute of High Energy Physics, Chinese Academy of Sciences, Beijing; ^(b) Department of Modern Physics, University of Science and Technology of China, Anhui; ^(c) Department of Physics, Nanjing University, Jiangsu; ^(d) School of Physics, Shandong University, Shandong; ^(e) Department of Physics and Astronomy, Shanghai Key Laboratory for Particle Physics and Cosmology, Shanghai Jiao Tong University, Shanghai; ^(f) Physics Department, Tsinghua University, Beijing 100084, China
³⁴ Laboratoire de Physique Corpusculaire, Clermont Université and Université Blaise Pascal and CNRS/IN2P3, Clermont-Ferrand, France
³⁵ Nevis Laboratory, Columbia University, Irvington NY, United States of America
³⁶ Niels Bohr Institute, University of Copenhagen, Kobenhavn, Denmark
³⁷ ^(a) INFN Gruppo Collegato di Cosenza, Laboratori Nazionali di Frascati; ^(b) Dipartimento di Fisica, Università della Calabria, Rende, Italy
³⁸ ^(a) AGH University of Science and Technology, Faculty of Physics and Applied Computer Science, Krakow; ^(b) Marian Smoluchowski Institute of Physics, Jagiellonian University, Krakow, Poland
³⁹ Institute of Nuclear Physics Polish Academy of Sciences, Krakow, Poland
⁴⁰ Physics Department, Southern Methodist University, Dallas TX, United States of America
⁴¹ Physics Department, University of Texas at Dallas, Richardson TX, United States of America
⁴² DESY, Hamburg and Zeuthen, Germany
⁴³ Institut für Experimentelle Physik IV, Technische Universität Dortmund, Dortmund, Germany
⁴⁴ Institut für Kern- und Teilchenphysik, Technische Universität Dresden, Dresden, Germany
⁴⁵ Department of Physics, Duke University, Durham NC, United States of America
⁴⁶ SUPA - School of Physics and Astronomy, University of Edinburgh, Edinburgh, United Kingdom
⁴⁷ INFN Laboratori Nazionali di Frascati, Frascati, Italy
⁴⁸ Fakultät für Mathematik und Physik, Albert-Ludwigs-Universität, Freiburg, Germany
⁴⁹ Section de Physique, Université de Genève, Geneva, Switzerland
⁵⁰ ^(a) INFN Sezione di Genova; ^(b) Dipartimento di Fisica, Università di Genova, Genova, Italy
⁵¹ ^(a) E. Andronikashvili Institute of Physics, Iv. Javakhishvili Tbilisi State University, Tbilisi; ^(b) High Energy Physics Institute, Tbilisi State University, Tbilisi, Georgia
⁵² II Physikalisches Institut, Justus-Liebig-Universität Giessen, Giessen, Germany
⁵³ SUPA - School of Physics and Astronomy, University of Glasgow, Glasgow, United Kingdom
⁵⁴ II Physikalisches Institut, Georg-August-Universität, Göttingen, Germany
⁵⁵ Laboratoire de Physique Subatomique et de Cosmologie, Université Grenoble-Alpes, CNRS/IN2P3, Grenoble, France
⁵⁶ Department of Physics, Hampton University, Hampton VA, United States of America

- ⁵⁷ Laboratory for Particle Physics and Cosmology, Harvard University, Cambridge MA, United States of America
- ⁵⁸ ^(a) Kirchhoff-Institut für Physik, Ruprecht-Karls-Universität Heidelberg, Heidelberg; ^(b) Physikalisches Institut, Ruprecht-Karls-Universität Heidelberg, Heidelberg; ^(c) ZITI Institut für technische Informatik, Ruprecht-Karls-Universität Heidelberg, Mannheim, Germany
- ⁵⁹ Faculty of Applied Information Science, Hiroshima Institute of Technology, Hiroshima, Japan
- ⁶⁰ ^(a) Department of Physics, The Chinese University of Hong Kong, Shatin, N.T., Hong Kong; ^(b) Department of Physics, The University of Hong Kong, Hong Kong; ^(c) Department of Physics, The Hong Kong University of Science and Technology, Clear Water Bay, Kowloon, Hong Kong, China
- ⁶¹ Department of Physics, Indiana University, Bloomington IN, United States of America
- ⁶² Institut für Astro- und Teilchenphysik, Leopold-Franzens-Universität, Innsbruck, Austria
- ⁶³ University of Iowa, Iowa City IA, United States of America
- ⁶⁴ Department of Physics and Astronomy, Iowa State University, Ames IA, United States of America
- ⁶⁵ Joint Institute for Nuclear Research, JINR Dubna, Dubna, Russia
- ⁶⁶ KEK, High Energy Accelerator Research Organization, Tsukuba, Japan
- ⁶⁷ Graduate School of Science, Kobe University, Kobe, Japan
- ⁶⁸ Faculty of Science, Kyoto University, Kyoto, Japan
- ⁶⁹ Kyoto University of Education, Kyoto, Japan
- ⁷⁰ Department of Physics, Kyushu University, Fukuoka, Japan
- ⁷¹ Instituto de Física La Plata, Universidad Nacional de La Plata and CONICET, La Plata, Argentina
- ⁷² Physics Department, Lancaster University, Lancaster, United Kingdom
- ⁷³ ^(a) INFN Sezione di Lecce; ^(b) Dipartimento di Matematica e Fisica, Università del Salento, Lecce, Italy
- ⁷⁴ Oliver Lodge Laboratory, University of Liverpool, Liverpool, United Kingdom
- ⁷⁵ Department of Physics, Jožef Stefan Institute and University of Ljubljana, Ljubljana, Slovenia
- ⁷⁶ School of Physics and Astronomy, Queen Mary University of London, London, United Kingdom
- ⁷⁷ Department of Physics, Royal Holloway University of London, Surrey, United Kingdom
- ⁷⁸ Department of Physics and Astronomy, University College London, London, United Kingdom
- ⁷⁹ Louisiana Tech University, Ruston LA, United States of America
- ⁸⁰ Laboratoire de Physique Nucléaire et de Hautes Energies, UPMC and Université Paris-Diderot and CNRS/IN2P3, Paris, France
- ⁸¹ Fysiska institutionen, Lunds universitet, Lund, Sweden
- ⁸² Departamento de Fisica Teorica C-15, Universidad Autonoma de Madrid, Madrid, Spain
- ⁸³ Institut für Physik, Universität Mainz, Mainz, Germany
- ⁸⁴ School of Physics and Astronomy, University of Manchester, Manchester, United Kingdom
- ⁸⁵ CPPM, Aix-Marseille Université and CNRS/IN2P3, Marseille, France
- ⁸⁶ Department of Physics, University of Massachusetts, Amherst MA, United States of America
- ⁸⁷ Department of Physics, McGill University, Montreal QC, Canada
- ⁸⁸ School of Physics, University of Melbourne, Victoria, Australia
- ⁸⁹ Department of Physics, The University of Michigan, Ann Arbor MI, United States of America
- ⁹⁰ Department of Physics and Astronomy, Michigan State University, East Lansing MI, United States of America
- ⁹¹ ^(a) INFN Sezione di Milano; ^(b) Dipartimento di Fisica, Università di Milano, Milano, Italy
- ⁹² B.I. Stepanov Institute of Physics, National Academy of Sciences of Belarus, Minsk, Republic of Belarus
- ⁹³ National Scientific and Educational Centre for Particle and High Energy Physics, Minsk, Republic of Belarus

- ⁹⁴ Department of Physics, Massachusetts Institute of Technology, Cambridge MA, United States of America
⁹⁵ Group of Particle Physics, University of Montreal, Montreal QC, Canada
⁹⁶ P.N. Lebedev Physical Institute of the Russian Academy of Sciences, Moscow, Russia
⁹⁷ Institute for Theoretical and Experimental Physics (ITEP), Moscow, Russia
⁹⁸ National Research Nuclear University MEPhI, Moscow, Russia
⁹⁹ D.V. Skobeltsyn Institute of Nuclear Physics, M.V. Lomonosov Moscow State University, Moscow, Russia
¹⁰⁰ Fakultät für Physik, Ludwig-Maximilians-Universität München, München, Germany
¹⁰¹ Max-Planck-Institut für Physik (Werner-Heisenberg-Institut), München, Germany
¹⁰² Nagasaki Institute of Applied Science, Nagasaki, Japan
¹⁰³ Graduate School of Science and Kobayashi-Maskawa Institute, Nagoya University, Nagoya, Japan
¹⁰⁴ ^(a) INFN Sezione di Napoli; ^(b) Dipartimento di Fisica, Università di Napoli, Napoli, Italy
¹⁰⁵ Department of Physics and Astronomy, University of New Mexico, Albuquerque NM, United States of America
¹⁰⁶ Institute for Mathematics, Astrophysics and Particle Physics, Radboud University Nijmegen/Nikhef, Nijmegen, Netherlands
¹⁰⁷ Nikhef National Institute for Subatomic Physics and University of Amsterdam, Amsterdam, Netherlands
¹⁰⁸ Department of Physics, Northern Illinois University, DeKalb IL, United States of America
¹⁰⁹ Budker Institute of Nuclear Physics, SB RAS, Novosibirsk, Russia
¹¹⁰ Department of Physics, New York University, New York NY, United States of America
¹¹¹ Ohio State University, Columbus OH, United States of America
¹¹² Faculty of Science, Okayama University, Okayama, Japan
¹¹³ Homer L. Dodge Department of Physics and Astronomy, University of Oklahoma, Norman OK, United States of America
¹¹⁴ Department of Physics, Oklahoma State University, Stillwater OK, United States of America
¹¹⁵ Palacký University, RCPTM, Olomouc, Czech Republic
¹¹⁶ Center for High Energy Physics, University of Oregon, Eugene OR, United States of America
¹¹⁷ LAL, Université Paris-Sud and CNRS/IN2P3, Orsay, France
¹¹⁸ Graduate School of Science, Osaka University, Osaka, Japan
¹¹⁹ Department of Physics, University of Oslo, Oslo, Norway
¹²⁰ Department of Physics, Oxford University, Oxford, United Kingdom
¹²¹ ^(a) INFN Sezione di Pavia; ^(b) Dipartimento di Fisica, Università di Pavia, Pavia, Italy
¹²² Department of Physics, University of Pennsylvania, Philadelphia PA, United States of America
¹²³ National Research Centre "Kurchatov Institute" B.P.Konstantinov Petersburg Nuclear Physics Institute, St. Petersburg, Russia
¹²⁴ ^(a) INFN Sezione di Pisa; ^(b) Dipartimento di Fisica E. Fermi, Università di Pisa, Pisa, Italy
¹²⁵ Department of Physics and Astronomy, University of Pittsburgh, Pittsburgh PA, United States of America
¹²⁶ ^(a) Laboratório de Instrumentação e Física Experimental de Partículas - LIP, Lisboa; ^(b) Faculdade de Ciências, Universidade de Lisboa, Lisboa; ^(c) Department of Physics, University of Coimbra, Coimbra; ^(d) Centro de Física Nuclear da Universidade de Lisboa, Lisboa; ^(e) Departamento de Física, Universidade do Minho, Braga; ^(f) Departamento de Física Teórica y del Cosmos and CAFPE, Universidad de Granada, Granada (Spain); ^(g) Dep Física and CEFITEC of Faculdade de Ciencias e Tecnologia, Universidade Nova de Lisboa, Caparica, Portugal

- ¹²⁷ Institute of Physics, Academy of Sciences of the Czech Republic, Praha, Czech Republic
¹²⁸ Czech Technical University in Prague, Praha, Czech Republic
¹²⁹ Faculty of Mathematics and Physics, Charles University in Prague, Praha, Czech Republic
¹³⁰ State Research Center Institute for High Energy Physics (Protvino), NRC KI, Russia, Russia
¹³¹ Particle Physics Department, Rutherford Appleton Laboratory, Didcot, United Kingdom
¹³² ^(a) INFN Sezione di Roma; ^(b) Dipartimento di Fisica, Sapienza Università di Roma, Roma, Italy
¹³³ ^(a) INFN Sezione di Roma Tor Vergata; ^(b) Dipartimento di Fisica, Università di Roma Tor Vergata, Roma, Italy
¹³⁴ ^(a) INFN Sezione di Roma Tre; ^(b) Dipartimento di Matematica e Fisica, Università Roma Tre, Roma, Italy
¹³⁵ ^(a) Faculté des Sciences Ain Chock, Réseau Universitaire de Physique des Hautes Energies - Université Hassan II, Casablanca; ^(b) Centre National de l'Energie des Sciences Techniques Nucléaires, Rabat; ^(c) Faculté des Sciences Semlalia, Université Cadi Ayyad, LPHEA-Marrakech; ^(d) Faculté des Sciences, Université Mohamed Premier and LPTPM, Oujda; ^(e) Faculté des sciences, Université Mohammed V, Rabat, Morocco
¹³⁶ DSM/IRFU (Institut de Recherches sur les Lois Fondamentales de l'Univers), CEA Saclay (Commissariat à l'Energie Atomique et aux Energies Alternatives), Gif-sur-Yvette, France
¹³⁷ Santa Cruz Institute for Particle Physics, University of California Santa Cruz, Santa Cruz CA, United States of America
¹³⁸ Department of Physics, University of Washington, Seattle WA, United States of America
¹³⁹ Department of Physics and Astronomy, University of Sheffield, Sheffield, United Kingdom
¹⁴⁰ Department of Physics, Shinshu University, Nagano, Japan
¹⁴¹ Fachbereich Physik, Universität Siegen, Siegen, Germany
¹⁴² Department of Physics, Simon Fraser University, Burnaby BC, Canada
¹⁴³ SLAC National Accelerator Laboratory, Stanford CA, United States of America
¹⁴⁴ ^(a) Faculty of Mathematics, Physics & Informatics, Comenius University, Bratislava; ^(b) Department of Subnuclear Physics, Institute of Experimental Physics of the Slovak Academy of Sciences, Kosice, Slovak Republic
¹⁴⁵ ^(a) Department of Physics, University of Cape Town, Cape Town; ^(b) Department of Physics, University of Johannesburg, Johannesburg; ^(c) School of Physics, University of the Witwatersrand, Johannesburg, South Africa
¹⁴⁶ ^(a) Department of Physics, Stockholm University; ^(b) The Oskar Klein Centre, Stockholm, Sweden
¹⁴⁷ Physics Department, Royal Institute of Technology, Stockholm, Sweden
¹⁴⁸ Departments of Physics & Astronomy and Chemistry, Stony Brook University, Stony Brook NY, United States of America
¹⁴⁹ Department of Physics and Astronomy, University of Sussex, Brighton, United Kingdom
¹⁵⁰ School of Physics, University of Sydney, Sydney, Australia
¹⁵¹ Institute of Physics, Academia Sinica, Taipei, Taiwan
¹⁵² Department of Physics, Technion: Israel Institute of Technology, Haifa, Israel
¹⁵³ Raymond and Beverly Sackler School of Physics and Astronomy, Tel Aviv University, Tel Aviv, Israel
¹⁵⁴ Department of Physics, Aristotle University of Thessaloniki, Thessaloniki, Greece
¹⁵⁵ International Center for Elementary Particle Physics and Department of Physics, The University of Tokyo, Tokyo, Japan
¹⁵⁶ Graduate School of Science and Technology, Tokyo Metropolitan University, Tokyo, Japan
¹⁵⁷ Department of Physics, Tokyo Institute of Technology, Tokyo, Japan
¹⁵⁸ Department of Physics, University of Toronto, Toronto ON, Canada

- ¹⁵⁹ ^(a) TRIUMF, Vancouver BC; ^(b) Department of Physics and Astronomy, York University, Toronto ON, Canada
- ¹⁶⁰ Faculty of Pure and Applied Sciences, and Center for Integrated Research in Fundamental Science and Engineering, University of Tsukuba, Tsukuba, Japan
- ¹⁶¹ Department of Physics and Astronomy, Tufts University, Medford MA, United States of America
- ¹⁶² Centro de Investigaciones, Universidad Antonio Narino, Bogota, Colombia
- ¹⁶³ Department of Physics and Astronomy, University of California Irvine, Irvine CA, United States of America
- ¹⁶⁴ ^(a) INFN Gruppo Collegato di Udine, Sezione di Trieste, Udine; ^(b) ICTP, Trieste; ^(c) Dipartimento di Chimica, Fisica e Ambiente, Università di Udine, Udine, Italy
- ¹⁶⁵ Department of Physics, University of Illinois, Urbana IL, United States of America
- ¹⁶⁶ Department of Physics and Astronomy, University of Uppsala, Uppsala, Sweden
- ¹⁶⁷ Instituto de Física Corpuscular (IFIC) and Departamento de Física Atómica, Molecular y Nuclear and Departamento de Ingeniería Electrónica and Instituto de Microelectrónica de Barcelona (IMB-CNM), University of Valencia and CSIC, Valencia, Spain
- ¹⁶⁸ Department of Physics, University of British Columbia, Vancouver BC, Canada
- ¹⁶⁹ Department of Physics and Astronomy, University of Victoria, Victoria BC, Canada
- ¹⁷⁰ Department of Physics, University of Warwick, Coventry, United Kingdom
- ¹⁷¹ Waseda University, Tokyo, Japan
- ¹⁷² Department of Particle Physics, The Weizmann Institute of Science, Rehovot, Israel
- ¹⁷³ Department of Physics, University of Wisconsin, Madison WI, United States of America
- ¹⁷⁴ Fakultät für Physik und Astronomie, Julius-Maximilians-Universität, Würzburg, Germany
- ¹⁷⁵ Fachbereich C Physik, Bergische Universität Wuppertal, Wuppertal, Germany
- ¹⁷⁶ Department of Physics, Yale University, New Haven CT, United States of America
- ¹⁷⁷ Yerevan Physics Institute, Yerevan, Armenia
- ¹⁷⁸ Centre de Calcul de l’Institut National de Physique Nucléaire et de Physique des Particules (IN2P3), Villeurbanne, France
- ^a Also at Department of Physics, King’s College London, London, United Kingdom
- ^b Also at Institute of Physics, Azerbaijan Academy of Sciences, Baku, Azerbaijan
- ^c Also at Novosibirsk State University, Novosibirsk, Russia
- ^d Also at TRIUMF, Vancouver BC, Canada
- ^e Also at Department of Physics & Astronomy, University of Louisville, Louisville, KY, United States of America
- ^f Also at Department of Physics, California State University, Fresno CA, United States of America
- ^g Also at Department of Physics, University of Fribourg, Fribourg, Switzerland
- ^h Also at Departamento de Física e Astronomia, Faculdade de Ciencias, Universidade do Porto, Portugal
- ⁱ Also at Tomsk State University, Tomsk, Russia
- ^j Also at CPPM, Aix-Marseille Université and CNRS/IN2P3, Marseille, France
- ^k Also at Universita di Napoli Parthenope, Napoli, Italy
- ^l Also at Institute of Particle Physics (IPP), Canada
- ^m Also at Particle Physics Department, Rutherford Appleton Laboratory, Didcot, United Kingdom
- ⁿ Also at Department of Physics, St. Petersburg State Polytechnical University, St. Petersburg, Russia
- ^o Also at Department of Physics, The University of Michigan, Ann Arbor MI, United States of America
- ^p Also at Louisiana Tech University, Ruston LA, United States of America
- ^q Also at Institutio Catalana de Recerca i Estudis Avancats, ICREA, Barcelona, Spain

- ^r Also at Graduate School of Science, Osaka University, Osaka, Japan
- ^s Also at Department of Physics, National Tsing Hua University, Taiwan
- ^t Also at Department of Physics, The University of Texas at Austin, Austin TX, United States of America
- ^u Also at Institute of Theoretical Physics, Ilia State University, Tbilisi, Georgia
- ^v Also at CERN, Geneva, Switzerland
- ^w Also at Georgian Technical University (GTU), Tbilisi, Georgia
- ^x Also at Ochadai Academic Production, Ochanomizu University, Tokyo, Japan
- ^y Also at Manhattan College, New York NY, United States of America
- ^z Also at Hellenic Open University, Patras, Greece
- ^{aa} Also at Institute of Physics, Academia Sinica, Taipei, Taiwan
- ^{ab} Also at LAL, Université Paris-Sud and CNRS/IN2P3, Orsay, France
- ^{ac} Also at Academia Sinica Grid Computing, Institute of Physics, Academia Sinica, Taipei, Taiwan
- ^{ad} Also at School of Physics, Shandong University, Shandong, China
- ^{ae} Also at Moscow Institute of Physics and Technology State University, Dolgoprudny, Russia
- ^{af} Also at Section de Physique, Université de Genève, Geneva, Switzerland
- ^{ag} Also at International School for Advanced Studies (SISSA), Trieste, Italy
- ^{ah} Also at Department of Physics and Astronomy, University of South Carolina, Columbia SC, United States of America
- ^{ai} Also at School of Physics and Engineering, Sun Yat-sen University, Guangzhou, China
- ^{aj} Also at Faculty of Physics, M.V.Lomonosov Moscow State University, Moscow, Russia
- ^{ak} Also at National Research Nuclear University MEPhI, Moscow, Russia
- ^{al} Also at Department of Physics, Stanford University, Stanford CA, United States of America
- ^{am} Also at Institute for Particle and Nuclear Physics, Wigner Research Centre for Physics, Budapest, Hungary
- ^{an} Also at University of Malaya, Department of Physics, Kuala Lumpur, Malaysia
- * Deceased